Exploring the Structure, Properties, and Applications of Highly Ordered Bionanocomposites

Zlopaša, Jure

DOI
10.4233/uuid:e47bfa54-4d58-4c82-829f-3cb2ceb6cfc7

Publication date
2017

Document Version
Final published version

Citation (APA)
Zlopaša, J. (2017). *Exploring the Structure, Properties, and Applications of Highly Ordered Bionanocomposites*. [Dissertation (TU Delft), Delft University of Technology]. https://doi.org/10.4233/uuid:e47bfa54-4d58-4c82-829f-3cb2ceb6cfc7

Important note
To cite this publication, please use the final published version (if applicable).
Please check the document version above.

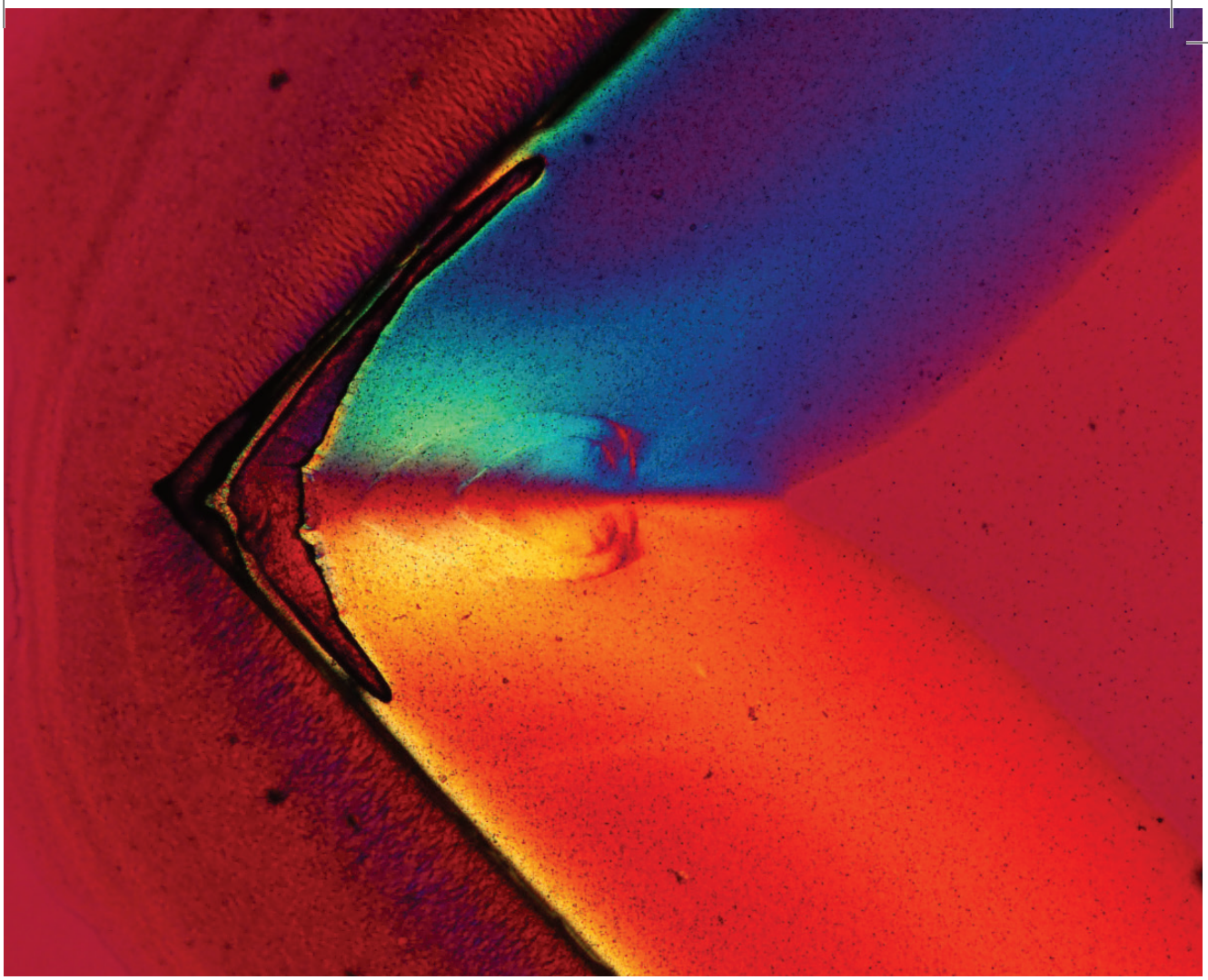

Exploring the Structure, Properties, and Applications of Highly Ordered Bionanocomposites

Jure Zlopaša

EXPLORING THE STRUCTURE, PROPERTIES, AND APPLICATIONS OF HIGHLY ORDERED BIONANOCOMPOSITES

Proefschrift

ter verkrijging van de graad van doctor
aan de Technische Universiteit Delft,
op gezag van de Rector Magnificus prof. ir. K. C. A. M. Luyben
voorzitter van het College voor Promoties,
in het openbaar te verdedigen op
vrijdag, 22 september 2017 om 12:30 uur

door
Jure ZLOPAŠA

Magistar Inženjer, University of Zagreb,
geboren te Zagreb, Kroatië.

This dissertation has been approved by the

Promotors: Prof. dr. S.J. Picken, Prof. dr. ir. K. van Breugel
and Prof. dr. ir. E.A.B. Koenders

Composition of the doctoral committee:

Rector Magnificus	voorzitter
Prof. dr. S.J. Picken	Technische Universiteit Delft
Prof. dr. ir. K. van Breugel	Technische Universiteit Delft
Prof. dr. ir. E.A.B. Koenders	Technische Universität Darmstadt, Duitsland

Independent members:

Prof. dr. R. Polder	CiTG, Technische Universiteit Delft
Prof. dr. ir. J. van der Gucht	Wageningen University & Research
Prof. dr. D. Bonn	Universiteit van Amsterdam
Prof. dr. A.D. Gotsis	Technical University of Crete, Griekenland
Prof. dr. dr. h.c. ir. M.C.M. van Loosdrecht	Delft University of Technology, reservelid

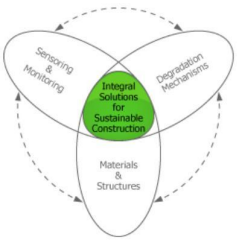

This research is supported by the Dutch Technology Fundation STW, which is part of the Netherlands Organisation for Scientific Research (NWO) as a part of the IS2C program (www.is2c.nl), number 10962.

Cover design by Ben Blumensheid. The image shows the influence of drying direction on the MMT alignement.

Printed in the Netherlands by Rijnja Repro.
ISBN 978-94-6186-849-7

Contents

Chapter 1

Introduction

The ambition to generate new innovations for efficient and sustainable construction is the basis on which this research started on. The main focus was on development and characterisation of environmentally friendly water-based curing compound for cement-based materials.

The extension of the range of filler dimensions to a nanometric size has lead to quite an considerable research in designing innovative materials and understanding the wide range of their resulting properties. The next challenge posed to the researchers is how to improve and/or tune specific material properties. This has lead to a vast body of knowledge in self-assembling materials or the use of external triggers, primarily by using a magnetic field, which enables a considerable control over the final structure/alignment of the nanocomposite that facilitates tuning of the desired properties of the material (Jestin et al. 2008). In the following work we have focused on control over the orientation of the filler of the bionanocomposites, and have provided deep understanding on how the highly organized structure is obtained. Furthermore, we have also looked at utilisation of the bionanocomposite as a curing compound for cement-based materials.

1.1 Polymer nanocomposites

Polymer nanocomposite, in broad terms, describes a material with polymer matrix where the filler has a nanometer size (smaller than 100nm) at least in one of the dimensions. In general the fillers can be classified in (1) particle, (2) layered and (3) fibrous materials. In this work we will focus on the layered inorganic fillers, and more specifically layered silicates (phyllosilicates).

A concept of polymer clay nanocomposites PCNs (then called polymer clay hybrids) was first presented at Toyota Central R&D labs in 1985. It was noticed that a small addition of randomly oriented and homogeneously distributed layered silicates resulted in superior mechanical, thermal and barrier properties of these materials compared to those of pristine polymer and/or conventional composite. This was achieved by a two-step process, which entails cation exchange and inter-

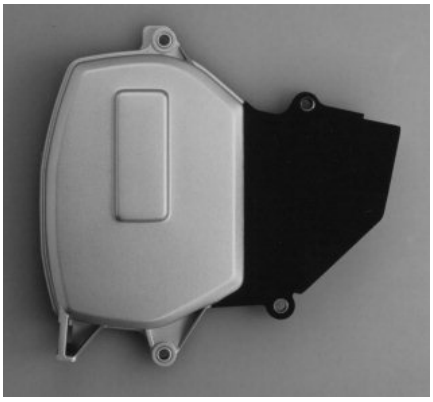

Figure 1.1: Injection molded PCH timing belt cover (Toyota) (Kawasumi, 2004).

calation of 12-aminolauric acid within the montmorillonite sheets, which allowed the ϵ-caprolactam to enter in-between the expanded layers. This was followed by polymerisation of ϵ-caprolactam, using the 12-aminolauric acid montmorillonite as the catalyst, by doing so the polymer pushes the montmorillonite sheets even more apart, producing a completely exfoliated nylon 6-clay hybrid (Kojima *et al.* 1993). Very soon afterwards, in 1989, Toyota started implementing the PCNs in their automotive parts, i.e. timing belt covers, figure 1.1(Kawasumi, 2004).

Phyllosilicates (from the Greek "*phyllon*" meaning leaf) presents a group of silicates that are defined by their layered structure. The structure of phyllosilicates are all based on a tetrahedral (T) and octahedral (O) sheet that form either in 1:1 layer structure in which one tetrahedral sheet is bonded to one octahedral sheet or 2:1 layer structure where one octahedral sheet is sandwiched between two opposing tetrahedral sheets, *i.e.* T-O or T-O-T layers. The dimensions of the individual layer make it an interesting filler, because the thickness is around 1 nm and the radium may vary from 10 to 1000 nm, resulting in high aspect ratio (Theng, 2012).

The ideal 2:1 structure is found in pyrophyllite ($Al_2Si_4O_{10}(OH)_2$), in which two octahedral sheets contain trivalent cations (M^{3+}) with a vacancy in the third octahedron and the tetrahedral sheet contains Si^{4+} in all tetrahedra. Such structure is electrically neutral and no cations are needed in the interlayers to balance the charge. The layers organize themselves to form regular galleries that are held together by van der Waals forces. These structures have no possibility of swelling of the layers, due to the lack of charge there is essentially no cation exchange capacity. This makes it rather difficult to completely exfoliate the individual layers and get the nanometer-size inorganic filler. Isomorphous substitution of Al^{3+} for Si^{4+} in

the tetrahedral and Al^{3+} or Mg^{2+} for lower charged cations in octahedral sheets or presence of vacancies of basic pyrophyllite structure results in negative layer charges where the charge imbalance is compensated by intercalation of exchangeable cations.

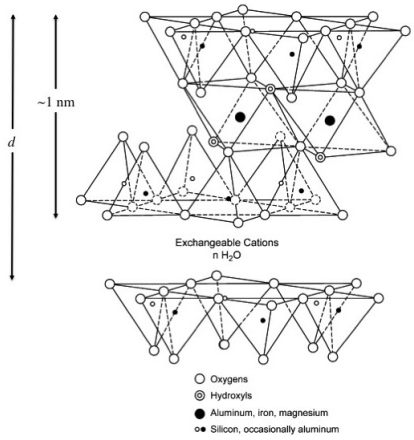

Figure 1.2: Idealized structure of montmorillonite (Ray & Okamoto, 2003).

One such group of swell-able phyllosilicates is the smectite group, which are widely available and cheap fillers making them an interesting material due to their high cation exchange capacities, surface area, surface reactivity, and adsorptive property. In PCNs they are used because of ease of swelling and complete exfoliation of the individual layers, which is necessary to profit from the nanometric dimensions of the platelets.

One of most investigated smectite clays for the use in PCNs is montmorillonite (MMT), which will also be used in this thesis. The montmorillonite structure is derived from the original pyrophyllite structure by partial isomorphous substitution of the Al^{3+} by Mg^{2+} in the octahedral layer, resulting in a negative charge of the T-O-T layers that is compensated by mono- and di-valent cations. Corresponding to the isomorphous substitution the general formulae of MMT is $(Na,Ca)_{0.3}(Al,Mg)_2Si_4O_{10}(OH)_2 \bullet n(H_2O)$. The presence of the exchangeable cations in the MMT structure allows the water to enter in between the layers, causing the increase in the d-spacing that can further swell, and under high shear stress can exfoliate to individual layers. Individual MMT platelets have a surface area of around 750 m^2/g and aspect ratio in range of 100-500 [Roderick, 1965].

Unfortunately, for most PCNs, the surface modification of clay platelets is necessary in order to achieve good dispersion and compatibility with the polymer matrix.

The reason for this is found in the hydrophilicity of the clay platelets that is incompatible with hydrophobic polymers. The surface modification is usually achieved by mixing aqueous clay suspension with a solution of a cationic organic surfactant (quaternary ammonium), which leads to an exchange of original interlayer cations by organic cations or by addition of chemical groups that form complexes with cations. The process is called intercalation that leads to expanded clays, thus producing organically modified clay (organoclay). The amount of cations that are exchanged is governed by the cation exchange capacity, CEC. The organic modification of clay does not only increases the compatibility with polymer matrix, but it also facilitates complete exfoliation of individual clay layers.

Figure 1.3: Schematic presentation of polymer clay (nano)composite. The microcomposite (1) has stacked clay platelets that leads to a tactoid structure with reduced aspect ration. The favorable polymer-clay interactions assist in (2) intercalation of polymer in the clay galleries and can further (3) fully exfoliate the clay platelets, leading to a nanocomposite structure.

The distribution of clay filler within the PCNs determines the properties of the final material. In Figure 1.3, the most common three types of polymer clay (nano)composite morphologies are presented: (1) phase separated (tactoid), (2) intercalated, and (3) exfoliated. In the case of phase separation, the polymer does not diffuse in between the clay layers, with no effect on the spacing between the layers. This in the end means that clay filler remains in the microscopic dimension and the resulting composite represents a microcomposite. In the intercalated PCNs, the clay galleries are expanded, where the distance between the individual layers is fixed. In the PCNs with completely exfoliated clay platelets, there is no fixed distance between the platelets and the full potential of the clay platelets as a filler is achieved, meaning the aspect ratio is the key factor. The influence of the layered silicates is depicted in Figure 1.4, where we see that high aspect ratio imposes a tortuous path to the penetrating molecules, making the PCNs an interesting material for membranes.

The final important factor, along with the distribution of the clay platelets, is the level of orientation, which is described as the orientational order parameter,

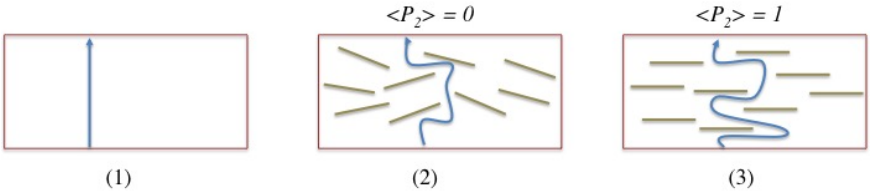

Figure 1.4: Illustration of a tortuous path imposed by clay platelets in polymer matrix film. In a film with no clay (1), molecules diffuse via pathway perpendicular to the film orientation. In a PCN film (2) and (3) the molecules diffuse around the clay platelets with futher increase in the tortuos path by orientation of the cay platelets.

$<P_2>$, which is the average orientation order of the molecules, in our case the clay platelets. The $<P_2>$ describes the level of orientational order of clay platelets in the nanocomposite. The highest value of $<P_2>$ of 1 is for clay platelets that are perfectly aligned parallel to the director, while for randomly distributed platelets the $<P_2>$ value is 0. The value of $<P_2>$ is very important for the transport properties of the final PCNs, as is presented in Figure 1.4. We can see that the higher the level of alignment the longer is the tortuous path the penetrating molecules need to pass, meaning the diffusion coefficient is significantly lowered.

Conventionally there are three production routes to achieve PCNs: (1) *in-situ* polymerization, (2) melt compounding and (3) solvent blending (Giannelis 1996, Tjong 2006).

The *in-situ* polymerization route consists of mixing suitable monomers together with completely exfoliated organoclay, or intercalated organoclay, followed by polymerisation that results in increase of volume between the layers pushing them to completely exfoliated structure. This method can give quite a good exfoliation of the clay platelets, which is reflected in the material properties, but it is not possible for all PCNs, also sometimes the degree of polymerisation is not sufficient.

Melt compounding of the PCNs entails the mixing of polymer melt with (surface modified) clay platelets, usually high shear forces are necessary to achieve high level of intercalation/exfoliation. It is broadly applicable to many commodities and engineering polymers, due to its flexibility as a process, that are produced on a large scale.

For making PCNs via solvent blending, a suitable solvent is needed to dissolve the polymer and disperse the organoclays, usually under high shear, after which the solvent evaporates. Both melt compounding and solvent blending methods have difficulties in getting completely exfoliated structures, which usually results in

tactoid PCNs morphologies, while all methods have no control over the orientation of the clay platelets.

1.2 Bio(nano)composites

Most of the earlier work on PCNs used petroleum-based polymers, with a volume fraction of the clay platelets rarely exceeding 10 wt.%, because of the dramatic decrease in the properties of PCNs. The reason for this is the occurrence of phase separation, absence of platelet orientation and the lack of exfoliation (low aspect ratio) of the clay platelets.

In search for survival, living organisms, such as molluscs, have used sophisticated biomineralisation mechanisms that provide the organism with hybrid structures that exhibit appealing combinations of strength, stiffness, resilience and energy absorbing capabilities. Interestingly, if we zoom in on materials found in nature we find a complex microarhictecture with a high hierarchical order and impressive mechanical properties. These biological structures are formed at ambient conditions from common materials (*e.g.* proteins and/or polysaccharides, $CaCO_3$, and FeOOH), yet they exhibit superior performance through the complex hierarchical utilisation of composition and architecture (Kakishava & Sumitomo, 2011). One such material found in nature that has been quite extensively explored is nacre, presented in figure 1.5, also known as the "mother of pearl". This composite material is found in the innerlayer of mollusc shells and apart from being interesting for research it has ornamental use. It is constituted of 95 wt.% of predominantly highly ordered aragonite platelets that are surrounded by proteins/polysaccharides that serve as an organic template for nucleation and growth of aragonite, but also it strongly contributes to the mechanical properties of nacre. The microarchitecture of nacre is typically presented as a "brick-and-mortar" arrangement, where the brick refers to the aragonite platelets and the mortar is a polysaccharide/protein glue (Jackson *et al.* 1988).

Nacre is not the only nature-made material that has sparked a lot of attention, recently limpet teeth has raised a considerable interest by surpassing spiders web as the *strongest natural material* and going toe to toe with some of the strongest man-made materials, i.e. carbon fibers, with a whopping tensile strength of 4.9 ± 1.9 GPa (Barber *et al.*, 2015). This should come as no surprise, considering the timescales over which these materials have been developed in Nature with the display of a remarkable efficiency following a general principle postulated by C. R.

Darwin *"natural selection is continually trying to economise in every part of the organisation"* (Darwin, 1859). By which the complex requirements posed by the way that plants and animals function in their surrounding environment shape the natural materials.

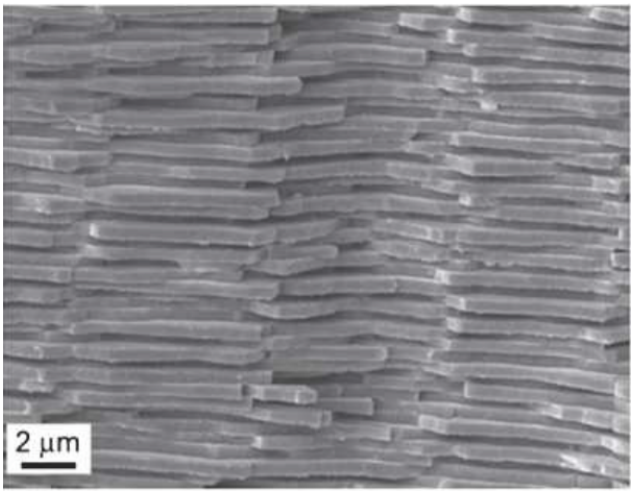

Figure 1.5: Hierarchical structure of a fractured red abalone shell showing the ordered aragonite crystals in the nacreous layer (Barthelat *et al.* 2006).

Recently, PCNs with a biopolymer matrix are being investigated to a great extent, where the researchers have started to explore biopolymer clay with a high volume fraction of clay filler. The inspiration was to produce materials with similar, or exceeding, properties to those found in nature, *e.g.* nacre, where the complex formation of aragonite platelets was replaced by phyllosilicates and most commonly one polysaccharide was used as a polymer matrix. Similar to nacre, PCNs with a biopolymer matrix were found to have a highly ordered structure that results in impressive mechanical and transport properties. There have been several methods proposed to produce the structure of nacre, most notably via layer-by-layer deposition.

Tang *et al.* were the first to explore the layer-by-layer deposition as a pathway to achieve an artificial analog to a nacre structure. This technique involves controlled sequential deposition of the polyelectrolytes and clays on a glass slide. The obtained highly ordered nanostructure resembles that of nacre, and this was also reflected in the mechanical properties of the obtained nanocomposite, which are remarkably high and can exceed those of nacre. The inconvenience of this technique is that it is quite laboursome and time consuming (Tang *et al.*, 2003).

Recently, there have been several attempts to produce such materials, particularly by suspension casting, doctor blading and by vacuum assisted self-assembly (Ebina & Mizukami, 2007, Walther *et al.* 2010, Yao *et al.*, 2010). These techniques show promise when considering the time needed for production and large-scale production of highly ordered (bio)polymer clay nanocomposites.

Although, in the initial polymer/clay system the clay particles are randomly distributed, with further processing either by vacuum assisted self-assembly, doctor blading, and/or solvent evaporation, the resulting structure is found to be highly ordered. As mentioned due to the anisotropy and high clay loading, the mechanical and transport properties of these highly ordered (bio)-nanocomposites are greatly improved, while a clear understanding of the formation mechanism is still lacking, making it difficult to improve on and control.

The nacre-like structures can also be made with different fillers, *e.g.* layer double hydroxides, gibbsite and graphene oxide. Putz *et al.* followed the development of highly ordered PEO/graphene oxide nanocomposite prepared by vacuum assisted self-assembly. From their observations they proposed that the highly ordered PEO/graphene oxide is developed through a formation of a semi-ordered accumulation of graphene sheets, which is followed by a compression of the sheets by further solvent removal (Putz *et al.*, 2011).

1.3 Curing of cement-based materials

Cement-based materials (*e.g.* concrete, mortar) are the most used materials in the world, and it can be simply presented as a composite material composed of sand, cement and water. The cement and water go through a chemical reaction, hydration, producing cement hydrates that are the building blocks of the cement-based material, acting as a glue between the sand particles. Hydration refers to chemical and physical changes that take place when Ordinary Portland Cement, CEM I, reacts with water (Richardson, 2000). Due to high CO_2 footprint of cement industry, nowadays, part of the cement is replaced by supplementary cementing materials (SCMs), *e.g.* fly ash, ground granulated blast-furnace slag or silica fume. The SCMs go through a pozzolanic reaction that extends the cement hydration period, making the curing of such structures an even more important issue (Siddique & Kahn, 2011). In marine environments, a very commonly used cement is CEM III/B which has a high replacement of cement by ground granulated blast furnace slag, GGBFS. The hydration mechanism of the combination of GGBFS and Portland cement is

slightly more complex than that of a Portland cement only. This pozzolanic reaction involves activation of the GGBFS by alkalis and sulphates to form its own hydration products. The result is a hardened cement paste with more very small gel pores and less capillary pores for the same total pore volume.

The extent of the hydration process in turn reflects on the final properties, *e.g.* bonding between the sand particles and the porosity. When the water activity drops below 0.8, the kinetics of cement hydration is at only 10% compared to sample cured at a water activity of 1 (Powers & Brownyard, 1946-1947). This implies that a high degree of hydration, will only be achieved in a completely water saturated space, and thus producing a dense microstructure with desired physical and chemical properties, which determine the durability of cement-based materials.

After the placement of fresh cement-based material, the surrounding environmental conditions, *i.e.* temperature, relative humidity, and wind, dictate the rate of drying, as illustrated in figure 1.6. Premature drying of young concrete affects the concrete both at early ages, *e.g.* plastic shrinkage and plastic cracking, and in the long term, *e.g.* strength and durability. If the potential of concrete with regards to strength and durability is to be fully realized, it is most essential that it be cured adequately (Hover, 2011, Meeks & Carino, 1999).

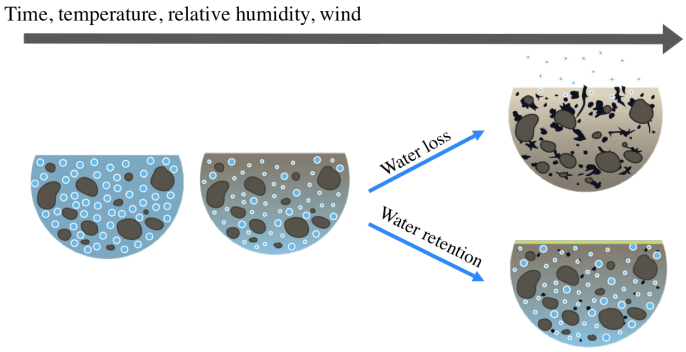

Figure 1.6: Influence of enviornmental conditions on water evaporation from the surface of cement-based materials.

Curing is the process of controlling the rate and the extent of moisture loss from cement-based materials during cement hydration. It represents the final stage in production of cement-based materials and is essential for the final properties of the material. By preventing the loss of water from cement-based materials, ongoing hydration could be achieved and drying shrinkage can be avoided, leading to a minimum of surface cracks, a stronger bond between aggregates, fewer voids, and lower

connectivity of pores (Neville, 1995). Such a microstructure is denser and can cause slower penetration of aggressive fluids that may be harmful, *e.g.* to prevent corrosion of the steel reinforcement, figure 1.7. Therefore, a properly cured cement-based material is better prepared for a long service life. This is especially important for cements that have partial replacement by pozzolans that have a longer hydration period and are more sensitive to water loss. But if cured properly the achieved microstructure surpasses the one of OPC by far. **The cement industry represents about 8.6 % of global anthropogenic CO_2 emissions, which indirectely means that poorly designed and executed (e.g. curing) cement-based materials increase the already high CO_2 footprint** (Miller et al. 2016)**.**

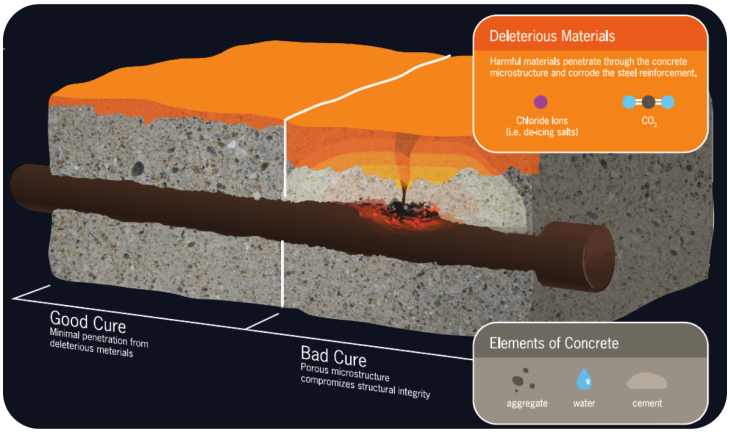

Figure 1.7: Illustration of the influence of "good" and "bad" cured cement-based material on the corrosion of steel reinforcement.

Generally, curing can be performed by adding water or by hindering water to escape from the cement-based material's surface. Continuously adding water to the surface, by means of water ponding, water spraying, and/or by the use of wet burlaps usually gives the best end results. However, this technique requires workers on site that keep the concrete moist, which can be costly. In addition, this method can be especially costly in places where there is a scarcity of water. As said, the second way of curing cement-based materials is by preventing water evaporation. This can be accomplished by covering the surface with plastic sheets or by spraying it with a curing compound (polymer solutions/emulsions) that creates a film that hinders water evaporation. Curing compounds can be water based or organic-solvent based. In general, curing compounds based on organic-solvents show better performance compared to water-based ones. As a drawback, there can be an environmental

impact, especially when using it in poorly ventilated environments. Covering the concrete structures with plastic sheets in general provides a good curing conditions, but applying it in practice can be quite tedious and sometimes unpractical, *e.g.* strong wind can blow the cover (Wang *et al.*, 1994, Al-Gahtani, 2010).

1.4 Outline of the thesis

In this thesis we report on the work on sodium alginate montmorillonite bionanocomposites. The mechanism behind the high level of alignment of the bionanocomposite was investigated. Furthermore, we examined the rheological behavior of the sodium alginate and montmorillonite in suspensions. In addition to that, we studied the mechanical and transport properties of the highly ordered Na Alginate/MMT bionanocomposites. Finally, we also explored the possibility of using sodium alginate as a novel bio-based curing compound for cement-based materials.

In chapter 2 a highly ordered alginate/montmorillonite bionanocomposite structure is presented. The alignment of the bionanocomposites has been determined by environmental scanning electron microscopy (ESEM) and wide-angle X-ray scattering (WAXS). The ESEM micrographs show a high in-plane orientation of the bionanocomposite, while 2D X-ray scattering images show a clear angle dependency that confirms preferential orientation of montmorillonite (MMT) platelets. The order parameter ($<P_2>$) was calculated from azimuthal intensity profiles derived from WAXS measured over the MMT 001 reflection, using the Maier–Saupe and the affine deformation model. The importance of the $<P_2>$ value is that it can be directly correlated to the anisotropic properties of the bionanocomposite, i.e. mechanical and transport properties. This will be further dealt with in chapter 4 and 5.

We observe that the $<P_2>$ values depend on the MMT concentration, which is explained by the MMT–alginate interaction. We propose an affine deformation model based on gel formation achieved by alginate adsorption on the edges of MMT, which develops yield stress and deforms the MMT platelets during drying resulting in high range $<P_2>$ values.

In chapter 3 we report on a study of a rheological behavior of sodium alginate and montmorillonite suspension. We find that viscoelastic behavior of this suspension is dramatically affected with increasing volume fraction of montmorillonite platelets. Addition of montmorillonite generally leads to gel formation, which is attributed to interactions of montmorillonite and alginate via H-bonding and attraction between the positive edges of the platelets and the anionic backbone of the

biopolymer. A critical concentration for the measured system was observed at 20 wt.% montmorillonite, where a crossover to a gel-like structure was detected. The observed gel has a rubber plateau, which develops further with higher montmorillonite concentration. In this physical gel the relaxation maximum was detected, which is associated with the breaking and reformation of the bonds between the platelets and the biopolymer. For this transient behavior, we find that a Maxwell type viscoelasticity quite well describes the relaxation time and the observed G'-G" crossover. We believe that this gel-like behavior plays an important role in formation of highly ordered nanostructures that are developed during the drying of these bionanocomposite suspensions.

In chapter 4 the mechanical properties of the Na Alg/MMT bionanocomposites is measured and discussed. The effect of MMT loading and the obtained "brick-and-mortar" structure of the bionanocomposite were studied by Dynamic Mechanical Analysis (DMA). We observe remarkably high stiffness values over a whole range of MMT concentration, with a small decrease for the sample with 80 wt.% MMT. We atribute this drop in the stiffness to the stacking of the MMT platelets that lowers the effective aspect ratio of the MMT, which leads to decrease in the stiffness of the bionanocomposites. The mechanical properties are described using the Halpin-Tsai model for which we have examined the interplay of the calculated order parameter, MMT concentration, and the aspect ratio on the stiffness of the Na-Alg/MMT bionanocomposite. The material at the same time displays a high heat distortion temperature that exceeds 240 °C for Na-Alg 80 wt.% bionanocomposite. As a result of the highly ordered structure, the bionanocomposite is self extinguishing and maintains its structure (minimal volume change) after burning.

In chapter 5 the water diffusion coefficient of Na Alg/MMT bionanocompoiste was examined from the sorption kinetics over the entire water activity range. We look at how the presence of impearmeabile disk-like filler influences the water vapor sorption kinetics by varying the filler concentration and taking into account the orientation of the filler. The Na-Alg/MMT bionanocomposite films demonstrate a considerable decrease in the sorption kinetics, which reflects the highly ordered structured that imposes a tuortuos diffusion path. The calculated water diffusion coefficient of the bionanocomposite and previously calculated order parameter were used to back-calculate the aspect ratio of the MMT platelets. The addition of the MMT platelets also influences the water absorbing capacity of the Na-Alg/MMT bionanocomposite, which could be caused by the interactions in the system reducing the hydrophilic nature of both individual components.

In chapter 6 an environmentally friendly, water-based curing compound, made of sodium alginate, has been tested. We address the principle in which the sodium alginate curing compound reacts on the surface of the cement-based materials. Rapid Chloride Migration test and ESEM are conducted on different samples to investigate the functional properties, e.g. ion transport, and microstructural investigation, of cement-based material to evaluate the performance of the new bio-based curing compound. Mortar samples were cured at 50% RH and 20 °C both with and without surface addition of the bio-based compound. Two different types of cement, CEM I and CEM III/B, were tested to study differences in curing performance. For both mortar samples we observed beneficial effects when applying the bio-based curing compound, which are reflected in reduction of the chloride migration coefficient. The results showed that using Na-Alg as a curing compound improved the surface quality with denser microstructure with fewer cracks compated to the control samples. Also, due to secondary pozzolanic reaction the mortar samples prepared with CEM III/B, we observed higher curing sensitivity compared to samples prepared with the CEM I.

In chapter 7 the most important findings of the research work within the scope of this thesis are summarized, along with outlook on future research. The emphasis is focused on the production of an high performance bionanocomposites from biopolymers extracted from wastewater treatment. We believe that using this technology we can contribute to the circular economy with development of bionanocomposites from a sustainable resource.

Chapter 2

Origin of Highly Ordered Sodium Alginate/Montmorillonite Bionanocomposites[1]

A highly ordered alginate/montmorillonite bionanocomposite structure is presented. The alignment of the bionanocomposites has been determined by environmental scanning electron microscopy (ESEM) and wide-angle X-ray scattering (WAXS). The ESEM micrographs show a high inplane orientation of the bionanocomposite, while 2D X-ray scattering images show a clear angle dependency that confirms preferential orientation of montmorillonite (MMT) platelets. The order parameter ($<P_2>$) was calculated from azimuthal intensity profiles derived from WAXS measured over the MMT 001 reflection, using the Maier−Saupe and the affine deformation model. We observed that the $<P_2>$ values depend on the MMT concentration, which is explained by the MMT−alginate interaction. We proposed an affine deformation model based on gel formation achieved by alginate adsorption on the edges of MMT, which develops yield stress and deforms the MMT platelets during drying resulting in high range $<P_2>$ values.

[1] J.Zlopasa, B.Norder, E.A.B. Koenders, S.J. Picken *Macromolecules* 2015, 48 (4), pp 1204–1209

2.1 Introduction

Polymers with only small additions of dispersed nanosized clay particles result in a polymer clay nanocomposite (PCN), with improved properties compared to the native polymer (Okada & Usuki, 1995). The addition of clays leads to a dramatic change in mechanical properties and reduced permeability, and it strongly enhances the flame retardance (Blumstein, 1965; Kojima et al., 1993; Okada & Usuki, 1995; Messersmith & Giannelis, 1995). The reason for this is the large aspect ratio of the clays that imposes a complex tortuous path to penetrating gases (Nielsen, 1967). Traditionally, clay concentrations in PCNs do not exceed 10 wt. % due to poor dispersion and low nanostructural ordering.

Recently, several studies have been reported on PCNs with large amounts of clay in the polymer matrix. All these studies used nacre as a template structure, which represents a highly ordered nanostructured system. Different methods are used to prepare such materials, namely a layer-by-layer deposition process, a water-based process similar to paper making, vacuum filtration, and a water evaporation induced self-assembly (EISA) (Tang, Kotov & Magonov 2003; Walther et al. 2010; Yao et al. 2010; Das et al. 2013; Kochumalayil et al. 2013). These approaches are based on the physical adsorption of polymers (e.g., PDDA, PVOH, and chitosan) onto the surface of the clay particles. During removal of the solvents the nanostructure starts to self-assemble, resulting in a system of alternating organic/inorganic layers. Because of the high clay concentration and remarkable nanostructural ordering, which is typical for a nacre-like nanocomposites, they present superior mechanical and transport properties compared to traditional PCNs.

In this study, a highly ordered bionanocomposite is discussed, based on sodium montmorillonite (Na^+ MMT) and sodium alginate (Na-Alg) with an inorganic particle concentration of up to 80 wt. %. Alginates are polysaccharides comprising (1 - 4) linked units of β-D-mannuronate (M) and α-L-guluronate (G) at different ratios and different distributions within the chains. The functional properties are strongly related to the polymer composition (M/G ratio) and level of block formation. Alginates are present in brown algae and can also be found in metabolic products of bacteria, e.g., pseudomonas and azotobacter (Linker & Jones 1966; Gorin & Spencer 1966; Grasdalen, Larsen, & Smidsrød 1981; Draget, Skjåk-Bræk, & Smidsrød 1997). Commonly, alginates are used as food additives, gelling agents, and wound dressings and are used for drug delivery (Matthew et al. 1995; Laurienzo 2010).

In a previous study, Ebina et al. described highly ordered saponite bionanocomposite films using anionic polymers, *viz.* sodium carboxymethyl cellulose (Na-CMC)

(Ebina & Mizukami 2007). The mentioned bionanocomposite is derived by film casting the CMC/saponite suspension and water evaporation after which the system was found to order itself. Because of the permanent negative charge of the saponite surface, the expected interaction between the anionic polymer and clay is on the positively charged clay edges (Tateyama et al. 1997). To our knowledge, so far there is no direct explanation why such a system should be ordered.

In the current paper, we aim to explain the mechanism responsible for the high nanostructural ordering between anionic polymers (alginate) and clays (Na^+ MMT). We observed a high order parameter for the MMT platelet determined by WAXS. The obtained ODF (orientation distribution function) is fitted to the Maier−Saupe model and the affine deformation model. The Maier−Saupe model is based on spontaneous, nematic ordering, while the affine deformation model assumes gel formation and compression of the MMT platelets that causes the alignment. Good agreement was found between the proposed models and the experimental results, although the affine deformation model appears to be somewhat better.

2.2 Materials and methods

A free film of Na-Alg with various concentrations of MMT was prepared according to the following procedure. Commercially available MMT (Cloisite Na^+ (MMT), Southern Clay Products Inc., Rockwood) was dispersed in deionized water under vigorous stirring for 24 h to achieve a 3 wt. % exfoliated dispersion. During that time all of the Na-MMT got dissolved and dispersed, without any remaining visible agglomerates. Na-Alg (M/G = 1.56, Mw = 150 kg/mol) purchased from Sigma-Aldrich was used as received. Na-Alg was dissolved using deionized water to form a 3 wt. % solution. The MMT suspension was subsequently mixed with Na- Alg solution and was further mixed for 24 h. The total solid content was kept at 3 wt. % but with different MMT concentrations, 0, 1, 2, 5, 10, 20, 50, and 80 wt. % with respect to the mass of Na-Alg. The obtained dispersions were poured into a 10 cm petri dish and dried at ambient conditions (20 °C, 50% RH) to form a thin film. Freestanding films were obtained by peeling the film off a petri dish. Furthermore, the films were vacuum-dried at 40 °C until constant weight. The final thicknesses were in the range of 100 μm. The free film formation experiment is summarized in figure 2.1.

The cross section of the bionanocomposite films was examined by environmental scanning electron microscopy (ESEM) using a Philips XL30 Series ESEM. Prior to

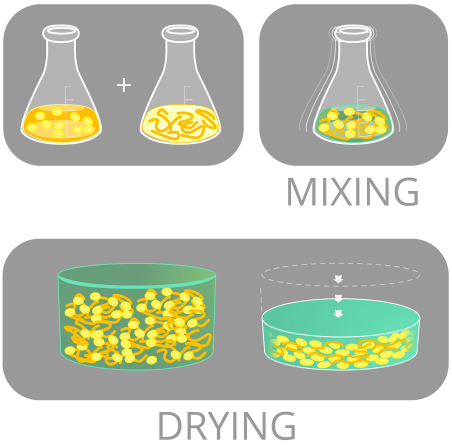

Figure 2.1: Preparation of Highly Ordered Na-Alg/MMT Bionanocomposites

ESEM investigation the films were coated with graphite using a Leica EM CED030 sputter coater. To determine the MMT concentration-dependent order parameter, wide-angle X-ray scattering (WAXS) was performed using a Bruker AXS D8 Discover X-ray diffractometer with a Hi-Star 2D detector and using Cu Kα radiation filtered by cross-coupled Göbel mirrors at 40 kV and 40 mA. The sample−detector distance was 10 and 13 cm for parallel and perpendicular to the film surface, respectively.

2.3 Orientation models

In this section the Maier−Saupe and affine deformation models are presented, which will be used for calculating the degree of MMT orientation. These models were chosen as two plausible extreme cases for analyzing the origin of nanostructural ordering of the Na-Alg/MMT bionanocomposite.

Maier−Saupe theory is founded on a molecular field treatment of long-range contributions to the intermolecular potential and ignores short-range forces (Luckhurst & Zannoni 1977). It is based on the mean-field potential that describes the average influence the nematic environment has on the orientation of one single particle (Picken 1990).

$$U(cos(\beta)) = -\in < P > P_2(cos(\beta)) \tag{2.1}$$

where $\in$ is the strength of the potential, $<P_2>$ is an average order parameter, and $P_2(cos(\beta))$ is a second-order Legendre polynomial of $cos(\beta)$. This model is often used in liquid crystals theory to describe spontaneous ordering of nematic crystals. The order parameter, $<P_2>$, of nematic phases can be derived by fitting the azimuthal intensity profiles using eq. 2.2 (Maier & Saupe 1959):

$$f(\beta) = I_0 + Ae^{\alpha cos^2(\beta)} \tag{2.2}$$

where I_0 is a baseline intensity, A is a normalization constant, a is the width of the curve and is directly related to $<P_2>$, and β is the azimuthal angle at maximum intensity. The Maier−Saupe theory has also been extended to the field of polymers (Picken et al. 1990). Recently, the Maier−Saupe orientational distribution function has also been used to fit the azimuthal intensity profile obtained by X-ray scattering measured on polymer gels with graphene nanosheets (Wu et al. 2014).

The affine deformation model, originally derived by Kuhn and Grün, has been used to describe the change in orientational order in an ideal rubber due to elongation (Kuhn & Grün 1942). It has also been used to describe the orientational order in aramid solutions during the fiber spinning process (Picken et al. 1991; Picken, van der Zwaag, & Northold 1992; Fan, Luckhurst, & Picken 1994). Here, we use the affine deformation model to describe the mechanism of high alignment of the MMT platelets. We assume that this high alignment is achieved due to interactions between the positively charged MMT edges and the negatively charged alginate backbone, which creates a network (pseudo gel) followed by a two stage drying process. During the first stage, water evaporation will result in an external volume change of the whole microstructure with no influence on the orientation of the MMT platelets until a critical total solid concentration has reached at which the system exhibits a yield stress. Once the yield stress is developed, the MMT platelets are immobilized, which during further drying causes alignment of the MMT platelets The affine deformation model allows calculation of the $<P_2>$ as a function of external deformation, which in this case is consolidation caused by drying. Here we modify the affine deformation model to measure the development of MMT orientation due to shrinkage (drying), following eq. 2.3:

$$f(\beta) = I_0 + \frac{1}{2}\lambda^2 \frac{cos^3(tan^{-1}(\lambda tan(\beta)))}{cos^3(\beta)} \tag{2.3}$$

in which I_0 is a baseline intensity, λ is a degree of (vertical) consolidation, and β is the azimuthal angle with respect to the z-axis. A detailed derivation of eq 2.3

is presented in the Appendix A. Considering that the cross-linking of the alginate is caused by the MMT platelets, we expect the <P_2> values to depend on the MMT concentration. In addition, the critical total solid concentration at which the yield stress develops should be inversely proportional to λ. The effect of an affine deformation in compression on the MMT platelets is shown schematically in Fig. 2.2.

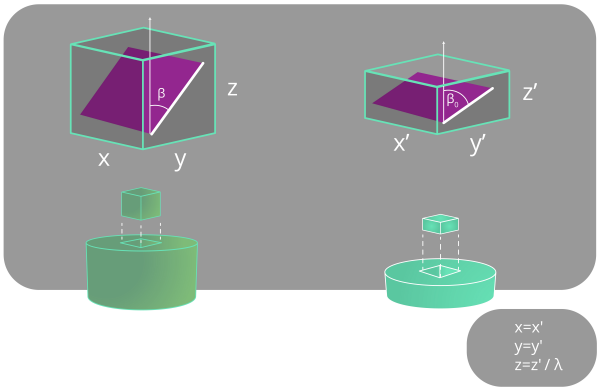

Figure 2.2: Effect of affine deformation during vertical shrinkage on the MMT platelets

The <P_2> value was calculated from the λ and a parameters, which were obtained from fitting the azimuthal intensity profile with affine deformation and the Maier−Saupe distribution, respectively, using eq 2.4:

$$< P_2 >= \frac{\int_{-1}^{1} P_2(cos(\beta)) f(\beta) dcos(\beta)}{\int_{-1}^{1} f(\beta) dcos(\beta)} \tag{2.4}$$

where $P_2(cos(\beta))$ is a second-order Legendre polynomial of cos(β):

$$P_2(cos(\beta)) = \frac{1}{2}(3cos^2(\beta) - 1) \tag{2.5}$$

The special case <P_2> = 0 represents an isotropic system while for a perfectly aligned system <P_2> = 1. To emphasize the shape difference between the affine deformation and Maier−Saupe orientation distribution functions, we have calculated these curves for the same <P_2> value, as shown in figure 2.3. These two orientation

distribution functions show a clear difference in the tails of the function, where the affine deformation curve displays a slower asymptotic decay compared to the Maier−Saupe function.

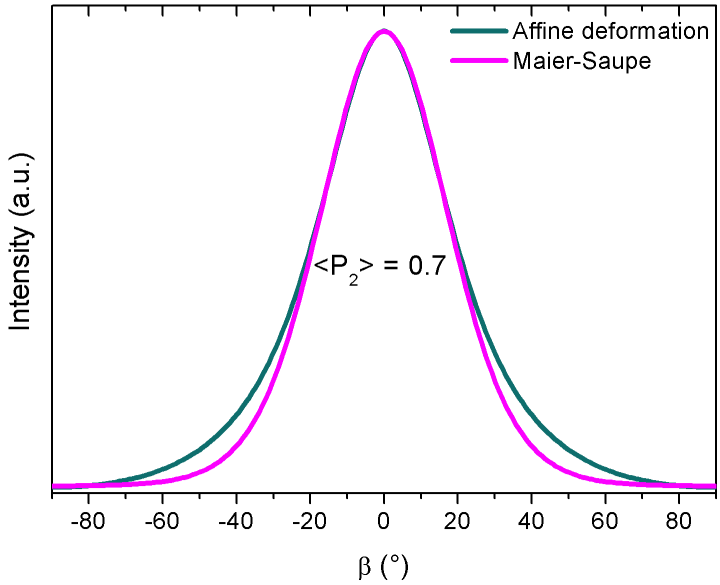

Figure 2.3: Calculated affine deformation (dark cyan) and Maier−Saupe (magenta) orientation distribution functions for $<P_2> = 0.7$. The orientation distribution functions are normalised to peak height.

In order to quantitatively show the difference in the calculated order parameter by two presented models, we used the technique of bootstrapping to randomly sample with replacements a set of 500 azimuthal intensity profiles from each of the measured azimuthal intensity profiles. For each of the scattering images of the bionanocomposite, the sample azimuthal intensity profiles were generated with the same number of counts as the original data, as well as with reduced statistics. A Maier-Saupe and affine deformation orientation distribution function was then fitted for each azimuthal intensity profile and the mean and standard deviation values of the $<P_2>$ values were obtained and were used for the calculation of the $<P_2>$.

2.4 Results and discussion

The ESEM micrographs (figure 4.1a,b) of the Na-Alg 50 wt. % MMT film cross section reveal a layered structure and clearly show the in-plane orientation of the

MMT platelets. A photo of Na-Alg with 80 wt. % MMT bionanocomposite film, shown in figure 4.1c, displays a strikingly high light transmittance that arises from the well-aligned lamellar microstructure.

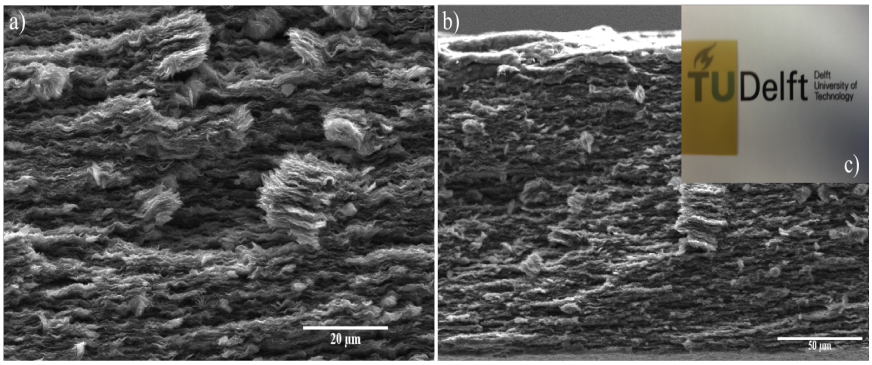

Figure 2.4: ESEM micrographs (a, b) of a cross section of an Na-Alg with 50 wt. % MMT. Inserted photo (c) of Na-Alg with 80 wt. % MMT shows high light translucency.

Another very interesting property of these bionanocomposites is that they display remarkable mechanical stiffness, even at higher MMT loadings, which is investigated in more detail in the following chapters.

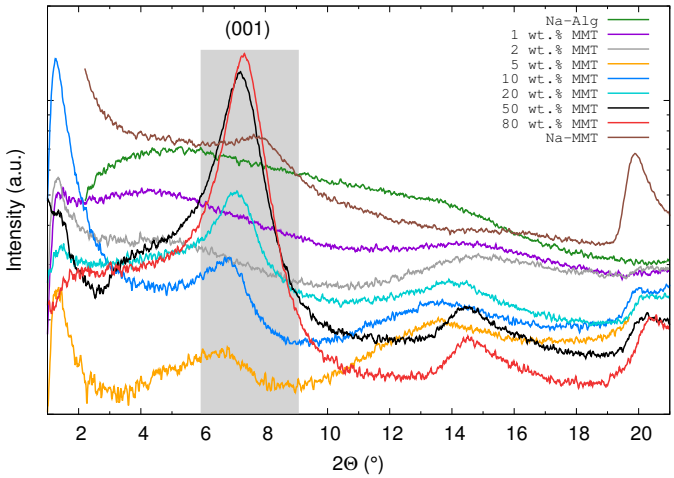

Figure 2.5: X-ray diffraction patterns of Na-Alg/MMT bionanocomposite measured parallel to the beam direction. The first appearance of a (001) reflection is noticed for 5 wt. % MMT system, and with further MMT addition the peak shifts toward higher angles, i.e., lower d-spacing.

The WAXS was used both to determine the d-spacing of MMT platelets and

to measure the order parameter. Figure 2.5 shows the radial scans of the WAXS patterns measured with the incident X-ray beam at a glancing angle parallel to the bionanocomposite film surface and the MMT powder pattern was measured with the material fixed to Scotch tape. Prior to the measurement, the bionanocomposite film samples were completely dried, while the MMT powder was kept at relative humidity (RH) of 50 % and fixed on Scotch tape. The diffractograms in figure 2.5 reveals the absence of the (001) reflection of MMT for 1 and 2 wt. % MMT in Na-Alg, which suggests an almost complete exfoliation of the MMT platelets.

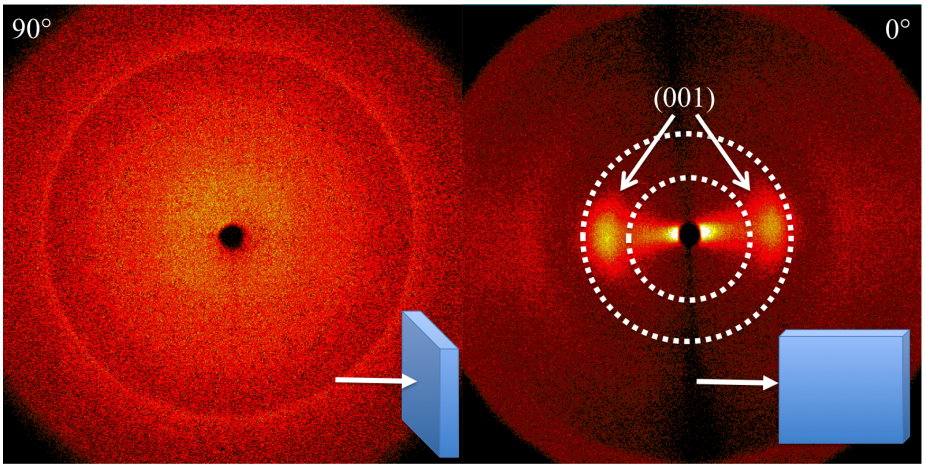

Figure 2.6: 2D scattering images of Na-Alg with 20 wt.% MMT at different beam inclinations with respect to the plane of the film (90° and 0°) where the sample−detector distance was 10 and 13 cm, respectively. The angle dependence of the (001) reflection confirms the anisotropy of the bionanocomposite.

The first appearance of the (001) reflection is visible for 5 wt. % MMT concentration, which corresponds to a d-spacing of around 15 Å, as calculated using the Bragg equation. This value is higher than the d-spacing for the monohydration layer of pure MMT (12 Å), which indicates the intercalation of Na-Alg within the MMT galleries (Watanabe & Sato, 1988). With increasing MMT concentration, the d-spacing for (001) reflection decreased down to a value of about 12 Å. These observations indicate that most of the alginate is located on the periphery of the MMT platelets and that some of it is intercalated between the galleries. The reflection at around 20° corresponds to the crystallographic planes inside the clay layer (020), and its position is independent of the (001) basal spacing.

For a quantitative determination of the average orientational order of the MMT, the bionanocomposite films were analyzed using WAXS. Samples were irradiated

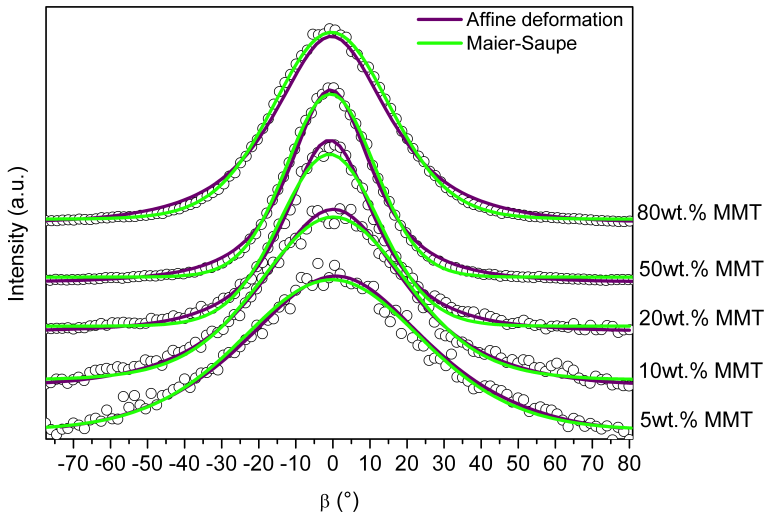

Figure 2.7: Azimuthal intensity profiles, corresponding to the (001) reflection for different MMT concentrations. The solid lines present the Maier−Saupe (magenta) and affine deformation (dark cyan) curve fits.

with the incident beam perpendicular and parallel to the film surface. In figure 2.6, the 2D scattering patterns for Na-Alg with 20 wt. % MMT show a clear angle dependence that corresponds with the anisotropy of the bionanocomposite. The presence of equatorial diffraction arcs with small azimuthal widths confirms a high preferential orientation of the MMT platelets. From figure 2.6 (0^o), the azimuthal profile of the (001) reflection was extracted for calculating the $<P_2>$. The azimuthal intensity profile was fitted to the Maier−Saupe and affine deformation orientation distribution functions for various MMT concentrations, using eqs (2.2) and (2.3). Bionanocomposite samples with 1 and 2 wt. % MMT were not used for calculating the $<P_2>$ due to absence of the (001) reflection and the lack of orientation.

From figure 2.7, we observe that both orientation distribution functions fit the azimuthal intensity profiles quite well. We notice that for the cases where the MMT concentration is lower than 50 wt. % the affine deformation model seems to fit the tails of the function more accurately than the Maier−Saupe distribution. However, for, bionanocomposites with 80 wt. % MMT the affine deformation orientation distribution function does not fit so well, and results are being closer to a Maier−Saupe-like distribution. We believe that at such high MMT concentrations in the system there is a jamming effect developing between the MMT platelets that hamper the aligning of the MMT platelets during drying, which results in a lower order parameter of the bionanocomposite.

Table 2.1: Residual Sum of Squares (RSS) Calculated for Maier−Saupe (MS) and Affine Deformation (AD)

sample	RSS (AD)	RSS (MS)
5 wt. % MMT	0.41839	0.50755
10 wt. % MMT	0.29038	0.40220
20 wt. % MMT	0.09724	0.22886
50 wt. % MMT	0.09995	0.05713
80 wt. % MMT	0.24730	0.03793

The residual sum of squares (RSS), calculated for both the Maier−Saupe (MS) and affine deformation (AD) orientational distribution functions, confirms this (see Table 2.1). This observation might be explained by the high volume fraction of the MMT platelets that introduces face−edge interactions between the platelets. These interactions may lead to gel formation at a different concentration, therefore causing a change in the ordering of the structure. The same phenomenon was observed for the calculated $<P_2>$ and the critical total solid concentration, which will be shown below.

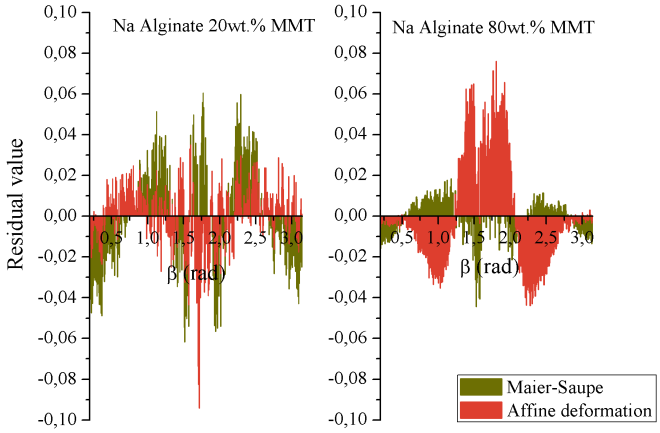

Figure 2.8: Residual plot for Maier−Saupe and affine deformation orientational distribution functions fits for Na alginate with 20 and 80 wt. % MMT bionanocomposite films.

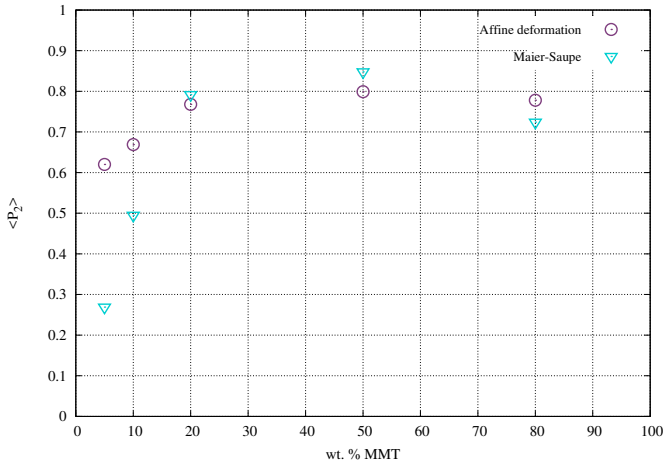

Figure 2.9: Order parameter, $<P_2>$, dependence on MMT concentration calculated using the Maier−Saupe (purple) and affine deformation (cyan) models from WAXS measurements.

The residual plots for Maier−Saupe and affine deformation fits are presented in figure 2.8. We show two cases, bionanocomposite films with 20 and 80 wt. % MMT, in which affine deformation or Maier−Saupe is favored.

From the fitted profiles we derived the width parameters, λ and a, for various MMT concentrations. These parameters were also used to calculate the $<P_2>$ values from eq 2.4. The resulting $<P_2>$ values are presented in figure 2.9. We observed remarkably high values of $<P_2>$ calculated with both models. Also noticeable is a very clear rise in $<P_2>$ values with increase with increasing MMT concentration. The highest $<P_2>$ values were observed for 50 wt. % MMT bionanocomposite, for both models.

As mentioned, the affine deformation model can also be used to determine the critical total solid concentration of the bionanocomposite suspension at which the system starts to develop a yield stress that immobilizes the MMT platelets.

In figure 2.10, by inverting the degree of compression (λ), we have determined the critical concentration of the bionanocomposite suspension for different MMT concentrations. The lowest critical total solid concentration is achieved for Na-Alg with 50 wt. % MMT, which corresponds to the highest reported $<P_2>$ value.

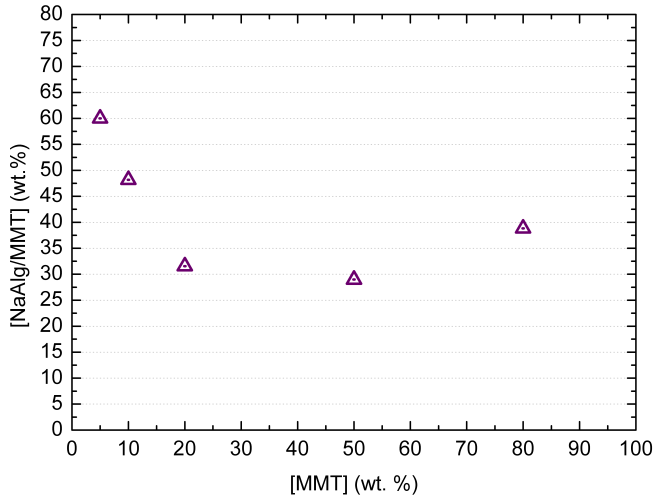

Figure 2.10: Critical total solid concentration of the bionanocomposite suspension at which the yield stress develops for various MMT concentrations calculated using the affine deformation model.

2.5 Conclusions

A highly ordered Na-Alg/MMT bionanocomposite was prepared using a simple film casting method. A highly dense and layered structure was observed on the ESEM micrographs. The orientational order of MMT platelets was measured by WAXS for various MMT concentrations. The *d*-spacing values from radial scans suggest that alginates are intercalated within the MMT galleries. High $<P_2>$ values were obtained by WAXS and calculated using the Maier−Saupe model and an affine deformation model. We conclude that the concentration dependence of $<P_2>$ values is described more accurately by the affine deformation model, in which the high alignment is a result of the vertical gel shrinkage. These results suggest that specific MMT−alginate interactions occur via the positive MMT edge and negative alginate backbone, forming a gel that immobilizes the MMT platelets. A clear increase in $<P_2>$ values was found at higher MMT concentrations, with a maximum value obtained for 50 wt. %. The $<P_2>$ for the 80 wt. % MMT bionanocomposite shows a slight decrease, which is attributed to the high volume fraction of MMT that introduces MMT−MMT interactions as well the as the MMT−alginate interactions. In addition, we used the affine deformation model to obtain the concentration of bionanocomposite suspension at which the yield stress develops immobilizing the MMT platelets. The critical concentration decreases with increasing MMT concen-

tration. In conclusion, the affine deformation model is found to be a useful tool to study the development of orientation of MMT in Na-Alg, which might be extended to other anionic polymers.

Appendix A

Under compression the orientation of the director changes as

$$tan(\beta) = \frac{1}{\lambda} tan(\beta_0) \tag{2.6}$$

where λ is degree of compression and is reversely proportional to critical total solid concentration at which yield stress immobilizes the MMT platelets. Equation 2.6 can be written as

$$\beta = tan^{-1}(\frac{1}{\lambda} tan(\beta_0)) \tag{2.7}$$

$$\beta_0 = tan^{-1}(\lambda tan(\beta)) \tag{2.8}$$

Under the change in director orientation the director density is conserved thus

$$f(\beta) dcos(\beta) = f(\beta_0) dcos(\beta_0) \tag{2.9}$$

$$f(\beta) = f(\beta_0) \frac{dcos(\beta_0)}{dcos(\beta)} \tag{2.10}$$

for the initial distribution we take the isotropic distribution $f(\beta 0) = ½$ of the MMT

$$f(\beta) = \frac{1}{2} \frac{dcos(\beta_0)}{dcos(\beta)} \tag{2.11}$$

and using relation

$$dcos(x) = -sin(x)dx = sin(x)cos^2(x)dtan(x) \tag{2.12}$$

with eq 2.11 we get

$$f(\beta) = \frac{1}{2} \frac{sin(\beta_0)cos^2(\beta_0)dtan(\beta_0)}{sin(\beta)cos^2(\beta)dtan(\beta)} \tag{2.13}$$

$$f(\beta) = \frac{1}{2}\lambda \frac{sin(\beta 0)cos^2(\beta_0)}{sin(\beta)cos^2(\beta)} \tag{2.14}$$

$$f(\beta) = \frac{1}{2}\lambda^2 \frac{cos^3(\beta_0)}{cos^3(\beta)} \tag{2.15}$$

And the final distribution of the director is found to be

$$f(\beta) = \frac{1}{2}\lambda^2 \frac{cos^3(tan^{-1}(\lambda tan(\beta)))}{cos^3(\beta)} \tag{2.16}$$

Appendix B

We used polarising optical microscopy to visualise the transition of randomly orientated to highly aligned MMT platelets in the Na-Alg/MMT bionanocomposite. For this purpose we prepared a Na-Alg/MMT (5/95) suspension and placed it on microscope slide with a cover glass placed over it. In this way we ensure that the drying of the suspension occurs on the edge of the cover glass (figure 2.11).

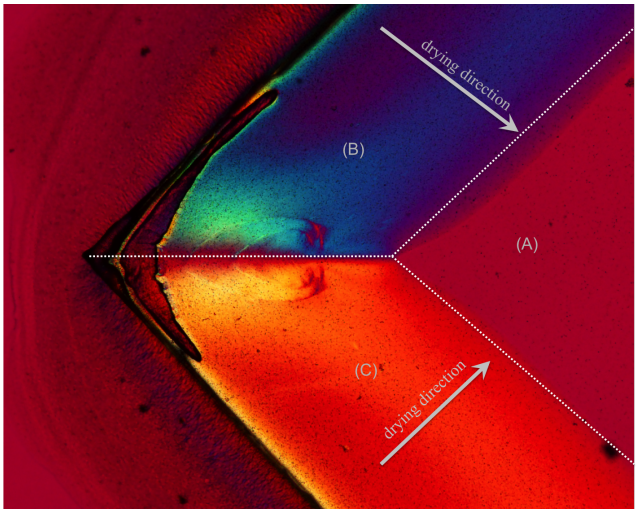

Figure 2.11: Anisotropic drying of the Na-Alg 95 wt.% MMT suspension between the microscope slide and a cover glass. (A) isotropic sample, (B) and (C) anisotropic samples perpendicular to each other.

The measurement was performed on a Nikon Eclipse E600 polarising microscope using a half-wave retardation plate. In figure 2.11 we are located on the corner edge

of the cover glass, where the system exhibits two drying directions that are perpendicular to each other. In the center of the cover slide (2.11-A) the suspension still has a randomly distributed MMT platelets, while at the edges the drying direction dictates how the system alignes (2.11-B and 2.11-C). This images confirms that the drying direction determines the alignment of the Na-Alg/MMT bionanocomposite.

Appendix C

Furthermore we have prepared the i-carrageenan with 20 wt.% MMT bionanocomposite with different starting total solid concnetrations. Iota carrageenan is a linear polysaccharide composed mainly of alternating α-1,3-D-galactose-4-sulfated and β-1,4-3,6-anhydro-D-galactose-2-sulfate groups. The i-carrageenan was used because it behaves as a thermoreversible gel, meaning that once the i-carrageenan/MMT suspension cools down to room temperature it immobilizes the MMT platelets. By doing so we can control the total strain applied on both MMT platelets and i-carrageenan during film formation (drying).

A i-carrageenan with 20 wt.% MMT was prepared by making i-carrageenan solution at 60 ^{o}C and adding exfoliated MMT suspension, with a varying total solid concentrations of the suspension (1, 3, and 5 wt.%). The suspension was poured in a petri dish and once it cooled down to room temperature, a hydrogel was formed with randomly distributed MMT platelets. The i-carrageenan/MMT bionanocomposite film was produced by further drying the hydrogel at ambient enviorment (50 % RH, 20 ^{o}C). The developed anisotropy in the bionanocomposite was measured using a WAXS with a sample-detector distance of 30 cm and an incendent beam parallel to the film surface.

In table 2.2 we have summarized the $<P_2>$ values calculated over the azimuthal intensity profile using an affine deformation ODF, and we note higher values of $<P_2>$ for the i-carrageenan/MMT system compared to Na-Alg/MMT bionanocomposites for the same MMT concentration. However we do not see the expected trend with varying the total solid content, where the highest $<P_2>$ value was for the 5 wt.% initial total solid content.

Table 2.2: Influence of the initial total solid content on the $<P_2>$ values of the i-carrageennan/MMT bionanocomposite.

total solid content [wt.%]	$<P_2>$
1	0.811
3	0.770
5	0.824

Acknowledgments

This work is part of the research program of Integral Solutions for Sustainable Construction (IS2C), which is financially supported by the Dutch National Science foundation (STW). Arjan Thijssen's assistance with ESEM measurement is acknowledged. Southern Clay Rockwood is acknowledged for supplying the Cloisite Na^+(MMT).

Chapter 3

Rheological investigation of specific interaction in Na Alginate and Na MMT suspensions[1]

Biopolymer clay nanocomposites can be produced by suspension casting, which results in a highly ordered structure. Here we report on a study of a rheological behavior of sodium alginate and montmorillonite suspension. We find that viscoelastic behavior of this suspension is dramatically affected with increasing volume fraction of montmorillonite platelets. Addition of montmorillonite generally leads to gel formation, which is attributed to interactions of montmorillonite and alginate via H-bonding and attraction between the positive edges of the platelets and the anionic backbone of the biopolymer. A critical concentration for the measured system was observed at 20 wt.% montmorillonite, where a crossover to a gel-like structure was detected. The observed gel has a rubber plateau, which develops further with higher montmorillonite concentration. In this physical gel the relaxation maximum was detected, which is associated with the breaking and reformation of the bonds between the platelets and the biopolymer. For this transient behavior, we find that a Maxwell type viscoelasticity quite well describes the relaxation time and the observed G'-G" crossover. We believe that this gel-like behavior plays an important role in formation of highly ordered nanostructures that develop during the drying of these bio-nanocomposite suspensions.

[1] J. Zlopasa, B. Norder, E.A.B. Koenders, S.J. Picken *Carbohydrate Polymers*, 151, pp 144-149

3.1 Introduction

The addition of clay platelets to polymers is a way to improve the properties of neat material, leading to a significant increase in stiffness (Young's modulus), a decreased permeability and reduced flammability (Blumstein, 1965; Kojima et al., 1993; Okada and Usuki, 1995; Messersmith and Giannelis, 1995). The reason for such material property enhancement comes from the nature of the filler, i.e. its high aspect ratio, which imposes a tortuous path to the diffusing molecules and the good interaction between the filler and the polymer (Nielsen, 1967). A variety of polymers have been used to produce such polymer clay nanocomposites (PCNs). In many systems the concentration of layered silicates rarely exceeds 5-10 wt.%, due to phase separation and loss of exfoliation. Recently, clay bio-nanocomposites have been made using biopolymers, such as chitosan, carboxymethyl cellulose, and xylogulcan. Using these biopolymers the concentration range of clay that can be successfully incorporated increases dramatically, with materials displaying unique properties, such as high level of alignment, and high volume fraction of the filler, which may result from favorable interaction between the biopolymer and the clay. All of the mentioned bio-nanocomposites have been produced via water casting of the biopolymer clay suspension (Ebina and Mizukami, 2007 and Kochumalayil et al., 2013; Yao et al., 2010; Zlopasa et al., 2015). Due to the nanostructure and the high volume fraction of the clay, these materials display superior mechanical and transport properties, when compared to conventional PCNs.

The present work is motivated by a high order parameter achieved in Na Alginate/MMT bio-nanocomposite system. Investigating the rheological behavior of the initial suspensions of the biopolymers (anionic and cationic) and clay platelets may give some answers in understanding how these nanostructures are formed. The interaction between the clay platelets and positively charged polyelectrolyte, e.g. chitosan, is likely to occur due to the electrostatic interactions between $–NH_3^+$ groups and the negatively charged sites on the clay surface, leading to a dynamic gel formation of the resulting suspension (Darder, Colilla, & Ruiz-Hitzky, 2003; Shchipunov, Ivanova, & Silant'ev, 2009). Subsequently, alignment of the montmorillonite platelets results in a nacre-like, highly ordered, microstructure that is proposed to occur via water evaporation induced self-assembly (Yao et al., 2010).

Miano et al. studied the influence of polyelectrolytes on the rheological behavior of montmorillonite suspension and found that face-edge interaction between montmorillonite platelets is inhibited by the presence of sodium polyacrylate, which is adsorbed on the edges of the clay particles (Miano and Rabaioli, 1994). Jaber et

al. measured the adsorption of negatively charged molecules on the montmorillonite platelets, where the interaction was hypothesized to occur on edges of the montmorillonite platelets via hydrogen bonding (Jaber et al., 2014).

Physical gelation occurs as a result of intermolecular association, leading to network formation. Unlike chemical bonding, where covalent attachments are typically permanent, these intermolecular associations are weak, reversible bonds or clusters produced by Van der Waals forces, electrostatic attractions, and/or hydrogen bonding (Larson, 1999).

The present work is intended to study the effect of the addition of montmorillonite platelets on the structure and rheology of Na-alginate solutions. Na-alginate is a negatively charged polyelectrolyte copolymer composed from mannuronic (M) and guluronic (G) acid. The functional properties of alginate are related to the ratio of the copolymers (M/G) and the level of block formation (Grasdalen, Larsen & Smidsrød, 1981). Alginate can be derived from brown algae, which is the main source for industrial use, and is also found in metabolic products of some bacteria, e.g. pseudomonas and azotobacter (Linker & Jones, 1966; Gorin & Spencer, 1966). Commonly, alginates are used as food additives (E400-405), gelling agents, wound dressings, membranes for curing cement-based materials, and potentially for drug delivery (Matthew et al., 1995; Laurienzo, 2010; Zlopasa, Koenders & Picken, 2014).

Na-alginate suspensions with a wide range of montmorillonite concentrations were characterized, in which a critical concentration for a gel-like behavior was measured. The intermolecular associations are hypothesized to occur between the positively charged montmorillonite edges and the negatively charged alginate backbone and/or via H-bonding. The transient behavior of the obtained bio-nanocomposite suspensions is described well by the Maxwell type viscoelasticity. The results from this study suggest that the gel-like behavior of the suspensions causes a strain-induced orientation, during drying. This leads to a formation of a highly ordered structure.

3.2 Materials and methods

Na-alginate (Na-Alg) suspensions with various concentrations of Na-montmorillonite (Na-MMT) were prepared according to the following procedure. Commercially available MMT, the apsect ratio (width/thickness) of the Cloisite is roughly 250:1, (Cloisite Na+ (MMT), Southern Clay Products Inc., Rockwood) was mixed in deionized water under vigorous stirring for 24 hours to achieve 3 wt.% exfoliated disper-

sion. During that time all of the Na-MMT was dispersed, without any remaining visual agglomerates. Na-Alg, (M/G=1.56, Mw=150 kg/mol) purchased from Sigma Aldrich was used as received. Na-Alg was dissolved using deionized water to form a 3 wt.% solution. The Na-MMT suspension was subsequently mixed with Na-Alg solution and was further mixed for 24 hours. The total solid content was kept at 3 wt.% but with different MMT concentrations, 0, 1, 5, 20, 40, 50, 60, 75, 80, 90, 95, 98, and 99 wt.% with respect to Na-Alg + Na-MMT.

The Na-Alg MMT suspensions were examined by small amplitude oscillatory shear (SAOS) experiments on a TA Instruments AR-G2 Rheometer, using parallel plate geometry with diameter of 40 mm. For each suspension, a strain sweep was performed, at the oscillatory frequency of 10 rad/s to determine the linear viscoelastic region. Frequency sweeps were performed in the linear viscoelastic region between 0.1 and 100 rad/s.

For time sweep experiment and for the dynamic oscillatory measurement at longer time scales (lower frequencies) we used a Couette geometry with stator radius 15.18 mm, rotor radius 14 mm and cylinder height 42.07 mm. The time sweep experiments were performed such that after sample loading, the samples underwent a pre-shear treatment at a shear rate of 100 s^{-1} for 120 s. All measurements were performed at 25 °C, using a solvent trap to avoid evaporation of water.

3.3 Results and discussion

For the Na-Alg solution and all the prepared suspensions, a strain sweep was performed at an oscillatory frequency of 10 rad/s to determine the linear viscoelastic region. The results are shown in figure 3.1, the pink dashed vertical lines indicate the strain used for the subsequent frequency sweeps. For Na-Alg suspension with Na-MMT concentrations higher than 40 wt.% we find that G' is higher than G", which is indicative for an elastic behavior rather than a viscous one, as is observed for the neat polymer solution and the pure Na-MMT suspension.

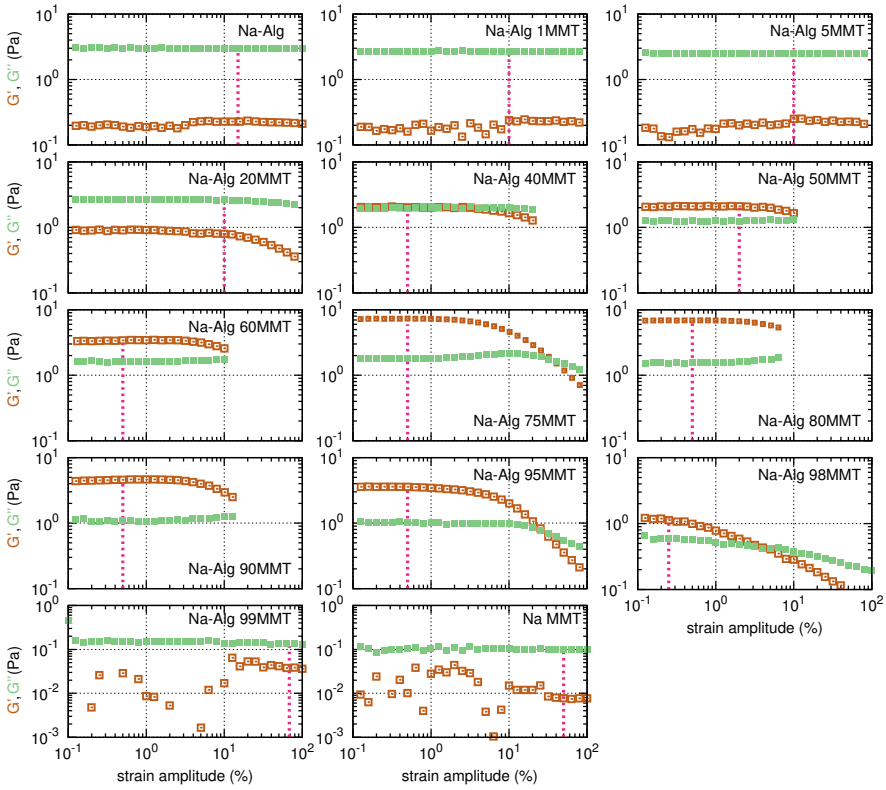

Figure 3.1: Storage (G') and loss (G") moduli, as a function of applied strain for Na-Alg solution, Na MMT and Na-Alg MMT suspension at different clay concentrations to investigate the strain independence (linear viscoelastic regime). Total solid concentration of suspensions was fixed at 3 wt.%. The measurements were performed at a frequency of 10 rad/s. The vertical lines indicate the strain used for the frequency sweep measurement. Note the different scale-bars for G' and G" in some of the figures.

A noticeable increase in G' is found upon the addition of Na-MMT platelets that at higher strains exhibits a sharp decrease, suggesting a critical strain for structure breakdown that imposes a limit of the linear regime (Ten Brinke, Bailey, Lekkerkerker & Maitland, 2007). For the Na-Alg with 99 wt.% Na-MMT we observe a similar behavior as is found for the pure Na-MMT suspension.

Figure 3.2 shows the storage and loss modulus, G' and G", of a 3 wt.% Na MMT suspension (open circles) and a 3 wt.% Na-Alg (open squares) solution as a function of angular frequency measured by parallel plate geometry. The Na-Alg solution has a liquid-like behavior showing scaling properties of approximately G'$\propto \omega^{1.5}$ and G"$\propto \omega$. The deviation from the behavior of a fully relaxed homopolymer (G'$\propto \omega^2$ and G"$\propto \omega$) might be attributed to polydispersity (Krishnamoorti, Vaia & Giannelis, 1996).

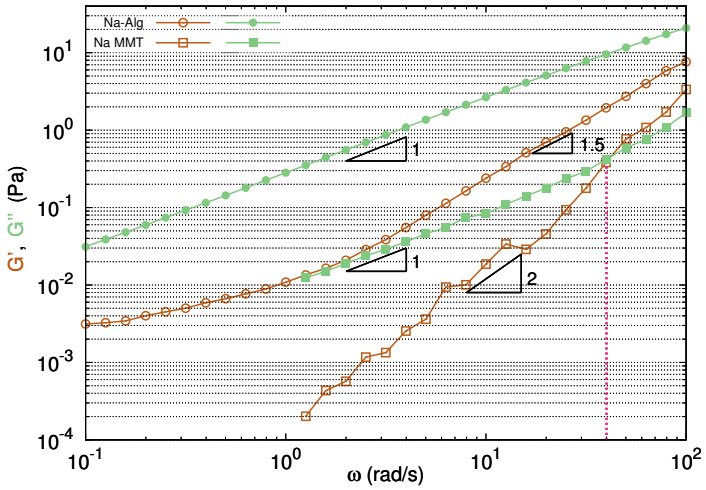

Figure 3.2: Storage (G') and loss (G") moduli of Na-Alg solution and Na-MMT suspension as a function of angular frequency. Total solid concentration of both suspension and solutions is 3 wt.%. The vertical line at 40 rad/s indicates the G'-G" crossover.

The aqueous dispersion of MMT exhibits a liquid-like behavior where the storage modulus scales with frequency as G'$\propto\omega^2$ and the loss modulus is linear in frequency G"$\propto\omega$. The 3 wt.% MMT suspension behaves as a solid at very short time scale of 0.025 s (40 rad/s crossover). This can be attributed to face-edge interaction and a formation of a transient network. Abend and Lagaly reported similar behavior of Na-MMT in this concentration range (Abend & Lagaly, 2000).

The storage and loss modulus for the Na-Alg system with 1 and 5 wt.% Na-MMT

platelets are shown as a function of angular frequency in figure 3.3. The addition of Na-MMT platelets up to 5 wt.% has little influence on the storage moduli. We still observe a liquid-like behavior of the suspension with G" values higher than the G' values at the studied frequency range.

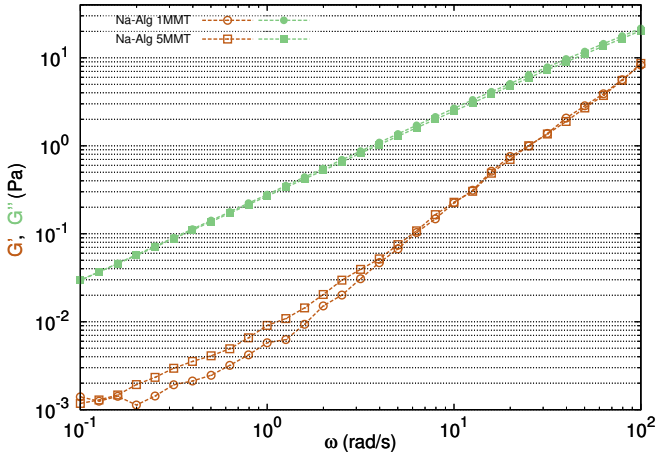

Figure 3.3: Storage (G') and loss (G") moduli of Na Alginate suspension with 1 and 5 wt.% MMT as a function of angular frequency. We observe a liquid-like behavior over the investigated timescales. Total solid content of the mixed suspension was 3 wt.%.

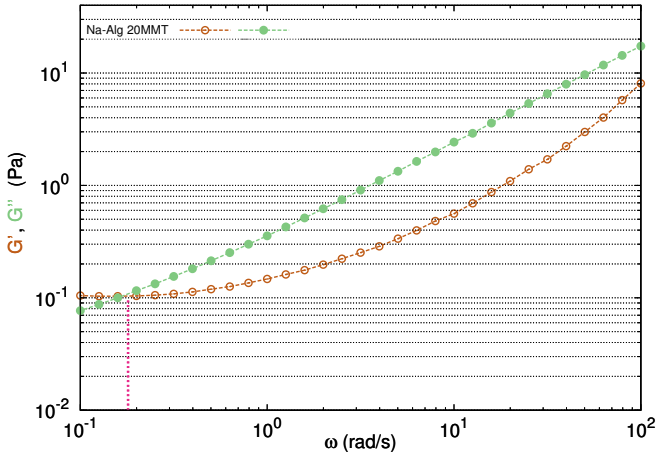

Figure 3.4: Storage (G') and loss (G") moduli as a function of angular frequency for Na-Alg suspension with 20wt.% MMT. The measured G'-G" crossover frequency is at 0.1673 rad/s.

A decrease in the terminal slope was noticed for the 5 wt.% Na-MMT compared to 1 wt.% Na-MMT that could be a result of interaction between the Na-MMT and alginate that can cause reduced mobility. We also notice that the extrapolated high frequency crossover relaxation time remains unaffected (roughly at 300 rad/s) and the high frequency regimes overlap.

With further addition of Na-MMT, at 20 wt.%, a crossover appears at lower frequencies with G' > G" and frequency independence of G', presented in figure 3.4. The corresponding frequency of the cross-over is 0.1673 rad/s. G' dominance falls in the region at large time-scales, which suggests that over longer timescales the suspension behaves like a viscoelastic soft solid as the long-range rearrangements are very slow.

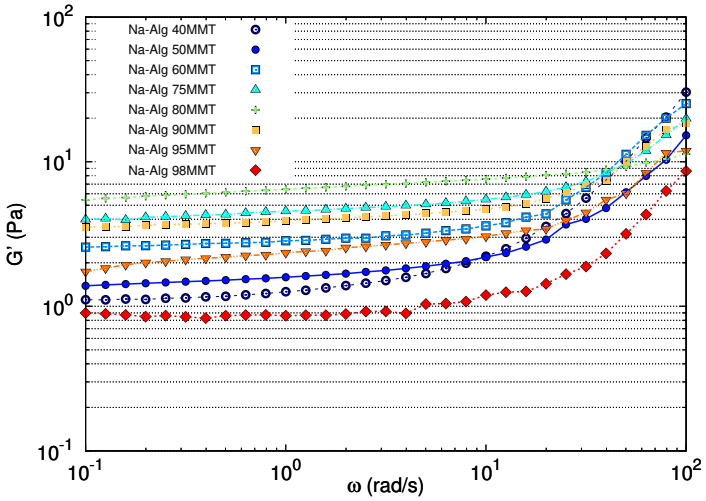

Figure 3.5: Storage moduli of Na-Alg suspension with 40, 50, 60, 75, 80, 90 and 98 wt.% MMT as a function of angular frequency. Total solid concentration is 3 wt.%.

Above the G'-G" crossover point, we have a the system has a viscous behavior, which implies that short-range rearrangements occur rapidly (Naficy et al., 2014). The reason for the crossover could be a result of an interaction between the edges of the Na-MMT platelets, which can be positively charged, and the negatively charged alginate backbone (Bradenburg & Lagaly, 1988). The Na-MMT platelets are linked to form a network structure, which can be disrupted by the flow. It is important to note that the formed cross-links appear to be transient that at rest allows the gel structure to rebuild to its initial structure.

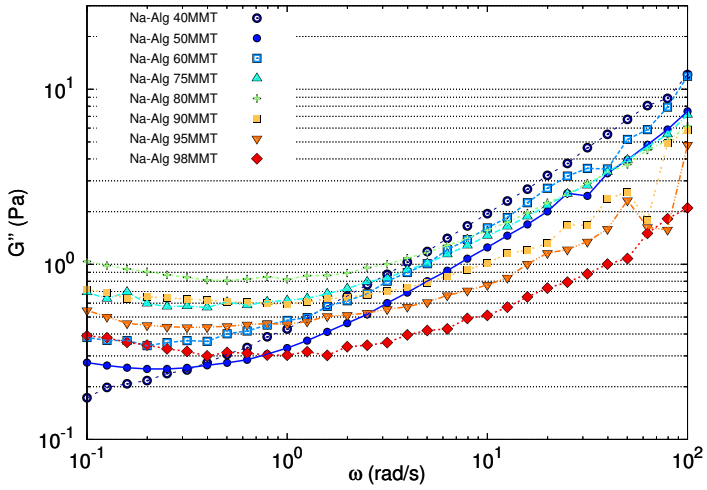

Figure 3.6: Loss moduli of Na-Alg suspension with 40, 50, 60, 75, 80, 90 and 98 wt.% MMT as a function of angular frequency. Total solid concentration is 3 wt.%.

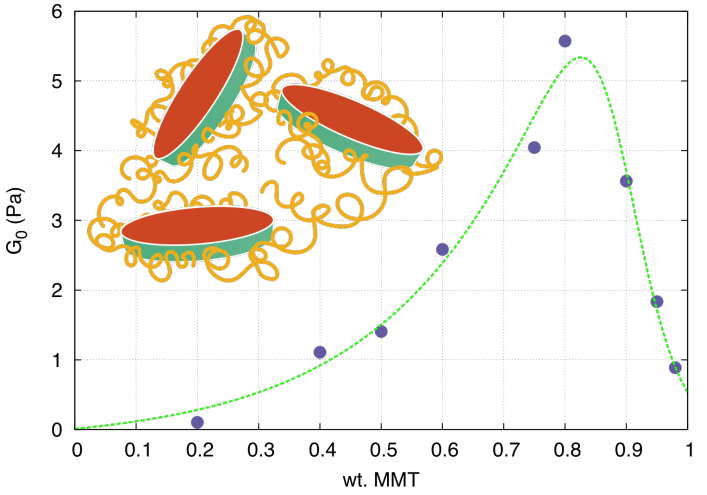

Figure 3.7: Plateau modulus G_0 of Na Alg-MMT gels measured at 0.1259 rad/s as a function of MMT concentration. The figure shows that above 20wt.% MMT we see an increase in plateau modulus with addition of MMT until 80wt.% MMT, followed by rapid decline. The lines are guides to eye. Schematic on the left of the figure is author's impression of the Na Alg-MMT network.

This is also characterized, as will be shown below, by a weak frequency dependence of the storage modulus and G' > G" over the measured frequency range,

indicating that the material behaves solid-like on the investigated time-scales. We also note that in broader terms the high frequency crossover seems to be independent of the MMT concentration up to 20 wt.%.

The frequency dependence of the storage modulus for suspensions with Na-MMT concentration above 40 wt.% up to 98 wt.% can be seen in figure 3.5. The storage modulus is greater than the loss modulus, compare Figures 3.5 and 3.6, over the entire frequency range which corresponds to a solid-like behavior, and G' is nearly frequency independent, i.e. we detect a plateau modulus. This plateau implies that for these time scales the suspension behaves as an elastic body. Aforementioned suggests the formation of an associative network, which could be attributed to the large number of connections between the polymer and the Na-MMT platelets. With further addition of Na-MMT platelets to the suspension a substantial increase in the plateau modulus is measured, suggesting that a strong reinforcement occurs in the system, in addition the plateau modulus is observed over a much larger frequency range. This plateau modulus is analogous to a classic rubber plateau.

In Figure 3.6, we observe that loss modulus, at lower frequencies, for the Na-Alg/MMT bio-nanocomposite suspensions show a distinct minimum in the loss modulus. This minimum shifts to higher frequency values with increased Na-MMT concentration. Further we observe that the minimum becomes less shallow and wider at higher volume fractions of Na-MMT platelets.

Because the interactions that form a continuous network are of a transient nature (physical cross-links), a structural relaxation that is characterized by a G'-G" crossover and G">G', is expected to occur at much longer timescales than measured here. This means that a maximum in viscous dissipation will be present at lower frequencies and will be followed by a decrease in the storage modulus, so that relaxation will take place and the suspension will start to flow (Te Nijenhuis, 2007). The relaxation can be attributed to the breaking and reforming of the transient MMT-alginate bonding. Such behavior is, as mentioned, characteristic for physical gels where the continuous network is portrayed by reversible links formed from temporary associations between the chains.

The measured values of plateau modulus, at 0.1259 rad/s, are presented in figure 3.7, were we observe that the associative network is formed at 20 wt.% Na-MMT and the measured values of the plateau modulus reach its peak at around 80 wt.% Na-MMT. Subsequently, by further addition of the Na-MMT we detect a rapid decline in the plateau modulus, which could be related to the formation of fewer bonds in the network with the decrease in concentration of Na-Alg.

In figure 3.8 we see that the Na-Alg with 99 wt. % Na-MMT behaves similarly to pure Na-MMT suspension, as seen in figure 3.2. We observe that a small addition of Na-Alg increases the viscous component of the Na-MMT suspension. Such behavior might be explained by the alginate adsorption around the edges of the MMT platelets, which inhibits the face-edge interactions between the platelets. Also, as a result of the low alginate concentration no entanglement and bridging occurs that could give rise to an elastic component in the rheology of the system.

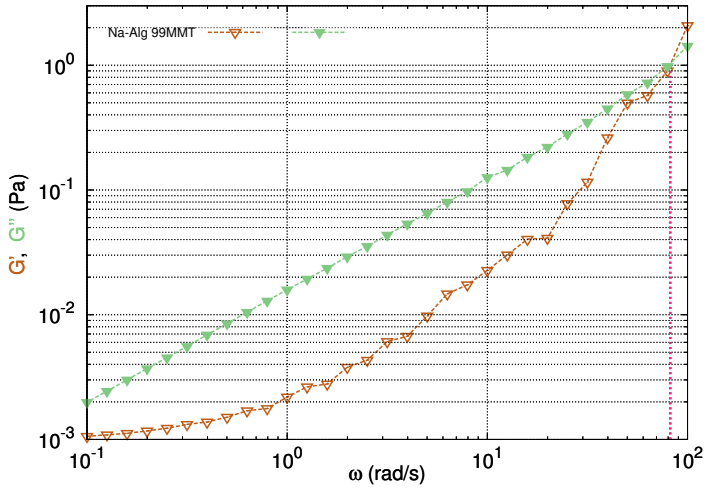

Figure 3.8: Storage (G') and loss (G") moduli for Na Alginate suspensions with 99 wt.% MMT as a function of angular frequency. The vertical line indicates a G'-G" crossover.

Figure 3.9 shows the result of a time sweep experiment at 2 % strain amplitude and 10 rad/s angular frequency at 25 °C, during which the kinetic evolution of the network during crosslinking of alginate with MMT platelets was monitored. Time sweep oscillation experiments were used to characterize the formation of a physical network for a Na-Alg suspension with 70 wt.% Na-MMT by measuring G' and G" recovery as a function of time.

After the gel formation is complete, the G' values should reach a constant value. Initial gelation was unfortunately not measurable due the rather fast kinetics of the gel formation. Since this is a physical gel with dynamic bonds we applied a shear rate of 100 s^{-1} for 120 s to break the gel, and measured the time it needed to rebuild the network. The measured gelation time is estimated by taking the crossover point of G' and G" at 10 rad/s, which marks a transition from liquid-like to solid-like behavior. We performed the measurement two times on the same sample and

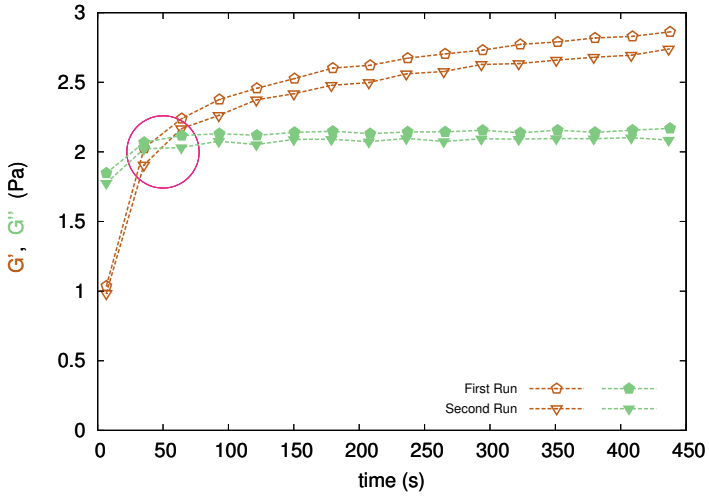

Figure 3.9: Evolution of storage (G') and loss (G") moduli over time for Na-Alg with 70wt.% MMT suspension measured at 10rad/s. Before each time sweep measurement a preshear of 100 s-1 for 120 s was performed on the suspension. Total solid concentration is 3 wt.%.

measured the crossover point to be 43 and 49 seconds for the first and the second run, respectively. We also note that there is an orientation induced reduction in the viscous component, G", which has a fast recovery, while intriguingly the network recovery of the elastic component, G', seems to be much slower.

Furthermore, we measured the viscoelastic response of the bio-nanocomposite suspension at longer time-scales. In figure 3.10, we measured the relaxation that is characterized by a peak in viscous dissipation at a value of around 6.8E-3 rad/s. The storage modulus is nearly constant over a large frequency range, corresponding to an elastic, solid-like response. The G'-G" crossover at very low frequencies is also visible, which implies a viscoelastic response with a finite relaxation time. This system shows a viscoelastic response, with an elastic behavior at the short timescales domain, and viscous behavior at larger timescales. The structural implications of the relaxation observed at very low frequency (G" maximum) is that the MMT platelets are not permanently attached to the polymer, but rather that there is a very slow dynamic (transient) cross-link. To investigate the long relaxation times associated with interaction of the MMT platelets with the alginate backbone the frequency sweep results, of Na-Alg 70wt.% Na-MMT, were fitted to a 2-mode Maxwell model (Ferry, 1980), see equation 3.1 and 3.2:

$$G'(\omega) = \frac{G_{P_1}\omega^2\tau_{R_1}^2}{1+\omega^2\tau_{R_1}^2} + \frac{G_{P_2}\omega^2\tau_{R_2}^2}{1+\omega^2\tau_{R_2}^2} \tag{3.1}$$

$$G''(\omega) = \frac{G_{P_1}\omega\tau_{R_1}}{1+\omega\tau_{R_1}} + \frac{G_{P_2}\omega\tau_{R_2}}{1+\omega\tau_{R_2}} \tag{3.2}$$

where, G_{P_1} and G_{P_2} are the shear moduli, τ_{R_1} and τ_{R_2} the specific times of the relaxations and ω is the angular frequency. This Maxwell-like viscoelastic model with two relaxation times fits the experimental results reasonably well.

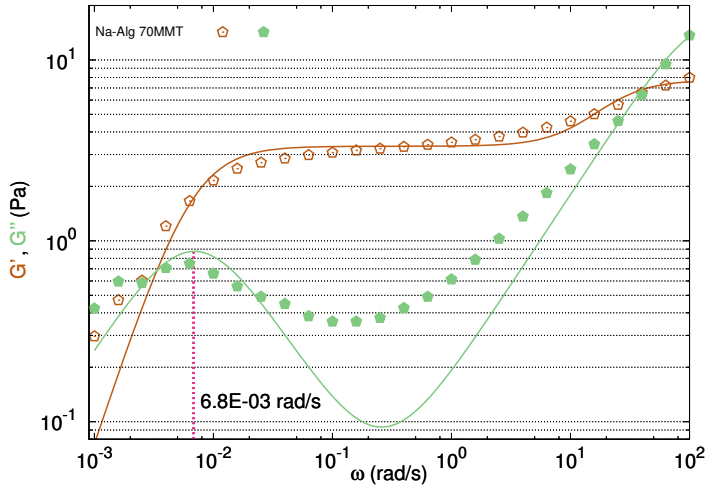

Figure 3.10: Storage (G') and loss (G") moduli as a function of angular frequency for Na-Alg suspension with 70 wt.% MMT over a longer timescale. The solid lines present the results of a dual-τ Maxwell model, see equations 3.1 and 3.2.

We also used a startup shear measurement to examine the nonlinear response of Na-Alg system with 70 wt.% Na-MMT. At shear rates higher than 0.01 s^{-1}, the system displays a stress overshoot at a critical strain before reaching steady state. Since we started from the same initial structure the increase in the stress overshoot with increasing shear rate reflects both the elastic response and the breakdown and rearrangement of the structure under flow. In broad terms, this is in agreement with the observed low frequency network dynamics at about 5E-3 rad/s, shown in figure 3.11.

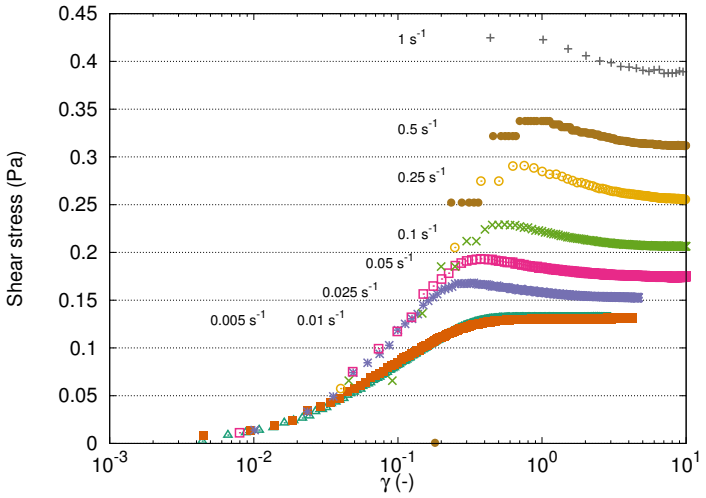

Figure 3.11: Stress-strain curves of a startup at various shear rates from 0.005 to 1 s^{-1} for Na-Alg suspension with 70 wt.% MMT. The stress over-shoot varies with the applied shear rates.

3.4 Conclusions

The viscoelastic properties of Na-Alg/MMT suspensions have been studied using dynamic and steady shear rheology to investigate specific interactions between the MMT platelets and the alginate polymer. The systems were observed to form a physical gel above a critical Na-MMT concentration, which in this study was 20 wt.%. The results indicate that alginate and MMT platelets form a three dimensional structure that forms as a result of specific interactions. These interactions are a result of attraction between the negatively charged alginate backbone with the positively charged MMT edges, possibly assisted by hydrogen bonding. We find an increase in the elasticity of the gel structure by addition of the Na-MMT platelets up to 80 wt.% Na-MMT, which we believe to be due to an increased level of interaction in the gel network. This gel formation, we propose, is responsible for the later development of the highly ordered nanostructure, which is achieved during water evaporation, as reported previously (Zlopasa et al., 2015).

We also observed that the Na-Alg with 99 wt.% Na-MMT behaves similarly to the pure Na-MMT system, where we find an increase in the viscous component for the 99 wt.% Na-MMT. This suggests that the alginate decorates the MMT platelets and thus reduces the face-edge interactions. A dynamic oscillatory measurement was performed for Na-Alg suspension with 70 wt.% Na-MMT over longer time scales,

and a relaxation time associated with the transient bonds of the physical gel occurs after which the suspension started to flow. The dual-mode Maxwell model that could be fitted to the experimental results seems to describe the relaxation of the MMT-alginate bond reasonably well.

A time sweep at fixed frequency was performed to investigate the microstructure recovery after breakdown due to high shear. We find that the structure reforms quite quickly (gel time around 40 s) indicating a transient bonding of the suspension, in agreement with the SAOS results.

Acknowledgments

The authors like to acknowledge the Dutch National Science foundation STW. The research conducted within this project is financed by STW as a part of the IS2C program (www.is2c.nl), number 10962.

Chapter 4

Mechanical properties of Na Alginate/Na MMT bionanocomposite: influence of orientation and MMT concentration

Self-supporting bionanocomposite films based on sodium alginate with wide range of montmorillonite concentration were successfully prepared by suspension casting. The obtained bionanocomposite displays a highly aligned structure where the order parameter has a dependence on the MMT concentration. In order to investigate the influence of unidirectional ordering of MMT on the mechanical properties of the bionanocomposite films we have analyzed the bionanocomposite films with dynamic mechanical thermal analysis, DMTA. The bionanocomposite films display a "brick-and-mortar" structure that is reflected with exceptional mechanical properties, which shows a MMT concentration dependence. To better understand the influence of the MMT addition on the mechanical properties, we used a conventional composite theory taking in consideration individual contributions of the filler, such as the level of alignment, aspect ratio, volume fraction, and the modulus of the MMT platelets.

4.1 Introduction

Bionanocomposites that combine biopolymers (e.g. polysaccharides) and layered silicates are getting more attention in the field of materials research. It is known for some time that the addition of layered silicates enhances the material properties such as permeability and stiffness, and results in reduced flammability (Blumstein 1965, Messersmith & Giannelis 1995, Okada & Usuki 1995, Fornes & Paul 2003). But unlike most conventional polymer clay nanocomposites (PCNs), in which the clay concentration rarely exceeds 10 wt.% due to poor dispersion, biopolymers display a remarkable nanostructural order and dispersion with clay concentration up to 90 wt.% (Ebina & Mizukami 2007). The reasons for such high affinity between clay and biopolymers are still not fully understood, yet the obtained bionanocomposites exhibit a highly ordered structure of the clay platelets that is reflected in superior mechanical, transport, and flame retardant properties.

Most reports compare the properties and the hierarchical structure of these materials to the ones found in nature, more specifically to nacre, where $CaCO_3$ bricks form an ordered brick-mortar arrangement within the biopolymer matrix (Tang et al. 2003, Munch et al. 2008, Walther et al. 2010). Such arrangement results in anisotropic properties of the composite, with the strength and stiffness of the bionanocomposite higher in the longitudinal than in the transverse direction. Furthermore, high stiffness and aspect ratio of the filler will impose tortuoisity to crack propagation and diffusion of molecules, making them go around the platelets instead through them (Liu et al. 2004).

The bionanocomposites we refer to are obtained by simply mixing completely exfoliated clay suspension and biopolymer solution that is followed by vacuum assisted self-assembly, doctor blading or solvent casting (Ebina & Mizukami 2007, Walther et al. 2010, Yao et al. 2010). We have found that the charge of the polysaccharides does not play a major role, since we find reports of highly ordered bionanocomposites from both positively and negatively charged polysaccharides with negatively charged clay platelets (Zlopasa et al. 2015). In Chapter 2, we have presented two plausible explanations why the Na-Alg/MMT system achieves high orientation, where 2D WAXS measurement of the bionanocomposite films revealed a MMT concentration dependence on the level of alignment. Furthermore, the order parameter $<P_2>$ was calculated using two models, the Maier-Saupe and the affine deformation model that describe the high orientation as a result of liquid crystal-like spontaneous self-assembly or by vertical shrinkage of a suspension that has a sufficient yield stress to immobilize the MMT platelets during drying, respectively. Moreover in Chap-

ter 3, we have probed the viscoelastic behaviour of the Na-Alg/MMT suspension and measured a solid-like response, which could be a result of specific interactions, *e.g.* positive clay edge-negative alginate backbone and/or H-bonding.This means that the stiffness of the Na-Alg/MMT gel will increase while the water evaporates during film formation and if the relaxation timescale is longer than water evaporation timescale a highly aligned bionanocomposite structure. This also means that the measured solid-like behaviour of the Na-Alg/MMT suspension excludes a self-assembly induced orientation of the Na-Alg/MMT bionanocomposite.

The present work is motivated by impressively good compatibility, of negatively charged polymer and filler, and the facile production of Na-Alg MMT bionanocomposite, resulting in the highly ordered, nacre-like, material. In this chapter we report on the mechanical properties of the Na-Alg/MMT bionanocomposites, where we look at the interplay of the order parameter, MMT loading, and the aspect ratio of the MMT platelets on the stiffness of the Na-Alg/MMT bionanocomposite.

4.2 Materials and methods

Sodium Alginate (Na-Alg) with an average molecular mass of approximate 150 000 g/mol and a M/G ratio of 1.56 was purchased from Sigma Aldrich and was used as received. Commercially available Sodium Montmorillonite, Cloisite Na+ (MMT), was kindly provided from Southern Clay Products Inc., Rockwood. To achieve completely exfoliated suspension, a 3 wt.% MMT suspension was prepared by dispersion in deionized water under vigorous stirring for 24 h. The 3wt.% suspension was added to 3 wt.% Na-Alg solution in various ratios to achieve different MMT loadings of the final films.

The bionanocomposite films were prepared by casting a Na-Alg MMT suspension on a plastic petri dish and allowing it to dry in ambient conditions (50 % RH, 20 °C). The final film thickness was around 100 μm. The bionanocomposite films were vacuum dried at 40 °C and kept in a desiccator prior to any measurements.

Wide Angle X-ray Scattering (WAXS) was collected on a Bruker AXS D8 Discover X-ray diffractometer with a Hi-Star 2D detector and using Cu Kα radiation filtered by cross-coupled Göbel mirrors at 40 kV and 40 mA. The sample−detector distance was 10 and 13 cm for parallel and perpendicular to the film surface, respectively.

Environmental Scanning Electron Microscope (ESEM), Philips XL30 Series ESEM, was used to examine the morphology of the bionanocomposite films. Prior to ESEM

investigation the films were coated with graphite using a Leica EM CED030 sputter coater.

To measure thermal behavior and the exact MMT loading Thermogravimetric Analysis (TGA) was carried out on a PerkinElmer TGA 7. The measurement were performed on samples of about 5 mg, placed in a corundum crucible, from 25 – 1000 °C at a heating rate of 10 °C/min, under nitrogen atmosphere, with an isothermal step at 1000 °C for 20 min.

Dynamic Mechanical Thermal Analysis (DMTA) was performed on a PerkinElmer DMA-7e. DMTA experiments on the Na-Alg MMT bionanocomposites were performed in a tensile mode at a frequency of 1 Hz from -50 to 200 °C temperature range at a heat rate of 2.5 °C/min, with film dimensions of 20.0x3.0x0.1 mm.

4.3 Results and discussion

Na-Alg/MMT bionanocomposite exhibits a high in-plane orientation of the MMT platelets, which was examined both by ESEM and WAXS measurements. Investigation of the bionanocomposite cross-section reveals a highly order, nacre-like structure, in which the MMT platelets are oriented perpendicular to the direction of drying, figure 4.1.

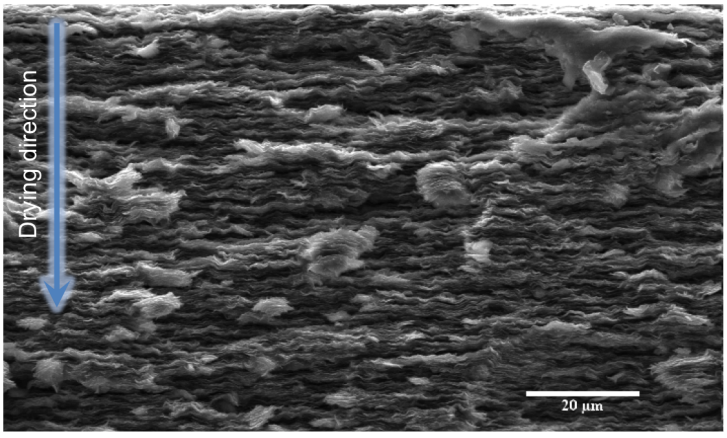

Figure 4.1: ESEM micrograph of Na-Alg 50wt.% MMT bionanocomposite cross-section.

We hypothesize that this is due to interaction of the MMT platelets and the Na-Alg, which during drying develops a yield stress and immobilizes the MMT platelets that are randomly dispersed and further drying forces the platelets to orientate. (Zlopasa et al., 2015, Zlopasa et al., 2016)

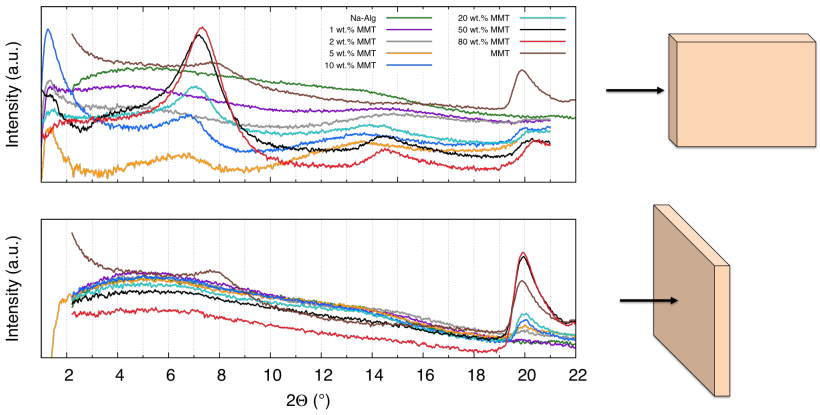

Figure 4.2: Radial scans of the WAXS data obtained for Na-Alg MMT bionanocomposites measured with an incident beam direction parallel (top) and perpendicular (bottom) to the surface of the films. Na MMT powder mounted on a scotch tape and measured perpendicular to the incident beam direction.

The radial scans presented in Figure 4.2 show that the Na-Alg MMT bionanocomposite samples exhibit anisotropic behavior. Measuring the samples with an incident beam parallel to the film surface reveal (001) of the MMT platelets, which is not present in the measurement with incident beam perpendicular to the film surface. The measured d-spacing of the (001) reflection indicates that the majority of Na-Alg is on the periphery of the platelets, which favors the hypothesis of adsorption of negatively charged alginate coil to the positively charged MMT edges and thus decorating the MMT platelets. We also note that the anisotropy of the bionanocomposite also had an influence on the relative diffraction intensity of the (001) reflection, resulting in higher values for 50 and 80 wt.% MMT than for the randomly dispersed MMT platelets as a result of preferred orientation.

The thermal stability and degradation behavior of Na-Alg and Na-Alg MMT bionanocomposite was followed by TGA at constant heat rate (10 °C/min) under inert conditions (N_2 atmosphere). The first mass loss is depicted in a temperature range from 80-150 °C, and is ascribed to removal of free and physically bound water. The second mass loss represents the main pyrolysis of Na-Alg, resulting in the decarboxylation of the alginate chains. This mass loss starts at around 200 °C and stretches until 325 °C, with the main peak at 250 °C for pristine Na-Alg. We notice that the onset temperature of the initial thermal decomposition of the Na-Alg in bionanocomposite has moved to a lower value than that of the pristine Na-Alg. But there is no clear trend, which could arise from the sample geometry,

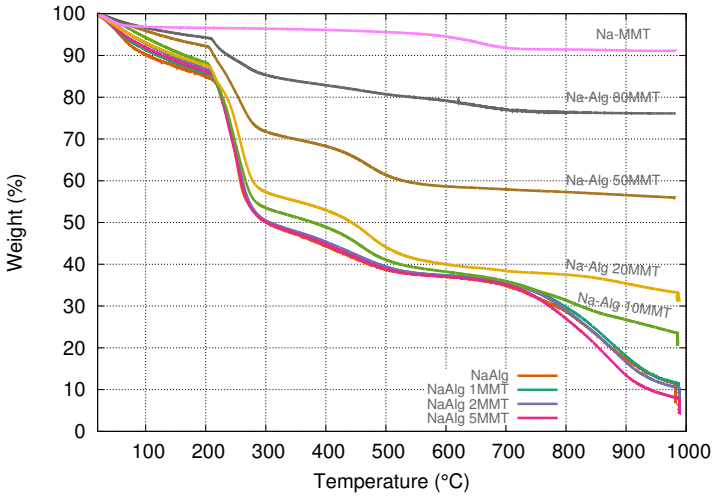

Figure 4.3: Thermogravimetry curves of Na-Alg and Na-Alg MMT bionanocomposite at 10 °C/min in nitrogen atmosphere.

the thickness was roughly the same while the snippets of the samples might deviate. From these results it is difficult to clearly claim the causes for the deviation of the onset temperature, other authors showed similar trends but have not addressed them, mostly due to sample geometry, but also as a result of the sample morphology, more specifically the effective MMT aspect ratio, and the order parameter.

The thermal response of the MMT was followed under the same temperature program as for the Na-Alg and Na-Alg/MMT bionanocomposite, which was later used to correct for the actual mass fraction of the MMT in the bionanocomposite. We observe two major mass losses, first in the temperature range of 60-110 °C, which is attributed to release of free and physically bound water, while the second mass loss, from 550-650 °C, which we believe is a result of dehydroxylation of the clay surface.

We have further looked at the derivative of a thermogravimetry, dTGA, in the temperature range of initial thermal decomposition, which for pristine Na-Alg sample shows an overlapping reaction, with a clear peak at 250 °C and a slight shoulder at 235 °C. This shoulder peak gets resolved when we follow the thermal decomposition of the bionanocomposite and two-step decomposition becomes more clear. Like for the onset temperature, we see that both peaks are shifting with different MMT concentration, and for the same reasons mentioned above we cannot clearly correlate this to a specific parameter (property) in the bionanocomposite. On the other

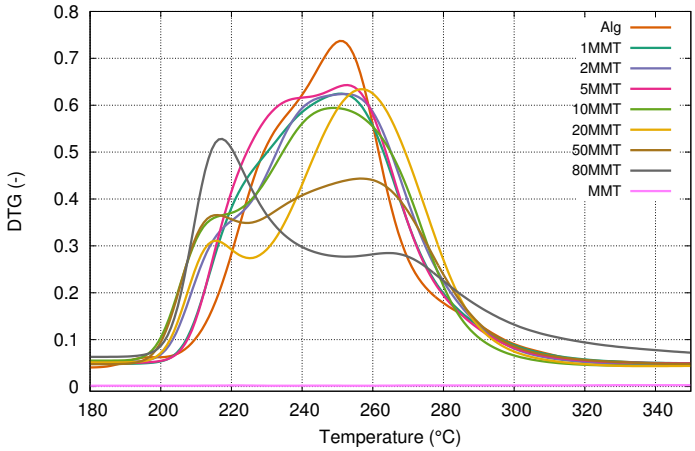

Figure 4.4: dTGA curves of pristine Na-Alg, MMT, and Na-Alg MMT bionanocomposite.

hand the peak height, the rate of the thermal degradation, shows a clear decrease with an increase in MMT concentration in the bionanocomposite. The decrease in the rate of the thermal degradation goes along with the highly ordered structure presented in figure 4.1, which acts as a thermal insulator by introducing abrupt interfaces (Losego *et al.,* 2012, Losego *et al.,* 2013).

The storage modulus over a wide temperature range for Na-Alg and Na-Alg/MMT bionanocomposites are reported in Figure 4.5. Firstly, we take a look at the pristine Na-Alg that has a very high storage modulus (10 GPa @ 20 °C) itself, which is originating from a rigid linear backbone and functional groups on the chain, e.g. electrostatic interactions. The glass transition of Na-Alg is reported to be at around 180 °C, but could not be clearly depicted, due to the overlapping with thermal decomposition of Na-Alg (Russo *et al.*, 2007). We observe a clear increase in storage modulus with the addition of MMT platelets, this increase reaches its maximum at 50 wt.% MMT, after which we see a slight decrease for 80 wt.% MMT bionanocomposite. Also, it is worth pointing out that both Na-Alg and Na-Alg/MMT bionanocomposites display a high heat distortion temperature at around 200 °C, while for the Na-Alg 80 wt.% MMT bionanocomposite has a heat distortion temperature higher than 240 °C.

As the samples go through a simultaneous glass transition and thermal decomposition (see TGA curve, figure 4.3) with onset temperature at around 180 °C, and as expected the films break. On the other hand Na-Alg/MMT bionanocomposites with high MMT content (>50 wt.%, but we also saw it for some samples with 10 and

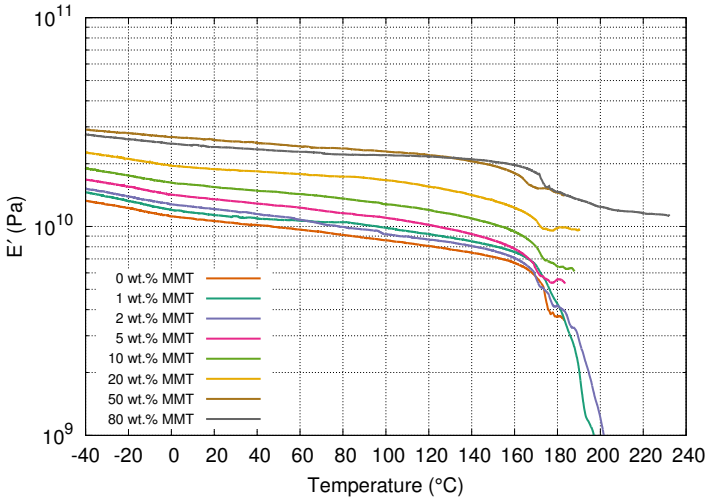

Figure 4.5: Measured dynamic storage modulus of Na-Alg/MMT nanocomposites with weight fractions of MMT up to 80wt.%

20 wt.% MMT) while going through thermal decompositions starts to sinter with the MMT platelets, which is reflected in the plateau values of the storage modulus. We believe that this is due to the formation of caramelised/MMT nanocomposite, which is a result of a very low oxygen diffusion of the sample, which means that the samples are burned under oxygen limiting atmosphere. This gives an interesting functionality to the bionanocomposite, as it can withstand high temperatures making it potentially a very attractive material for fireproofing. We note that the storage modulus values of the sintered Na-Alg 80 wt.% MMT bionanocomposite is around 10 GPa, which is especially intriguing for a sample where polymer matrix is totally decomposed.

Furthermore, we have used the Halpin-Tsai model to interpret the mechanical properties of the Na-Alg/MMT bionanocomposite. The Halpin-Tsai model, eq 4.1, was originally derived to describe the mechanical properties of semi-crystalline polymers (also falls in nanocomposite definition), and it is widely used to estimate reinforcement effects of fillers in composites such as fibre-reinforced composites, as well as polymer clay nanocomposites (Halpin & Kardos 1976.).

$$E_c = E_m \frac{E_f(1+\zeta\varphi_f) + E_m(\zeta - \zeta\varphi_f)}{E_f(1-\varphi_f) + E_m(\zeta + \varphi_f)} \tag{4.1}$$

in which E_c, E_m, $E_f$are the moduli values of the Na-Alg/MMT bionanocompos-

ite and pristine Na-Alg, respectively, Φ_f is the volume fraction of MMT, and ζ is a shape factor of the filler, which depends on the geometry, orientation and the aspect ratio of the filler.

The volume fraction of the MMT was determined from the weight fraction, w(MMT) obtained from TGA:

$$\Phi_f = \frac{\rho(Alg) \cdot w(MMT)}{\rho(MMT) \cdot w(Alg) + \rho(Alg) \cdot w(MMT)} \tag{4.2}$$

where the *ρ(MMT)* is the density of MMT, *ρ(Alg)* is the density of Na-Alg, *w(Alg)* is the weight fraction of Na-Alg.

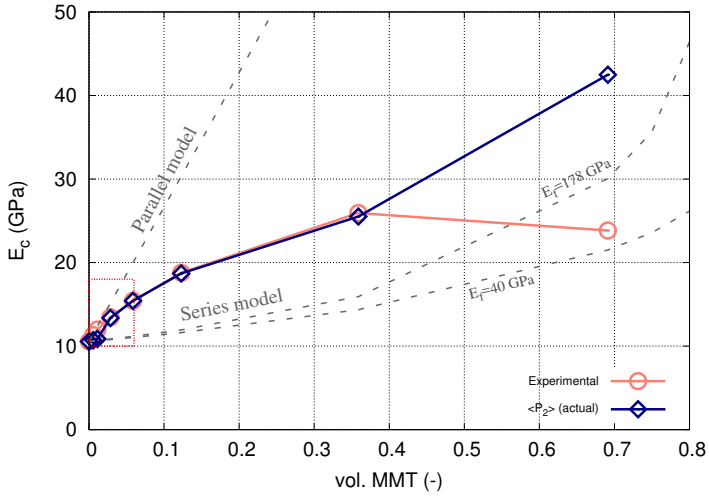

Figure 4.6: Storage modulus of Na-Alg/MMT bionanocomposites with highly aligned MMT platelets. Red rectangle is a guide for a typical concentration range of the filler for conventional PCNs.

From equation 4.1, considering the shape factor of the filler, we can see that in the case when the aspect ratio of the filler is much smaller than the modulus ratio of the filler and polymer matrix ($\zeta << E_c/E_m$), the Halpin-Tsai model converges to a series model:

$$E_c = \left(\frac{1 - \Phi_f}{E_m} + \frac{\Phi_f}{E_f} \right)^{-1} \tag{4.3}$$

In the case when the aspect ratio of the filler is much higher than the modulus of the filler and the polymer matrix ($\zeta >> E_c/E_m$), the Halpin-Tsai model converges to a parallel model:

$$E_c = (1 - \Phi_f)E_m + \Phi_f E_f \tag{4.4}$$

For the bionanocomposite with layered silicates with high aspect ratio, the series model underestimates the modulus of the bionanocomposite. While the parallel model overestimates the modulus, since it assumes a continuous phase for the reinforcement (MMT). Parallel and series model give good boundary conditions when describing the bionanocomposites, since realistically the effective aspect ratio is expected to be roughly the same as the ratio of the filler and polymer matrix modulus. This is especially true for very high MMT loadings, where we expect some restacking to occur, effectively reducing the aspect ratio of the filler.

The value for the E_f is assumed to be 172 GPa, a value that has been previously reported for perfect mica crystal (Shell & Ivey, 1989). In this way we can calculate the effective modulus for perfectly and randomly orientated MMT, since we have previously calculated order parameter for each MMT concentration, we can correct the values for calculated orientation for each bionanocomposite.

$$E_c = \left(\frac{< P_2 >}{E_{\|}} + \frac{1 - < P_2 >}{E_{\perp}} \right)^{-1} \tag{4.5}$$

where $E_{\|}$ and $E_{\perp}$ are tensile moduli of platelet reinforced composite in the radial direction of the platelets and perpendicular to the platelets, respectively. For this Van Es previously derived the shape factors for $E_{\|}$*(ζ=2/3*(L/D))* and for $E_{\perp}$ *(ζ=2)* *(*Van Es, 2001*).* Here we use the <P_2> values (Chapter 2) of MMT platelets in the bionanocomposite calculated from the azimuthal intensity profile derived from the WAXS measurements and fitted with the affine deformation model.

For a better illustration of the effect that the MMT concentration has on the stiffness of the bionanocomposite films, see figure 4.6, we have displayed storage modulus values at 20 °C. The results of the parallel and series model are also presented in figure 4.6 to illustrate the boundary conditions for the investigated system. As mentioned above, the bionanocomposite system shows a clear increase in the storage modulus with increasing MMT loading, with a maximum at 50 wt.% MMT loading that is followed by a slight decrease in the stiffness with 80 wt.% MMT. The measured decrease in the stiffness of the 80 wt.% MMT bionanocomposite might be caused by the stacking of the MMT platelets and a decrease of the effective aspect ratio of the filler. This results in overestimation of the stiffness of the 80 wt.% MMT by the Halpin-Tsai model, compared to experimentally measured ones.

Since the stiffness of the Na-Alg/MMT bionanocomposite, Na-Alg, and MMT

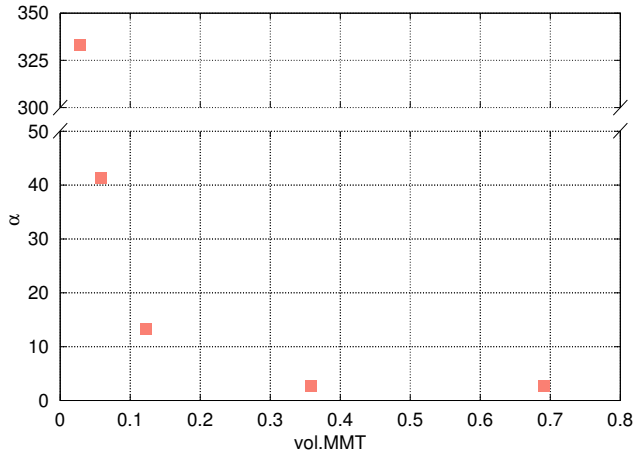

Figure 4.7: Back-calculated effective aspect ratio as a function of MMT concentration from the mechanical measurements using a Halpin-Tsai model

are known, we can use the Halpin-Tsai model to back calculate the effective aspect ratio of the platelets for different MMT concentrations.

In figure 4.7 the results of the calculated effective aspect ratio are presented, and we can see a decrease in the effective aspect ratio with increase in MMT content, which can be explained by the restacking of the MMT platelets.

We note that the effective aspect ratio for the bionanocomposites with 50 and 80 wt.% MMT seem to be underestimated, which could be due to other factors influencing the stiffness of the sample, e.g. MMT-MMT interactions and/or free volume increase (Das *et al.,* 2013, Choudalakis *et al.*, 2011). As we saw in figure 4.5, the Na-Alg/MMT bionanocomposites with high MMT content, after the initial thermal degradation, appear to go through a sintering of Na-Alg and MMT with relatively no dimension changes and considerable stiffness. In figure 4.8, we see the cross-section of Na-Alg 80 wt.% MMT bionanocomposite pyrolised at 1000 °C, which shows that the highly ordered structure remains relatively intact, we notice a slight expansion of the structure that is attributed to gases (CO_2, CO, and H_2O) leaving the structure.

Furthermore we have expolored how the Na-Alg 80 wt.% MMT bionanocomposite performs when exposed to a flame, and we observe in figure 4.9 no melting or flaming of material, as well as no smoke production. This property of the material directly arrises from the highly ordered structure of the bionanocomposite, lowering oxygen diffusivity making the material self-extinguishing. Considering that most

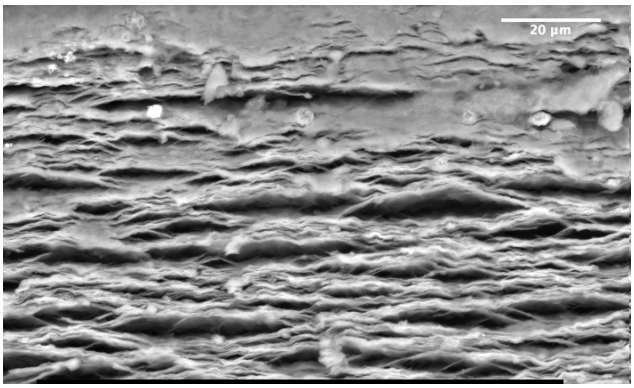

Figure 4.8: ESEM micrographs of Na-Alg 80wt.% MMT bionanocomposite cross-section after pyrolysis at 1000 °C.

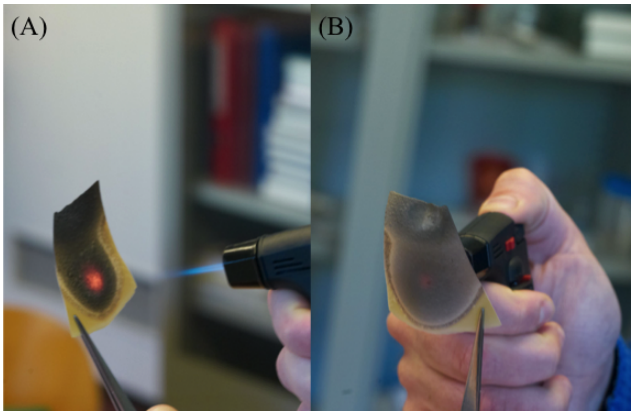

Figure 4.9: Na-Alg 80wt.% MMT bionanocomposite film exposed to flame (A) front side and (B) back side.

efficient flame retardants show toxicity, which presents a major problem for polymeric materials, this could position Na-Alg/MMT bionanocomposite as a superior material in view of flame retardancy. We also note that for a 80 µm thick film, the bionanocomposite displays a significant heat shield, as observed in the reduction in the glow intensity of the back side of the film compared to the front side of the film.

4.4 Conclusions

All natural-based bionanocomposites have been successfully prepared using a simple suspension casting and drying method at ambient conditions. We report on

ease of preparation of the bionanocomposites with MMT concentrations exceeding those explored in traditional petroleum based polymer clay nanocomposites. The bionanocomposites displays a highly ordered "brick-and-mortar" structure, starting from 5 wt.% MMT concentrations.

The XRD radial scans reveal that the d-spacing (intercalation of Na-Alg within MMT galleries) decreases with addition of MMT in the bionanocomposite. The d-spacing at 80 wt.% MMT is equivalent to the d-spacing for the monohydration layer of pure MMT platelets, which indicates some level of intercalation of Na-Alg within the MMT galleries, but suggests that most of the Na-Alg is located on the periphery of the MMT platelets.

Interestingly even the pristine Na-Alg sample has already a relatively high stiffness (10 GPa), which is considerably increased by addition of the MMT platelets. We measure that continuous addition of the MMT platelets leads to an increase in the stiffness of the bionanocomposite with a maximum being reached at 50 wt.% MMT. Further increase in the MMT concentration leads to a decrease in the stiffness that can be attributed to the restacking of the MMT platlets, resulting in reduction of the appearant aspect ratio, which reduces the effectivness of the MMT as reinforcement.

The developed bionanocomposite displays a favorable tunability of the mechanical properties that can maintain their shape, and quite high stiffness for MMT concentrations, after pyrolysis at 1000 °C. The material exhibits complete flame retardation by reducing the oxygen diffusion through the film, and substantial heat shielding over a 80 μm thick film.

Acknowledgments

This work is part of the research program of Integral Solutions for Sustainable Construction (IS2C), which is financially supported by the Dutch National Science foundation (STW). Arjan Thijssen's assistance with ESEM measurement is acknowledged. Southern Clay Rockwood is acknowledged for supplying the Cloisite Na^+(MMT).

Chapter 5

Characterisation of the water vapor barrier properties of Sodium Alginate and Sodium Alginate/Montmorillonite bionanocomposite

In this work we report on the influence of the MMT addition on the barrier properties of self-supporting Na-Alg/MMT bionanocomposite films with a wide range of MMT concentration and water activity. Motivated by a highly aligned structure of the bionanocomposite, we have investigated how the variation in the obtained order parameter and MMT concentration has an influence on the water vapor sorption kinetics. The bionanocomposite films showed a decrease in the amount of water absorbed with increasing MMT content. From the water vapor sorption experiments we have determined the diffusion coefficients of Na-Alg/MMT bionanocomposite films, which demonstrate a considerable reduction that reflects the imposed tortuous diffusion path by the aligned structure. The effective aspect ratio of the MMT platelets was back-calculated from the diffusion coefficients, and we notice a stacking of the platelets with increasing MMT concentration, which we find to be in agreement with the results obtained from the measured mechanical properties.

5.1 Introduction

The study and improvement of the barrier properties of polymer-based materials is an important factor due to their wide range of application in membranes and coatings, *e.g.* packaging membranes to slow down the spoiling of food, curing compounds to facilitate cement hydration. It is well established that addition of platelet-shaped filler with high aspect ratio and surface area improves the barrier properties of the polymers to the transport of water and oxygen, which is most dramatically noticeable in the reduced flammability of these nanocomposites (Kojima et al. 1993, Messersmith & Giannelis 1995).

In the literature it is described that the addition of platelet-shaped filler improves the barrier properties (i) by introducing a tortuous path to the diffusing gas molecules by the presence of an impermeable disk-shaped filler, and (2) by increasing the degree of crystalline phase that like the filler is impermeable as well. The addition of the clay platelets can also have an effect on the free volume of the matrix polymer (Giannelis 1992, Harrats & Groeninckx 2007, Choudalakis et al. 2011). In conclusion, it is about balancing the beneficial and adverse effects of the addition of the clay as a filler in the nanocomposites.

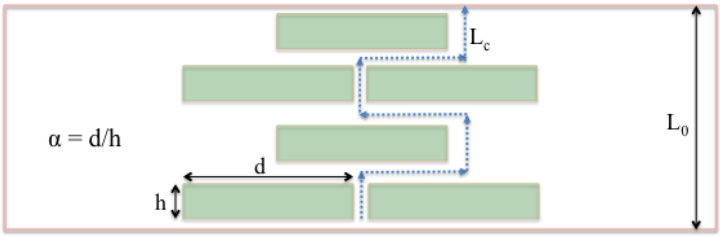

Figure 5.1: Tortuous path imposed by a high aspect ratio platelet-like filler.

Nielsen defined a simple model for the tortuous path as a ratio of the distance a molecule must travel through the film (L_c) and the film thickness (L_0), where the clay platelets are perfectly orientated and overlapped, figure 5.1(Nielsen 1967). It assumes that the platelet-shaped filler is monosized and has no influence on the diffusivity of the polymer matrix (D_m), defining the diffusion reduction as:

$$\frac{D_c}{D_m} = \frac{L_0}{L_c} = \frac{1}{1 + \frac{1}{2}\alpha\varphi_f} \tag{5.1}$$

where D_c represent the diffusion coefficient of the composite, a is the width (d) to thickness (h) ratio, and φ_f is the volume fraction of the filler. Following the

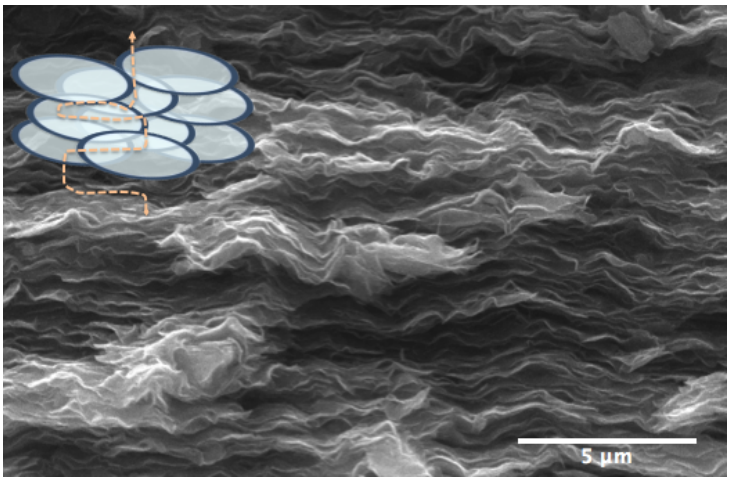

Figure 5.2: Highly ordered structure of Na-Alg/MMT, with inset schematic of an imposed tortuous path, by the aligned MMT platelets, to pentetrating molecules.

tortuous path imposed by the presence of impermeable platelet filler the barrier properties of polymer clay nanocomposite is governed by the concentration, aspect ratio, overlap factor, and the orientation of the filler (Van Es 2001).

A vast body of knowledge has been produced on polymer clay nanocomposites (PCNs) with clays added in a minor amount (<10 wt.%), which showed a drastic improvement in the stiffness of the composites and the gas-barrier properties (Kojima et al. 1993). In recent years, development of bionanocomposites with high loading of the platelet filler has been presented, resulting in barrier properties that far exceed the ones reported for PCNs (Ebina & Mizukami 2007, Doblhofer et al. 2016). The inspiration for this work is found in nature, where a high loading of the inorganic filler together with a sophisticated architecture is often found, e.g. mollusk shells, enamel, and bones. The highly ordered arrangement of the impermeable filler, like the one found in mollusk shells, is an ideal template structure for making membranes and coatings from these bionanocomposites, see figure 5.2, due to the longer diffusion path of the gas molecules.

The process of making such structures is found to be quite favourable from both technical and environmental aspect (Walther et al. 2010, Yao et al. 2010). This is quite encouraging in terms of the scaling up process to produce this type of materials on a large scale. In previous studies we have characterized the highly ordered structure and the mechanical properties of the Na-Alg/MMT bionanocomposite, and the viscoelastic behavior of the Na-Alg/MMT suspension that is responsible

for the formation of such structure by the interaction of negatively charged alginate backbone and positively charged MMT platelets edge.

We have previously, chapter 4, observed that the highly ordered Na-Alg/MMT structure dramatically reduces the oxygen diffusion, which results in non-flammability of this bionanocomposite. In this chapter, we explore the barrier properties of the highly ordered Na-Alg/MMT bionanocomposite, by measuring the influence of MMT concentration, orientation, and effective aspect ratio on the water vapor sorption kinetics. Furthermore, we analyse the effect that the addition of MMT has on the water sorption capacity.

5.2 Materials and methods

The bionanocomposite films were prepared by casting a Na-Alg MMT suspension into a plastic petri dish (PS) and allowing it to dry in ambient conditions (50 % RH, 20 °C). Firstly, a 3 wt.% suspension of Na-MMT (Sodium Montmorillonite, Cloisite Na+ (MMT) was completely exfoliated in water overnight and without any visual remaining agglomerates. After which a 3 wt.% polymer solution of Sodium Alginate (Na-Alg, Sigma Aldrich) was added to the Na-MMT suspension under vigorous stirring to ensure homogeneity. The MMT concentrations in the final films were controlled by the initial Na-Alg to Na-MMT ratio. To completely dry the bionanocomposite films were vacuum dried at 40 °C and kept in a desiccator prior to any measurements. The final film thickness was around 100 μm.

Sorption isotherms were obtained using a TA Instruments Q5000 SA by measuring the mass uptake of water vapor of the Na-Alg and Na-Alg/MMT bionanocomposite films. The isotherm measurement was conducted in 4 steps by varying the water activity (a_w), in which the humidity was maintained using a laminar flow with wet-dry vapor mixing at a constant mass flow rate with feedback control.

The water sorption measurement was performed as follows. Firstly the samples were dried at 60 °C at 0.01 a_w until the weight change was stabilized to less than 0.001 % for a period of 10 min. In the second step the temperature was stabilized to 20 °C at 0.01 a_w, after which the humidity was increased in a stepwise fashion, where each step represents an increase of 0.2 a_w. After each step the mass was measured for five hours or until mass change was less than 0.001 % for a period of 10 min. After the final water activity step has stabilized, desorption was performed by setting the water activity to a_w 0.01. This sorption/desorption isotherm set profile is shown in figure 5.3.

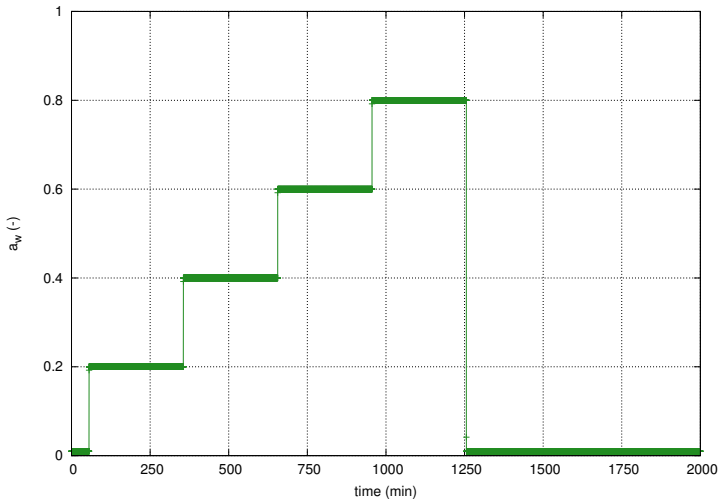

Figure 5.3: Designed water vapor sorption/desorption isotherms.

Due to the hydrophilic nature of the polymer and the filler we expect swelling of the films and to correct for the thickness of the sample we assume that the swelling is one-dimensional, which is a reasonable approximation due to the large surface area to volume ratio, where the density of the absorbed water in the film is estimated to be 0.998 g/cm^3.

$$\frac{1}{d_{RH}} = \frac{1}{d_{dry}}(1 - \Phi_{H_2O}) \tag{5.2}$$

where d_{RH} and d_{dry} is the thickness of the sample at a specific water activity and the dry sample, respectively, and Φ_{H_2O} is the volume fraction of water absorbed at a specific water activity.

As mentioned above, the water sorption was measured gravimetrically, and is presented as a weight gain of water sorbed by the material at initial time and at equilibrium. The measured accumulation of water in the sample as a function of time, we use Crank derivation to calculate the diffusion coefficient assuming Fickian behaviour with an infinite sheet geometry and a constant initial concentration throughout the sample and a constant concentration at the film surface (Crank 1975):

$$\frac{\Delta M_t}{\Delta M_\infty} = 1 - \frac{8}{\pi^2}\sum_{n=0}^{\infty}\frac{\exp\left(\frac{-(2n+1)^2 D\pi^2 t}{4l^2}\right)}{(2n+1)^2} \tag{5.3}$$

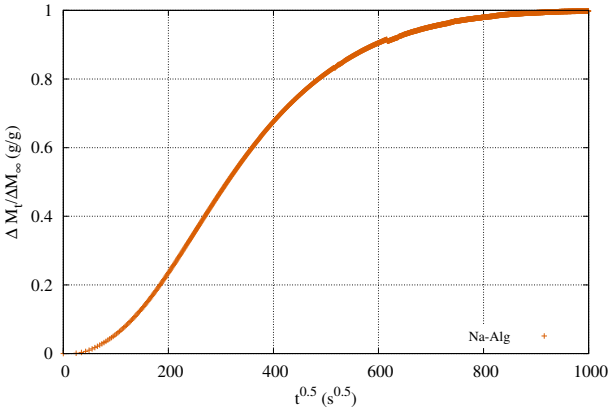

Figure 5.4: Sorption kinetics of water in Na-Alg membrane film at 20 °C and water vapor activity of 0.6-0.8.

where ΔM_t and ΔM_∞ represent mass uptake of water by the sample at time t and at equilibrium, respectively, and D is the diffusion coefficient, and l is the half thickness of the film sample.

As we can see from the example presented in figure 5.4, of the weight gain by the membrane film, at 20 °C and 0.6-0.8 a_w, as a function of the ratio between the square root of time and sample thickness. We observe a sigmoidal shape of the sorption kinetics curve, which suggests an initial time lag that is followed by Fickian diffusion (eq 5.3). The origin of the initial time lag could indicate anomalous sorption kinetics, but in absence of strong evidence we attribute it to an instrumental time constant and does not represent a fundamental property of the sample. In order to calculate the diffusion coefficient from such sorption curves we used a variable surface concentration model developed by Long and Richman, in which they formulated that at set water activity the water surface concentration approaches the equilibrium water concentration as an exponential function of time (Long & Richman 1960):

$$C(x = \pm l, t) = C_0 \left[1 - \exp\left(-\frac{t}{\tau}\right)\right] \tag{5.4}$$

where l is the half thickness of the film, and τ is the characteristic time for attaining saturation at the polymer/water-vapor interface. This means that at very early times the sorption is dominated by a relaxation step (in absence of evidence we believe it represents an instrumental anomaly rather than a property of the sample) that is not controlled by/or overlapped with the diffusion step. The subsequent

diffusion is assumed to be Fickian, with the boundary conditions as given in eq.5.4 and with a constant diffusion coefficient (Arce et al. 2004):

$$\frac{\Delta M_t}{\Delta M_\infty} = 1 - \exp\left(-\frac{t}{\tau}\right)\sqrt{\frac{D\tau}{l^2}}tan\sqrt{\frac{l^2}{D\tau}} - \frac{8}{\pi^2}\sum_{n=0}^{\infty}\frac{\exp\left[\frac{-D(2n-1)^2\pi^2 t}{4l^2}\right]}{(2n+1)^2\left\{1-(2n+1)^2\left[\frac{D\pi^2\tau}{4l^2}\right]\right\}} \tag{5.5}$$

From the sorption kinetics measurements we examine how the addition of the MMT and its orientation influences the diffusion coefficient of the Na-Alg/MMT bionanocomposites. Furthermore, the obtained diffusion coefficient values will be used to back-calculate the effective aspect ratio of the MMT platelets for all bionanocomposite samples.

5.3 Results and discussion

The water vapor sorption results are separated for each step of the water activity profile and to the appropriate equilibrium water content levels, as shown in figure 5.5. We observe that the fit using eq. 5.5 is found to be in good agreement with the experimental data for Na-Alg and Na-Alg/MMT bionanocomposite films at 20 ^{o}C for all measured water activities. As mentioned above, due to lack of strong evidence we believe the origin of the sigmoidal shape represents an instrumental constant rather than a property of the material. Also, we see that the kinetics of moisture sorption is clearly reduced with the increasing MMT concentration as a consequence of improved barrier properties, which will be discussed further in the text.

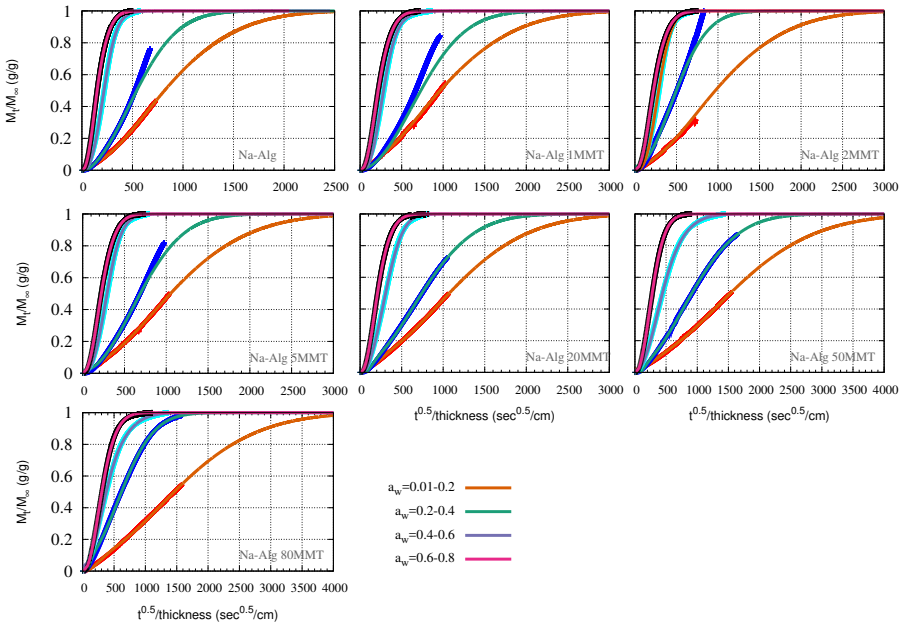

Figure 5.5: Kinetic water sorption of Na-Alg and Na-Alg/MMT bionanocomposite at 20 ºC. The sorption at different water activities.

Equilibrium sorption isotherms, figure 5.6, for Na-Alg and Na-Alg/MMT bionanocomposites are shown as a ratio of the weight of water sorbed by the sample for a given water vapor activity and the dry weight of the sample. Interestingly, both components in the examined system are hydrophilic, however, we observe that addition of MMT platelets causes a decrease in the total sorbed water of the Na-Alg/MMT bionanocomposites. This could be explained by favored interaction between Na-Alg and MMT platelets that reduces the water sorption of the bionanocomposite, by increasing the hydrophobicity of the system (Sehaqui et al. 2013).

The equilibrium isotherm exhibits a slight upturn at high water activities, which could be caused by the plasticisation of the Na-Alg by water, and/or clustering of water molecules. These effects are competitive with the opposite effect on how the diffusion coefficient changes with the increasing water activity. Plasticisation results in an increase of the diffusion coefficient with water activity due to increased segmental polymer mobility caused by the water molecules, while the water clustering increases the water diameter that decreases the diffusion coefficient with increasing water activity (Schult & Paul 1996).

From the water sorption kinetics we examine how the calculated water diffusion

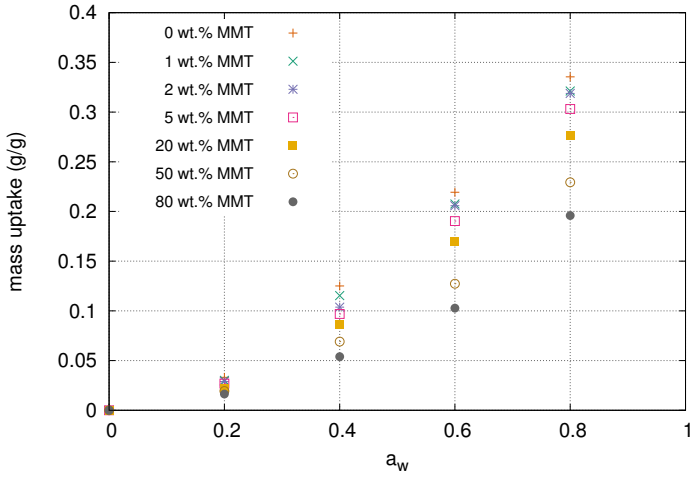

Figure 5.6: Equilibrium water vapor sorption isotherms for Na-Alg and Na-Alg/MMT bionanocomposites at 20 ºC.

coefficient changes by the introduction of the MMT platelets in the Na-Alg/MMT, as calculated by eq. 5.5.

In general, from figure 5.7 we see that the diffusion coefficient is dependent on the set water activity values, for which we see an increase in the diffusion coefficient with increasing water activity. This increased mobility at high water activities is induced by the plasticisation effect of the water on the Na-Alg, which is probably because of the hydrophilicity of the biopolymer.

Also, in figure 5.7 we observe that the presence of the impermeable MMT platelets within the Na-Alg matix causes a drastic decrease of the diffusion coefficient, which is achieved by increasing the average path length of water molecules through the Na-Alg/MMT film. As mentioned previously, the tortuous path of the diffusing molecules imposed by the MMT platelets also depends on the orientation, overlap factor, and the aspect ratio of the MMT platelets.

We used a modified Nielsen model, developed by Baharadwaj, to back-calculate the aspect ratio of the MMT with varying <P_2> values and MMT concentration in the Na-Alg/MMT bionanocomposite (Baharadwaj 2003).

$$\frac{D_c}{D_m} = \frac{1}{1 + \frac{1}{2}\alpha\varphi\frac{2}{3}\left(< P_2 > + \frac{1}{2}\right)} \tag{5.6}$$

where the <P_2> value is the order parameter of the MMT platelets in the

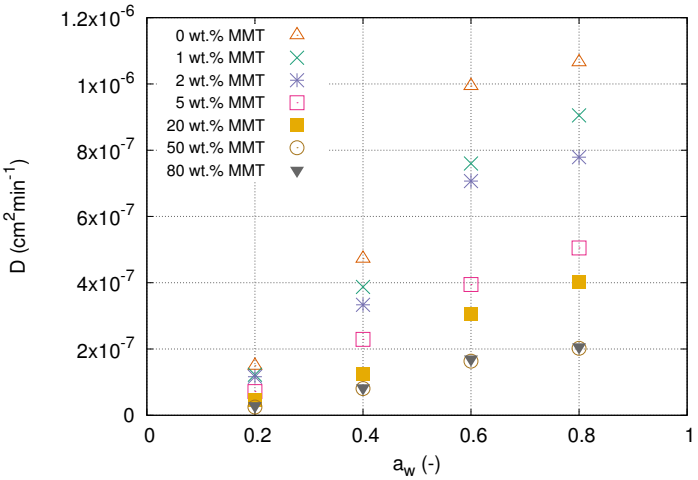

Figure 5.7: Water diffusion coefficient calculated with eq.5.5 from the sorption curves at different water activities for Na-Alg and Na-Alg/MMT bionanocomposites at 20 ºC.

system. We note three extreme cases of the $<P_2>$ values (i) -1/2 for platelets orientated parallel to the layer normal, (ii) 0 for randomly orientated platelets, and (iii) 1 for perfectly aligned platelets. The equation is formulated such that if the $<P_2>$ value is - 1/2 the diffusion coefficient is the same as the diffusion coefficient of the polymer and if the $<P_2>$ value is 1 it returns to eq 5.1. As we have reported previously in Chapter 2 the $<P_2>$ values calculated over the azimuthal intensity profile obtained by WAXS and fitted to the affine deformation ODF are ranging from completely random for 1 and 2 wt. % MMT to highly aligned for 5 wt.% MMT and higher. These values will be used to back-calculate the effective aspect ratio of the MMT platelets.

The effective aspect ratio of the MMT platelets are back-calculated from the diffusion coefficients for the Na-Alg and the Na-Alg/MMT bionanocomposites using eq. 5.6, and are presented in figure 5.8. As mentioned, in the Nielsen model one of the assumptions is that the clay platelets are perfectly overlapped and are monodispersed in size, which we believe is improbable for our system. We should view these results as an underestimation of the effective aspect ratio of the MMT platelets, however they can be used for comparison and can be viewed as the bottom values.

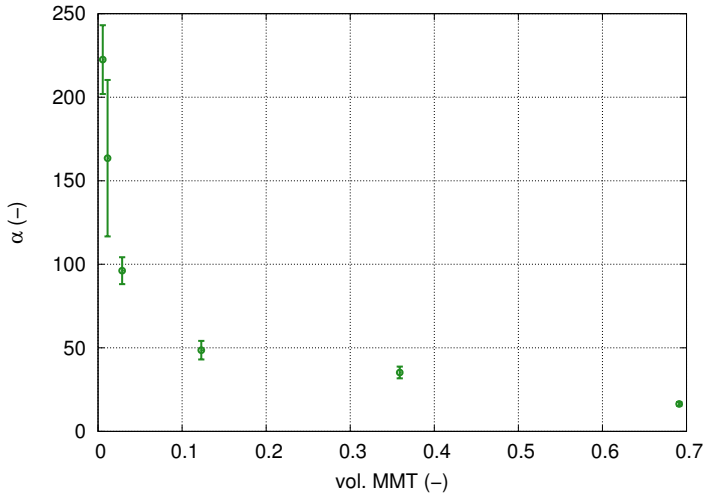

Figure 5.8: Aspect ratio of the MMT back-calculated from diffusion coefficient for various MMT loadings and wide relative humidities.

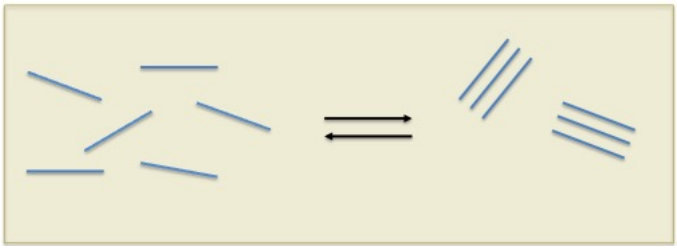

Figure 5.9: Reversible exfoliation and restacking of the MMT platelets during the development of the Na-Alg/MMT bionanocomposite.

We observe that the calculated effective aspect ratio is strongly dependent on the MMT concentration, and shows a decrease with the increasing MMT content. Although we observe an improved barrier properties for the bionanocomposites samples, the decrease of the effective aspect ratio results in reduced effectiveness of the MMT. The stacking of the MMT platelets occurs as a result of being thermodynamically more favorable and it leads to intercalated or immiscible MMT platelets within the polymer matrix (Fornes & Paul 2003). The stacking of MMT platelets develops during the drying of the Na-Alg/MMT system increasing the probability of MMT-MMT interaction, where a dynamic process of stacking and exfoliation is occurring, which is schematically presented in figure 5.9. We find this process similar to the one found in the living (equilibrium) polymerisation, in which the av-

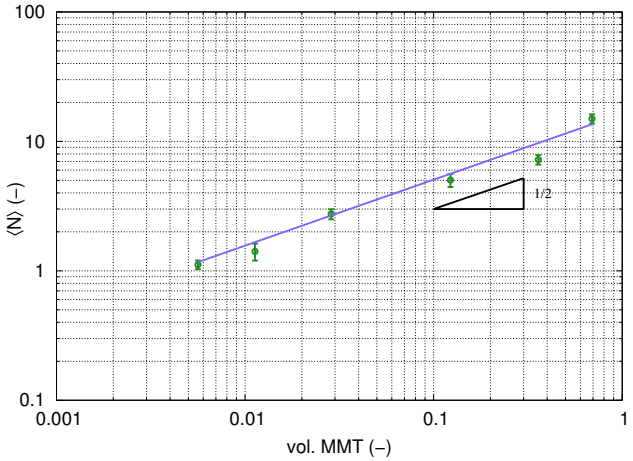

Figure 5.10: The dynamic restacking of the MMT platelets as a function of the MMT concentration.

erage polymer chain length, <N>, results from an equilibrium of reversible breakage and reformation of the bonds and is expressed by a mean-field theory as (Cates & Candau 1990, van der Gucht & Besseling 2002):

$$< N > \approx \sqrt{\varphi_f} \exp\left(\frac{E}{2k_bT}\right) \tag{5.7}$$

where the φ_f is the total volume fraction, E is the scission energy that is required to break a bond between two monomers, and the temperature T. For our system the average chain length represents the average number of the MMT stacks, which is dependent on the volume fraction of the MMT. Following eq. 5.7 the restacking of the MMT platelets scales with the MMT as $<N> \propto \varphi_f^{0.5}$, which we observe in figure 5.10.

5.4 Conclusions

This work explores the water vapor diffusion of the highly ordered Na-Alg/MMT bionanocomposites by varying the concentration of the MMT platelets. The addition of impermeable platelet-like filler to the host Na-Alg poymer matrix is controlled by the dimensions, concentration, overlap factor, and the level of the MMT alignment.

The water sorption capacity is reduced by the addition of the MMT platelets, which we attribute to the preferred MMT-alginate interaction that occurs via polar

(hydrophilic) functional groups of both components and consequently reduces the hydrophilicity of the system. At higher water activities there is a slight upturn in the water sorption, which is due to the plasticization of the alginate macromolecule by water, i.e. increased segmental mobility.

Both the filled and unfilled systems show water activity dependance of the diffusion coefficient.

The presence of the impermeable MMT platelets increases the tortuous path of water molecules and thus decreases the water diffusion coefficient. The reduction of the water diffusion coefficient corresponds to the volume fraction, orientation and the aspect ratio of the MMT platelets.

The aspect ratio of the MMT platelets is an important parameter that determines the effectiveness that the MMT addition to the polymer matrix has on the extent of improvement of barrier properties of the nanocomposite. In this work we have used the values of the diffusion coefficient to back-calculate the effective aspect ratio of the MMT and observe a reduction of the aspect ratio with the increasing MMT concentration. This results in the plateauing of the diffusion coefficient values for the system with MMT concentration higher than 50 wt.%.

Acknowledgments

This work is part of the research program of Integral Solutions for Sustainable Construction (IS2C), which is financially supported by the Dutch National Science foundation (STW). Southern Clay Rockwood is acknowledged for supplying the Cloisite Na^+(MMT).

Chapter 6

Bio-Based Curing Compound for Cement-Based Materials[1], [2]

Most concrete structures are designed to last for at least 100 years or more. During their lifetime these structures are exposed to various environmental actions. On going cement hydration guarantees a stronger concrete in terms of bond between the aggregates, fewer voids, and depercolation of capillary pores, which is of particular importance for cover concrete. Thus, a properly cured cement-based material is essential for a long service life. A new environmentally friendly, water-based curing compound, made of sodium alginate bio-polymers, has recently been developed at TU Delft that could help to achieve these goals. Experimental Rapid Chloride Migration tests and Environmental Scanning Microscope observations are conducted on different samples to investigate the functional properties, e.g. ion transport, and microstructural investigation, to examine the performance of the new bio-based curing compound. Mortar samples were cured at 50% RH and 20 °C both with and without surface addition of the bio-based compound. Two different types of cement, CEM I and CEM III/B, were tested to study differences in curing performance. Significant beneficial effects were observed at the mortar surface when applying the bio-based curing compound showing reduced diffusivity of the cement-based material. The results showed a very good quality surface with a high quality and dense microstructure. Also, a higher curing sensitivity was observed for the CEM III/B samples compared to samples prepared with CEM I.

[1] J.Zlopasa, E.A.B. Koenders, S.J. Picken *Dresden* 2014
[2] J.Zlopasa, E.A.B. Koenders, S.J. Picken *AMS* 2014

6.1 Introduction

Most cement-based structures are designed to last for at least 100 years or more. Cement-based materials are composite construction materials that primarily consist of a continuous phase of cement paste and a discontinuous phase of aggregates. The aggregate phase is viewed as an inert filler that contributes to volume stability and higher durability, which is bonded by hydration products of cement clinker in a cement paste (Neville 1995). Cement clinker is composed of four mineral phases Ca_3SiO_5 Ca_2SiO_4, $Ca_3Al_2O_6$ and $Ca_4Al_2Fe_2O_{10}$. Two major phases (around 80 % for most cements) of cement clinker are tri- and di-calcium silicate. Tri-calcium silicate reacts faster and is responsible for strength development during the first weeks, whereas di-calcium silicate reacts slower and contributes to the long-term strength of cement-based materials. In general, the reactions of both silicate phases are presented as follows:

$$(CaO)_b(SiO_2)+(b-{}^{Ca}/_{Si}+y)(H_2O)\rightarrow(CaO)_{Ca/Si}(SiO_2)\times y(H_2O)+(b-{}^{Ca}/_{Si})Ca(OH)_2 \tag{6.1}$$

where b=2 or 3 (di- or tri calcium silicate, respectively), Ca/Si=1.7-1.8, and y=4 (Richardson 2000). Nowadays, it is becoming common practice to replace a certain fraction of Ordinary Portland Cement (OPC) by pozzolanic materials, e.g. silica fume, fly ash or blast furnace slag. In marine environments, a very commonly used cement is CEM III/B, which has a high replacement of cement by ground granulated blast furnace slag GGBS. The hydration mechanism of the combination of GGBS and OPC is slightly more complex than that of OPC only. This pozzolanic reaction involves activation of the GGBS by alkalis and sulphates to form its own hydration products. The result is a hardened cement paste with more very small gel pores and less capillary pores for the same total pore volume (Siddique & Khan 2011). This means that durability properties of such hardened blended cement-based materials are higher than that of Portland cement alone.

Since water is an essential component in hydration, and cement hydration will only proceed in a water-filled environment, sustaining the hydration process requires that inter-particle voids remain filled with water (Hover 2011). Powers et al. showed that hydration of cement is greatly slowed down when the relative humidity in cement capillary pores goes below 80%, which most likely happens at the surfaces of e.g. concrete elements (Powers & Brownyard 1946-1947). Curing is a name given to mitigation procedures that aim to avoid this. They are used for ensuring

ongoing the hydration of cement, and consists of a control of moisture movement (and temperature) from and into the cement-based materials, through the exposed surfaces (Neville 1995).

By preventing the loss of water from cement-based materials, ongoing hydration could be achieved and drying shrinkage can be avoided, leading to a minimum of surface cracks, a stronger bond between aggregates, fewer voids, and lower connectivity of pores. Such a microstructure is denser and can cause slower penetration of aggressive fluids that may be harmful, e.g. to prevent corrosion of the steel reinforcement (Meeks & Carino 1999). Therefore, a properly cured cement-based material is better prepared for a long service life. As mentioned, cements that have partial replacement by pozzolans have a longer hydration period and are more sensitive to water loss. It is reported that cements in combination with puzzolans achieve, if cured properly, considerably densere miocrstructure than OPC (Ramezanianpour & Malhorta 1995, Bentz *et al.* 2000). Generally, continous hydration can be ensured by adding water or by hindering water to escape from the cement-based material's surface. Continuously adding water to the surface, by means of water ponding, water spraying, and/or by the use of wet burlap usually gives the best end results. However, this technique requires workers on site that keep the concrete moist, which can be costly. In addition, this method can be especially costly in places where there is a scarcity of water. As said, the second way of curing cement-based materials is by preventing water evaporation. This can be accomplished by covering the surface with a plastic sheets or by spraying it with a curing compound (polymer solutions/emulsions) that creates a film that hinders water evaporation. Curing compounds can be water based or organic-solvent based (Wang, Dhir, & Levitt 1994). In general, curing compounds based on organic-solvents show better performance compared to water-based ones (Al-Gahtani 2010). As a drawback, there can be an environmental impact, especially when using it in poorly ventilated environments.

In this study, we propose the use of a water-soluble bio-based polymer, sodium alginate, as potential curing compound for cement-based materials. Alginates are linear water-soluble polysaccharides comprising (1— 4) linked units of β-D-mannuronate (M) and ∝-L-guluronate (G) at different proportions and different distributions within the chains. The functional properties are strongly related to composition (M/G ratio) and with the sequence of the uronic acids. Alginates are present in brown algae and can also be found in metabolic products of bacteria, e.g. pseudomonas and azotobacter. The alginate synthesised by some bacteria is expressed

as a exopolysaccharide, EPS, and it can have a protective effect, *i.e.* prevent lethal desiccation. (Linker & Jones 1966; Gorin & Spencer 1966; Draget, Skjåk-Bræk, & Smidsrød 1977; Grasdalen, Larsen, & Smidsrød 1981).

Alginates are commonly used as food additives, gelling agents, wound dressings and for drug delivery (Laurienzo 2010; Matthew *et al.* 1995). The gelling property of this polymer gives a unique opportunity to be applied in various fields. Alginates gel either by lowering the pH below the pKa value of the uronic residue or in the presence of polyvalent cation ions (Russo, Malinconico, & Santagata 2007; Narayanan *et al.* 2012). Polyvalent ions act as bridges between different G units of chains, as shown in figure 6.1.

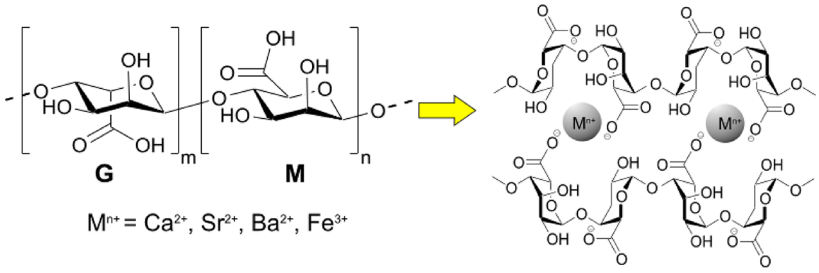

Figure 6.1: Structure of alginic acid (left) and schematic representation of crosslinking of alginate by polyvalent ions (right). (Narayanan et al. 2012)

As follows from equation 6.1, a large amount of Ca^{2+} is produced by cement hydration, which is freely available. The free calcium ions are available for further reaction with the pozzolanic materials or CO_2. Since sodium alginate cross-links rapidly with Ca^{2+}, forming a non-water soluble calcium alginate gel and later a film, we have investigated the possibility to use sodium alginate as an external curing compound. The principle of a sodium alginate curing system is presented schemactialy in figure 6.2.

For this purpose, we compared air-cured and alginate-cured mortar samples prepared with CEM III/B. We have examined functional properties and microstructure of mortar samples with and without the application of sodium alginate solution. This was achived by the use of Environmental Scanning Microscope (ESEM) and Rapid Chloride Migration (RCM) Tests. The calculated non-steady state migration of chloride ions, from the RCM test, in CEM III/B was compared to mortar samples made with Ordinary Portland cement, as studied previously, to compare the transport properties for different cements (Zlopasa, Koenders, & Picken 2014).

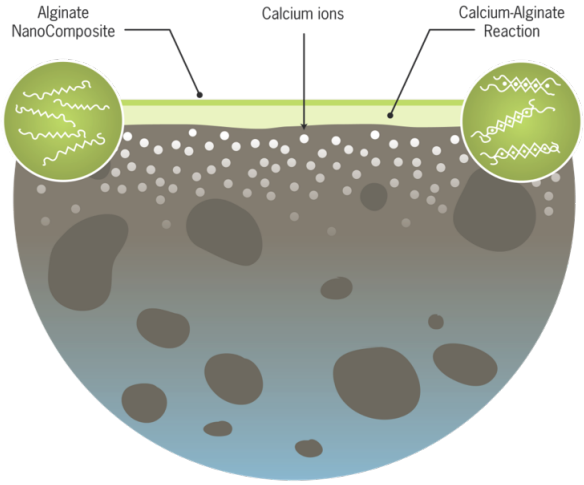

Figure 6.2: Schematic representation of the principle working of the alginate-based curing compound.

6.2 Materials and Methods

Sodium alginate, Na-Alg, with an average molecular weight of 150,000 g/mol and M/G ratio of 1.56 was obtained from Sigma Aldrich Co. A water solution of 3 wt.% Na-Alg was prepared using demineralised water under vigorous stirring. The mortar samples were prepared using two different cements, namely, ordinary portland cement CEM I/52.5R and blast furnace slag cement CEM III/N 52.5N (produced by ENCI Heidelberg Cement group) with a W/C of 0.5 and aggregate particles that follow Fuller's distribution. Table 6.1 give the exact mixture proportions of the mortar.

Table 6.1: Mortar mixture proportions

Cement type [-]	CEM I 52.5 R	CEM III/B 52.5 N
Cement content [kg/m^3]	507	494
Aggregates 0.125-2 mm [kg/m^3]	1522	1521
Water [kg/m^3]	254	247
W/C	0.50	0.50

Samples were cast in cylindrical moulds with 100 mm diameter which was followed by compaction using a vibration table. After compaction 25 ml of 3 wt.% Na-Alg solution was poured on top of the mortar samples, while the control samples

were left uncovered, all samples were made in triplicates. Once the Na-Alg solution is poured on the fresh mortar samples, a rapid gel formation was observed. This gel formation is due to reaction of (mainly) free Ca^{2+}, produced from cement hydration, and the applied Na-Alg solution on the surface of the mortar sample. Thus producing a continuos film on the surface of the mortar sample, which prevents water evaporation and enables uninterupted cement hydration. Also worth noticing is that when the Ca-Alg gel is formed on the surface of the mortar sample it does not flow, which prevents the alginate to penetrate inside the mortar sample and potentially disturb the cement hydration.

Furthermore, samples were placed in an environment with stable conditions of 50 % RH and 20 °C for 28 days, after which they were de-moulded and further analysed.

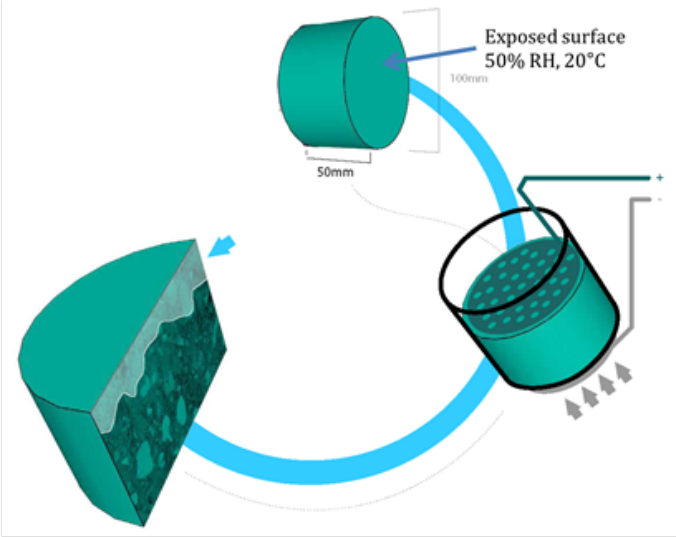

Figure 6.3: Schematic representation of RCM test.

In order to evaluate differences in transport properties of diffrently cured mortar samples, the chloride migration coefficient is determined by use of the Rapid Chloride Migration (RCM) test. The method is described in NT Build 492 (NT Build 492 1999). The principle behind this method is the application of an external electrical field axially across the mortar specimen which forces the chloride ions to migrate into the specimen at a high rate. Since curing of cement-based materials mostly affects the near surface area, we have modified the standard RCM test slightly by not removing the first 10-20 mm of the mortar surface from the samples.

A sketch of the RCM test is shown in figure 6.3. After 28 days the samples were de-moulded, the alginate coating was removed from the mortar surface to avoid any influence on the chloride migration coefficient. Preconditioning of the samples was performed by placing them in vacuum for 3 hours and then, with the vacuum pump still running, a saturated $Ca(OH)_2$ solution was introduced and the samples were completely submerged in it. After 1 hour the vacuum pump was turned off and air was allowed to enter the container and the specimens were further kept in the saturated $Ca(OH)_2$ solution for 18 hours. Once preconditioning was completed the samples were placed in the RCM setup, which consists of a rubber sleeve in which the samples are placed.

Electrodes are immersed in the anolyte (0.3 M NaOH) and catholyte (2 M NaCl) solutions and connected to the power supply unit. The initial current through the sample at 30 V is recorded and the voltage was adjusted according to the standard which also states the duration of the test. The voltage is adjusted allowing the chlorides to penetrate through about half of the sample. Initial and final temperatures of both anolyte and catholyte were also determined. After the described test duration the specimens were removed from the RCM setup and split axially, into two pieces. On the freshly split surface 0.1 M $AgNO_3$ was sprayed and after few minutes white silver chloride started to precipitate (see figure 6.4) causing a color change.

The precipitated silver chloride represents the chloride penetration depth, from which the migration coefficient is calculated using equation 6.2:

$$D_{nssm} = \frac{0.0239 \times (273+T) \times L}{(U-2) \times t} \times \left(x - 0.0238 \times \sqrt{\frac{(273+T) \times L \times x_d}{U-2}} \right) \tag{6.2}$$

where T is the temperature in $°C$, L is thickness of the sample in mm, t is the test duration in *hours*, U is the applied voltage and x_d is the chloride penetration depth in mm. Differences in developed microstructure of mortar samples were investigated using environmental scanning microscope (ESEM) in the backscattered electron mode (BSE), in conjunction with energy-dispersive spectroscopy for qualitative elemental analysis (Ca, Si, C, Al, Mg, Fe, Na, K).

Polished sections for ESEM and energy-dispersive X-ray spectroscopy (EDS) are made as follows. To examine the influence on the curing, which is most pronounced in the near-surface area, the sampling was done 30 mm from the surface, cement hydration was stopped by submerging the samples in liquid nitrogen and subse-

quently placing into a freeze-dryer (sublimation of H_2O) at a temperature of -24°C, under vacuum, for 21 days. The dried samples were impregnated under vacuum with epoxy resin. When the resin has hardened, the surface of interest was first ground and then polished.

6.3 Results and discussion

Measuring the penetration depth, after white silver chloride precipitation, the chloride non-steady state migration coefficient was calculated using equation 6.2. Figure 6.4 (right) depicts a substantial decrease in the D_{nssm} for samples that were treated with Na-Alg as an external curing compound compared to control sample. The non-steady state migration coefficient of chloride ions for alginate-cured mortar was 1.60 and 2.74 times lower than for the air-cured mortar samples of CEM I and CEM III/B, respectively. These results are fully comparable to results obtained by Bouwmeester - van den Bos and Schlangen, for both types of cements, in which the values of the chloride migration coefficient for Na-Alg cured mortar sample are almost equal to the mortar samples cured under water and in sealed conditions (Bouwmeester-van den Bos & Schalngen 2008).

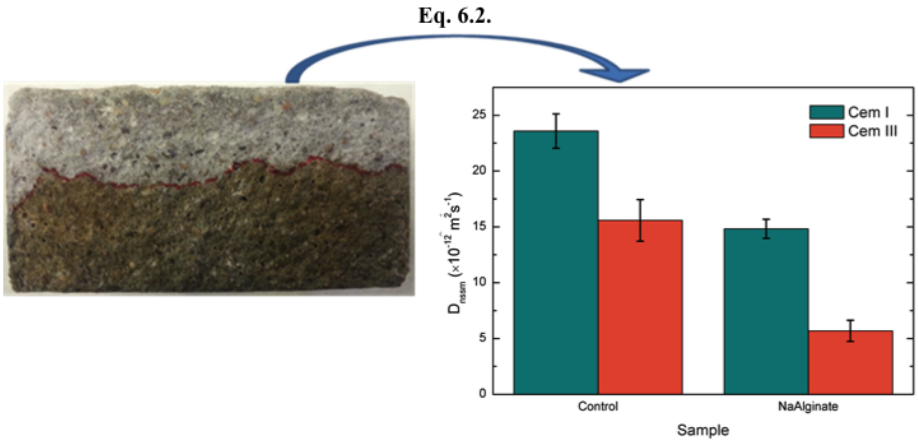

Figure 6.4: Chloride penetration (left) visualized with $AgNO_3$ producing the white AgCl, and chloride migration coefficient obtained from RCM test results (right).

As mentioned before, CEM III/B has an up to 80% cement replacement by GGBS, which makes it more sensitive to curing, due to secondary hydration reactions that are usually slower than primary cement hydration. What can be also seen

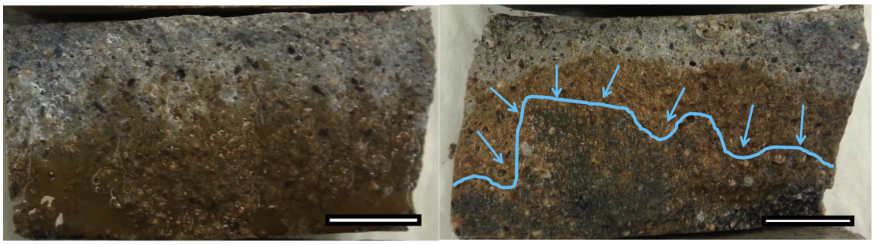

Figure 6.5: Split surfaces of air cured (LEFT) and alginate cured (RIGHT) mortar sample after RCM test. Scale bar is 20 mm.

is that if cured properly the transport properties of mortar samples made with CEM III/B is significantly lower than that of a mortars made with CEM I. This result also confirms that using CEM III/B cement is more suitable for marine environments than CEM I.

Split mortar samples after the RCM test are shown in figure 6.5. Since GGBS is a by-product of iron production, there is a considerable concentration of iron sulphide. Once cement hydration starts the iron sulphide oxidises to blue-green colored iron(II)sulphate. Further oxidation of iron produces iron(III)oxide and iron(III)sulphate that have a brown color. The presence of the blue colour is dependent on the quality of curing conditions, indicating the samples samples with a blue-green color as being properly cured (Sioulas & Sanjayan 2001). We can see that the characteristic blue coloration is visible only in the alginate-cured mortar sample, while the air-cured mortar sample was completely brown, which is further supporting the claim that the alginate-cured mortar sample is cured more adequately.

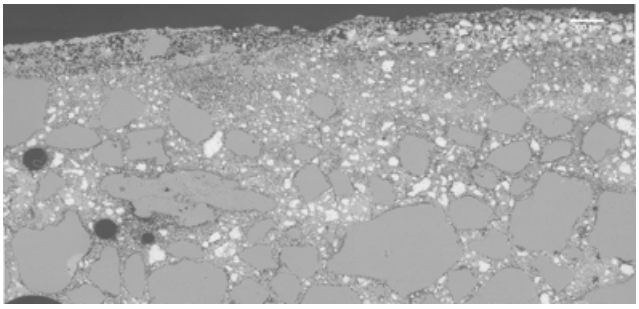

Figure 6.6: ESEM-BSE micrograph of near surface area of alginate-cured mortar sample made with CEM I.

In figure 6.6 and 6.7 we observe the difference in the microstructure of the mortar samples (CEM I) in the near surface area by means of ESEM, for the alginate-cured

and air-cured mortar sample. We can see that the microstructure of the mortar sample that was treated with Na-Alg solution is clearly denser and with fewer cracks compared to the microstructure of the mortar sample that was air-cured. The origin of cracks comes from drying or plastic shrinkage that is usually visible for cement-based samples that had excessive drying of freshly cast sample.

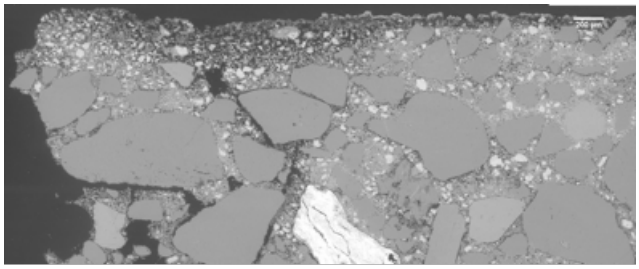

Figure 6.7: ESEM-BSE micrograph of near surface area of air-cured mortar sample made with CEM I.

In figures 6.8 and 6.9 a near surface area of the mortar samples was analysed by ESEM in BSE mode in conjunction with element mapping, in which for our research the the elements of interest are calcium and carbon.

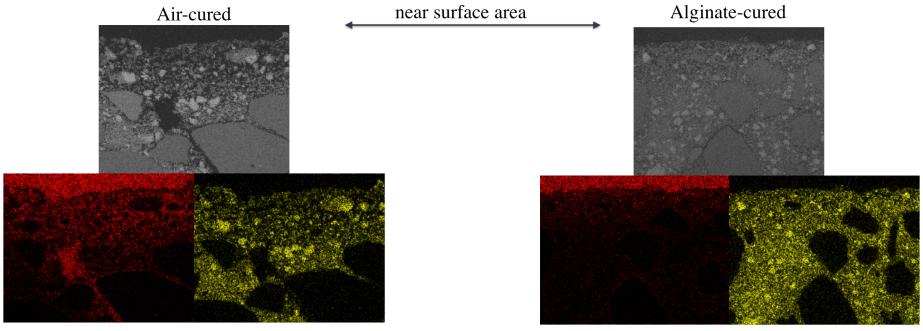

Figure 6.8: ESEM-BSE image with EDS mapping of Calcium (yellow) and Carbon (red) of near surface area of (LEFT) alginate-cured mortar sample and (RIGHT) air-cured mortar sample with CEM I.

We believe that the dominant reaction of Na-Alg on the sufrace of the mortar sample was free Ca^{2+} ions, which are present in abundance due to cement composition and hydration. This would indicate if there is any significant leaching of calcium due to alginate reaction. Since the samples were prepared by impregnating with the epoxy resin, analysis of carbon content will indicate the porous and cracked areas in the sample. The air-cured mortar samples made both with CEM

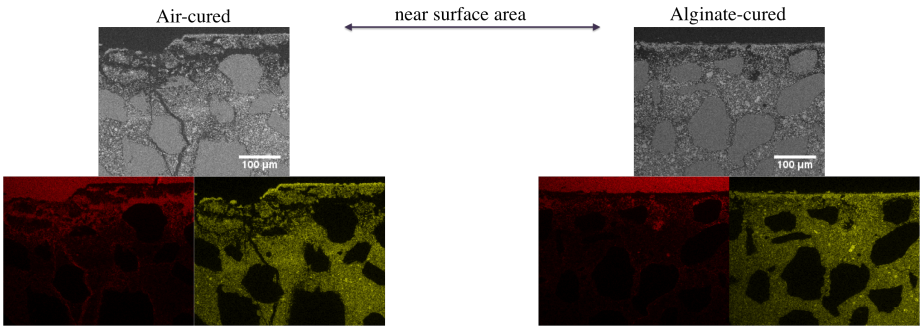

Figure 6.9: ESEM-BSE image with EDS mapping of Calcium (yellow) and Carbon (red) of near surface area of (LEFT) alginate-cured mortar sample and (RIGHT) air-cured mortar sample with CEM III.

I and CEM III showed a considerably higher porosity of the microstructure in the near surface area compared to alginate-cured samples.

In contrast to what we expected, due to the calcium reaction with Na-Alg, we observe a lower calcium content at the near surface area for the air-cured sample than for the alginate-cured sample. The leaching of calcium for the air-cured samples occurs due to reaction of free Ca^{2+} ions with CO_2, and precipitation of $CaCO_3$, which further develops a concentration gradient causing leaching of calcium. In research by Belcarz et al., sodium alginate was added to gypsum in order to reduce calcium leaching and authors observed positive effect of alginate to reduce leaching, which was found to be dependent on the initial concentration of alginate (Belcarz *et al.* 2013).

6.4 Conclusions

In this work, we have examined the influence the application of Na-Alg solution on the surface of the mortar sample as an external curing compound has on the transport properties and the microstructure. The objective was to see whether a water-soluble bio-based polymer, Na-Alg, can be used as an external curing compound for cement-based materials. The principle working of the alginate-based curing is in a rapid reaction of the biopolymer with free divalent and trivalent cations that are present on the surface of freshly cast cement-based sample. The formation of a continous membrane results in a reduction of water release and enables undistrubed cement hydration.

After 28 days of curing in 50% RH and 20 °C, the RCM test was performed

and a significant differences in chloride migration were observed for the alginate-cured and air-cured mortar samples. Alginate-cured samples showed a substantial decrease of the chloride migration coefficient for mortar samples made with both CEM I and CEM III/B cements. This difference was a 1.6 and 2.74 times lower migration coefficient for alginate cured samples compared to air-cured samples for CEM I and CEM III/B, respectively.

We also noticed a distinque blue coloration of the split surface of the mortar samples made with CEM III/B cement, indicating adequate curing, which was absent for air-cured sample.

The microstructure of the near surface area of the mortar samples was examined by ESEM and also in conjunction with EDS. The alginate-cured mortar sample displayed a denser microstructure with fewer cracks, while the air-cured sample also showed considerably higher calcium leaching.

Acknowledgments

The authors like to acknowledge the Dutch National Science foundation STW. The research conducted within this project is financed by STW as a part of the IS2C program (www.is2c.nl), number 10962. Arjan Thijssen's assistance in ESEM measurement is acknowledged.

Chapter 7

General discussion and future outlook

One of the more inspiring aspects of materials found in nature comes from their spontaneously occuring high level of hierarchical organisation, while they are producted under mild environmental conditions. Making use of the intricate hierarchical organisation and the interplay of components these materials exhibit a variety of advanced functional properties that are primarily determined by the demands of the environment that they are in. Some intriguing properties are, to name a few: high toughness, good adhesion, formation of structural colors, high stiffness and strength, low density, self reparing, dynamic adaptation to external stimuli, etc. The basic ingredients and the processes at which these biological materials are formed, unlike many man-made products, are made in an energy and resource efficient manner. There is a considerable desire to make materials with as as little waste as possible, while remaining economically effective, therefore the bio-based processes present themselves as a logical source of inspiration in materials science.

7.1.1 Orientation of biopolymer clay bionanocomposites

We have observed that the Na-Alg/MMT suspension goes from complete disorder to a highly ordered structure after drying. This phenomenon, also observed by others has raised a lot of attention in the analysis of the properties resulting from such structures, but there has been a lack of understanding how these structures are actually formed. This transition from disorder to order is achieved by a facile method of puring a Na-Alg/MMT suspension and allowing it to dry.

From the results presented in this work we have demonstrated that the formation of such ordered structures can be achieved via the gel network that immobilizes the randomly distributed MMT platelets and limits the number of degrees of freedom. This gel network is caused by interaction of the negatively charged alginate backbone and positively charged MMT edges and/or H-bonding**.** We have studied the rheological response of the Na-Alg/MMT suspension to examine the interactions that occur in the system, and observed a critical concentration of the MMT platelets that causes a solid-like response of the suspension. The corresponding Na-Alg/MMT gel-like structure is dynamic in nature, as we have observed a structural relaxation at long timescales that is attributed to the breaking and reforming of the transient MMT-alginate network.

The formation of the gel network is just one part of the formation of the ordered structure. The second part is the speed of drying that has to be faster than the relaxation times of the network itself. In addition to the gel dynamics and the drying speed we have also investigated the effect of the drying front, which we

find determines the alignment direction of the organized structure. This has been observed using optical polarisation microscopy.

In our opinion this unexplored topic should be examined in more detail due to the large number of possibilities to create optically interesting and potentially useful materials.

This research has also been extended to other biopolymers, as shown in Chapter 1, namely k-carrageenan, which is a thermally reversible polysaccharide, where the intention was to show that decreasing the total solid content of the k-carrageenan/MMT suspension resulted in a higher strain on the MMT platelets during drying. We find that this indeed was the system with the highest order parameter described in this thesis.

7.1.2 Properties of the Na-Alg/MMT bionanocomposite

Next, we have looked at how the addition of the MMT platelets and the resulting highly ordered structure is reflected on the properties of the Na-Alg/MMT bionanocomposites. We have measured the stiffness of the material over a wide range of temperatures for various MMT concentrations and find that unidirectional reinforcement of the Na-Alg with MMT platelets results in considerable increase in the stiffness of the bionanocomposite films, with a maximum at 50 wt.% MMT. We observe a drop in the stiffness for the 80 wt.% MMT system, which we believe is a result of restacking of the MMT platelets, which reduces the effective aspect ratio. The Halpin-Tsai model was useful to investigate the influence of the level of alignment and the MMT concentration on the stiffness of the bionanocomposite, also allowing to quantify the restacking behaviour of the MMT platelets.

A very interesting property of the Na-Alg/MMT bionanocomposite is a quite high heat deflection temperature at around 200 °C, while for the Na-Alg with 80 wt.% MMT we observe a new network formation during thermal decomposition that is responsible for extension of the heat deflection temperature above 240 °C. After the heat treatment the Na-Alg with 80 wt.% MMT has been completely charred, but it remained structurally intact with minimal volume change, which provides an important advantage for various application where thermal stability is of high importance, e.g. using as a covering for electrical cables to prevent short circuits caused by over heating. The non-flammability of this material is induced by the high level of order in the system, which considerably decreases the diffusion of oxygen and volatile degradation molecules, which in turn does not allow a flame to be sustained.

The search for bio-based, non-toxic, and biodegradable materials for packaging or

as coatings is increasing due to the environmental risk concerns and desire to create a circular economy. The addition of platelet-shaped filler with a high aspect ratio, e.g. bentonite clay, is already a proven way to enhance the barrier properties of polymers, which allows the thickness of the coating film to be reduced. Motivated by the highly ordered Na-Alg/MMT bionanocomposite, we have shown that the addition of the MMT platelets significantly reduces the water vapor sorption kinetics. As a result of the high aspect ratio of the MMT platelets the penetrating water molecules have a longer tortuous path trough the bionanocomposite. At high MMT concentrations the diffusion coefficient is still reduced, but the effectiveness is decreased due to restacking of the MMT platelets reducing the effective aspect ratio. We observe that the restacking behaviour of the MMT platelets during film formation scales with the MMT concentration as $<N> \propto \varphi_f^{0.5}$. We find such behavior in living polymers, where the average polymer chain length, expressed by the mean-field theory, is in equilibrium of bond breaking and reforming.

In addition, the bionanocomposites show a clear decrease in the water sorbing capacity, which we attribute to the preferred MMT-Alg interactions.

The highly ordered films developed in this work have a potential as free standing membrane materials, but further work needs to be performed to reduce the water uptake capacity, since the properties of these bionanocomposites are humidity dependent. This could be achieved by crosslinking the structure an form an alginate-based termoset or modification of the carboxylic group via amidizing and or esterification. Future work should be done on measuring the barrier properties of this bionanocomposite for other gases, such as H_2, O_2, methanol vapor, and CO_2.

7.1.3 Applications of the Na-Alg/MMT bionanocomposite

We have shown in Chapter 6 that the Na-Alg solution can be successfully applied as a curing compound for cement-based materials by ensuring that the water is kept in the cement-based material during the hydration reaction. Using the water-based Na-Alg solution we take advantage of the rapid gel-forming ability of Na-Alg with divalent cations (mainly Ca^{2+}) that are readily available on the surface of fresh cement-based materials to produce a water insoluble membrane. The quality of the curing was examined by electron microscopy and the chloride migration test. This showed a very dense structure with less cracks and substantial decrease in the non-steady state chloride migration coefficient, compared to untreated control sample. In addition, we have shown that even though the Na-Alg reacts with the free Ca^{2+} from the surface of the cement-based material, we find a higher leaching of calcium

from the control sample compared to the Na-Alg cured sample.

The advantage of using this system is that it is an all natural-based bionanocomposite, free of volatile organic solvents, and the gel forming ability prevents flowing of the curing compound into the cement-based material, which allows proper cement hydration to occur. Also, we have shown that the addition of the MMT platelets drastically decreases the water diffusion coefficient, which we expect will improve the performance of cement-based materials in harsh environments that normally promote the loss of water.

7.2 The future of nacre-like bionanocomposites

New and innovative developments in the field of wastewater treatment technology have been introduced in the form of aerobic granular sludge that has led to a considerable increase in separation efficiency of biomass and water compared to conventional flocculent sludge. This means that the operation, construction costs, and spatial requirements are greatly reduced (De Kruek et al. 2010). This process has been commercialised under the trade name Nereda®.

Looking more closely we observe that the aerobic granules themselves are a composite materials composed of bacteria, phosphates, sand, and biofilm (Yuemei et al. 2010). Here, we focus on a specific part of the granule, namely the exopolymeric substance (EPS), which has a binding and protective property. The name EPS is a generic name for macromolecules that are synthesized as an external protection by microbial cells, and which can vary greatly in their chemical and physical properties (Sutherland 2001). A large fraction of the granular sludge has been identified as an alginate-like exopolymer (ALE) (Felz et al. 2016). Considering the rapid success of the aerobic granular sludge technology with at present over 30 operational full scale wastewater treatment plants built all over the world, there is an enormous potential in harvesting and obtaining the ALE polymer. This can lead to a totally new class of materials that are likely to have a broad appeal due to their excellent properties, low cost, and low environmental impact.

To show the potential of this biopolymer, we have performed some preliminary experiments and have replicated the Na-Alg/MMT bionanocomposite by replacing Na-Alg with Na-ALE. The ALE was obtained from the aerobic granular sludge, using the alkaline extraction method described elsewhere (Yuemei et al. 2010, Yuemei et al. 2013). The ALE was concentrated to a 3 wt.% solution, to which a 3 wt.% MMT suspension was added, and was further mixed overnight. The total solid content was

kept at 3 wt.%, with MMT concentrations of 5, 10, 20, 50, and 80 wt.% with respect to mass of Na-Alg. The suspensions were poured on to a petri dish and dried under ambient conditions (20 °C and 50% RH) and further dried completely in a vacuum oven at 40 °C. The bionanocomposite film samples were kept in a desiccator prior to any measurement.

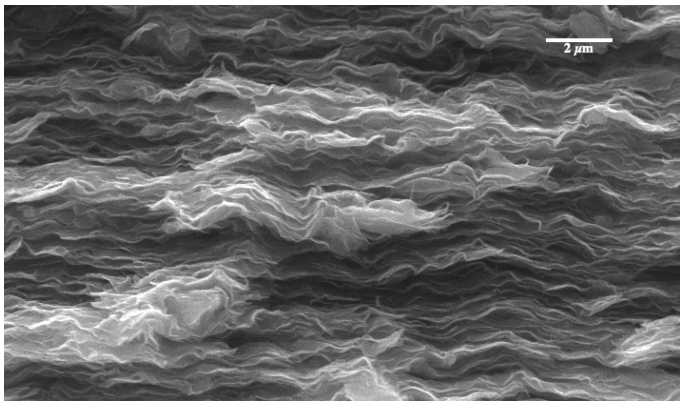

Figure 7.1: ESEM micrographs of a cross section of a Na-ALE with 80 wt.% MMT.

As we can see from the ESEM micrograph presented in figure 7.1, it is indeed possible to achieve the same highly aligned, nacre-like, microstructure using Na-ALE and MMT. To our knowledge this is the first reported nacre-like bionanocomposite produced with a biopolymer extracted from wastewater treatment process. From the WAXS we also see increased d-spacing of the 001 reflection for the bionanocomposite samples with Na-ALE, which means that higher levels of exfoliation and intercalation within the MMT galleries, compared to the Na-Alg/MMT system, which might be due to the lower molecular mass of the Na-ALE.

To quantify the degree of orientation, as we have shown previously, we integrated over the azimuthal intensity profile and fitted the curves to the affine deformation ODF and calculated the $<P_2>$ value. In figure 7.2, we observe slightly lower order parameters for the Na-ALE-/MMT bionanocomposite compared to the Na-Alg/MMT although the same trends are found.

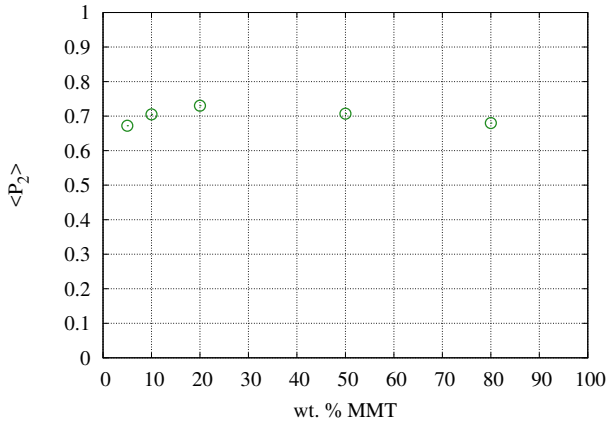

Figure 7.2: Order parameter of ALE/MMT bionanocomposite as a function of the MMT concentration.

In figure 7.3, we report on the thermomechanical response of the Na-ALE/MMT bionanocomposite with 50 and 80 wt.% MMT where we can see the similarly high storage modulus as measured for Na-Alg/MMT bionanocomposite. The mechanical properties at lower MMT concentrations were not found, due to a higher brittleness of the films, making them difficult to handle.

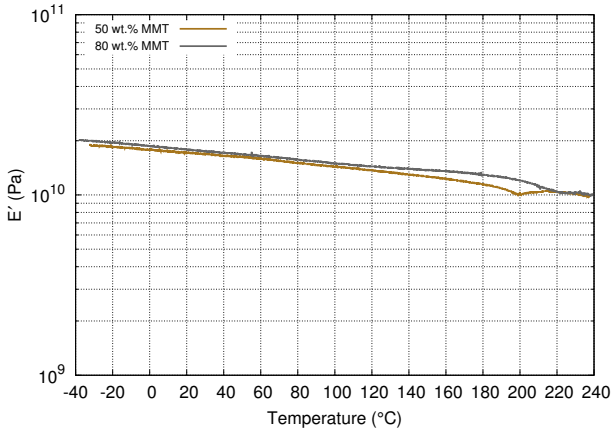

Figure 7.3: Measured dynamic storage modulus of Na-ALE/MMT nanocomposites with 50 and 80 wt.% MMT.

The potential of making high performance bionanocomposite using the biopolymers harvested from wastewater treatment presents itself as a possible breakthrough in polymer nanocomposite science and technology.

The Na-ALE/MMT system can also be used for curing cement-based materials, and we believe that due to the reported higher hydrophobicity of this material it has the possibility to even surpass the performance of the Na-Alg/MMT bionanocomposite, Chapter 6, in keeping the water tightly inside during the cement hydration (Lin et al. 2015).

7.3 Concluding remarks

The materials found in nature meet the requirements posed by the environment using a design solution developed via evolution, taking into account the constrain on the available constituents and the conditions of the surroundings. We are strongly convinced that the development of nature inspired materials presents itself as a legitimate way forward in material science that will be based primarily on the functionality and the required performance, with the added benefit of using components that are sustainable and biodegradable. Furthermore, there is an urgent demand to understand the synergic effect of the building blocks that make up these lightweight bionanocomposites, which surpass those of their individual components by orders of magnitude (Wang et al. 2001, Meyers et al. 2007, Wegst et al. 2011).

The anisotropic behavior of the materials developed in this work opens a wide range of application possibilities. Furthermore, our procedure to make highly ordered structures can be applied for a multitude of different polymers (including synthetic ones) and for different fillers, which offers a facile production of anisotropic membranes with different functional properties.

The biggest impact we see in further development of (nano)composite materials made with biopolymers extracted from aerobic granular sludge. By presenting itself as a efficient technology in both wastewater treatment and materials science, we see a potential strategy to produce high performance lightweight materials that have a combination of stiffness, barrier, and functional (conductivity, binding, etc.) properties. While this can be done at high volume, low cost, which is compatible with the desire to obtain a fully circular economy.

References

Abend, S.; Lagaly, G. "Sol-gel transition of sodium montmorillonite dispersions." *Applied Clay Science* **2000**, 16, 201-227.

Al-Gahtani, A. S. "Effect of curing methods on the properties of plain and blended cement concretes." *Construction and Building Materials* **2010**, 24, 308-314.

Arce, A.; Fornasiero, F.; Rodríguez, O.; Radke, C. J.; Prausnitz, J.M. "Sorption and transport of water vapor in thin polymer films at 35 ºC." *Physical Chemistry Chemical Physics* **2004**, 6, 103-108.

Barber A. H.; Lu, D.; Pugno, N.M. "Extreme strength observed in limpet teeth." *Journal of the Royal Society Interface* **2015**, 12(105), p. 20141326.

Barthelat, F.; Li, C. M.; Comi, C.; Espinosa, H. D. "Mechanical properties of nacre constituents and their impact on mechanical performance." *Journal of Materials Research* **2006**, 21, 1977-1986.

Bentz, D.P.; Jensen, O.M.; Coats, A.M.; Glasser, F.P. "Influence of silica fume on diffusivity in cement-based materials: I. Experimental and computer modeling studies on cement pastes." *Cement and Concrete Research* **2000**, 30(6), 953-962.

Bharadwaj, R. K. "Modeling the barrier properties of polymer-layered silicate nanocomposites." *Macromolecules* **2001**, 34, 9189-9192.

Bhushan, B. "Biomimetics: lessons from nature - an overview." *Philosophical Transaction of the Royal Society A* **2009**, 367, 1445-1486.

Blumstein, A. "Polymerization of adsorbed monolayers. II. Thermal degradation of the inserted polymer." *Journal of Polymer Science Part A: General Papers* **1965**, 3, 2665−2672.

Bouwmeester - van den Bos, W.J.; Schlangen E. "Influence of curing on the pore structure of concrete." Walraven & Stoelhorst (eds) *Tailor Made Concrete Structures*, London, Taylor & Francis Group, **2008**.

Bradenburg, U.; Lagaly, G. "Rheological properties of sodium montmorillonite dispersions." *Applied Clay Science* **1988**, 3, 263-279.

Cates, M. E.; Candau, S. J. "Statics and dynamics of worm-like surfactant micelles." *Journal of Physics: Condensed Matter* **1990**, 2, 6869-6892.

Choudalakis, G.; Gotsis, A. D.; Schut, H.; Picken, S. J. "The free volume in acrylic resin/laponite nanocomposite coatings." *European Polymer Journal* **2011**, 47 (3), 264-272.

Crank, J. *The mathematics of diffusion*, 2nd ed.; Oxford University Press, Oxford **1975**.

Darwin, C. R. *On the origin of species*, John Murray, London **1859**.

Das, P.; Schipmann, S.; Malho, J. M.; Zhu, B.; Klemradt, U.; Walther, A. "Facile access to large-scale, self-assembled, nacre-inspired, high-performance materials with tunable nanoscale periodicities." *ACS Applied Materials & Interfaces* **2013**, 5, 3738−3747.

De Kreuk, M. K.; Van de Poel, I. R.; Zwart, S. D.; Van Loosdrecht, M. C. M. "Ethics in innovation: Cooperation and tension" In I. R. van Poel & D. E. Goldberg (Eds.), Philosophy and engineering: An emerging Agenda, **2010**, 215-226, Dordrecht: Springer.

Doblhofer, E.; Schmid, J.; Reiß, M.; Daab, M.; Suntinger, M.; Habel, C.; Bargel, H.; Hugenschmidt, C.; Rosenfeldt, S.; Breu, J.; Scheibel, T. "Structural insights into water-based spider silk protein-nanoclay composites with excellent gas and water vapor barrier properties." *ACS Applied Materials & Interfaces* **2016**, 8, 25535-25543.

Draget, K. I.; Skjåk-Bræk, G.; Smidsrød, O. "Alginate Based New Materials." *International Journal Biological Macromolecules* **1997**, 21, 47−55.

Ebina, T.; Mizukami, F. "Flexible Transparent Clay Films with Heat-Resistant and High Gas-Barrier Properties" *Advanced Materials* **2007**, 19, 2450-2453.

Fan, S. M.; Luckhurst, G. R.; Picken, S. J. "A deuterium nuclear magnetic resonance investigation of orientational order and director kintetics in aramid solutions." *Journal of Chemical Physics* **1994**, 101, 3255−3267.

Felz, S.; Al-Zuhairy, S.; Aarstad, O.A.; van Loosdrecht, M.C.M.; Lin, Y.M. "Extraction of structural extracellular polymeric substance from

aerobic granular sludge." *J. Vis. Exp.* **2016**, 115.

Ferry, J. D. *Viscoelastic properties of polymers* Wiley (3rd edition), New York, **1980**.

Fornes, T.D.; Paul, D.R. "Modeling properties of nylon 6/clay nanocomposites using composite theories." *Polymer* **2003**, 44, 4993-5013.

Giannelis, E. P. "A new strategy for synthesizing polymer-ceramic nanocomposites." *JOM* **1992**, 44(3), 28-30.

Giannelis, E. P. "Polymer layered silicate nanocomposites" *Advanced Materials* **1996**, 8(1), 29-35.

Gorin, P. A. J.; Spencer, J. F. T. "Exocellular alginic acid from azotobacter vinelandii." *Canadian Journal of Chemistry* **1966**, 44, 993−998.

Grasdalen, H.; Larsen, B.; Smidsrød, O. "^{13}C-NMR studies of monomeric composition and sequence in alginate." *Carbohydrate Research* **1981**, 89, 179−191.

Van der Gucht, J.; Besseling, N. A. M. "Statistical thermodynamics of equilibrium polymers at interfaces." *Physical Review E* **2002**, 65, 051801.

Halpin, J. C.; Kardos, J. L. "Halpin-Tsai equatons - review." *Polymer Engineering and Science* **1976**, 16(5), 344-352.

Harrats, C.; Groeninckx, G. "Features, questions and future challenges in layered silicates clay nanocomposites with semicrystalline polymer matrices." *Macromolecular Rapid Communications* **2007**, 29, 14-26.

Hover, K.C. "The influence of water on the performance of concrete." *Construction of Building Materials* **2011**, 25, 3003-3013.

Jaber, M.; Georgelin, T.; Bazzi, H.; Costa-Torro, F.; Lamber, J. F.; Bolbach, G.; Coldic, G. "Selectivities in adsorption and peptidic condensation in the (arginine and glutamic acid)/montmorillonite clay system." *Journal of Physical Chemistry C* **2014**, 118, 25447-25455.

Jackson, A. P.; Vincent, J. F. V.; Turner, R. M. "The mechanical design of nacre." *Proceedings Of The Royal Society B* **1988**, 234, 415-440.

Jestin, J.; Cousin, F.; Dubois, I.; Ménager, C.; Schweins, R.; Oberdisse, J.; Boué, F. " Anisotropic reinfocement of nanocomposites tuned

by magnetic orientation of the filler network." *Advanced Materials*, **2008**, 20, 2533-2540.

Kakisawa, H.; Sumitomo, T. "The toughening mechanism of nacre and structural materials inspired by nacre." *Science and Technology of Advanced Materials* **2011**, 12:6, 064710.

Kochumalayil, J. J.; Bergenstråhle-Wohlert, M.; Utsel, S.; Wågberg, L.; Zhou, Q.; Berglund, L. A. "Bioinspired and highly oriented clay nanocomposites with a xyloglucan biopolymer matrix: extending the range of mechanical and barrier properties." *Biomacromolecules* **2013**, 14, 84−91.

Kojima, Y.; Usuki, A.; Kawasumi, M.; Okada, A.; Fukushima, Y.; Kurauchi, T.; Kamigaito, O. "Mechanical properties of nylon 6-clay hybrid." *Journal of Materials Research* **1993**, 8, 1185−1189.

Kojima, Y.; Usuki, A.; Kawasumi, M.; Okada, A.; Kurauchi, T.; Kamigaito, O. "Sorption of water in nylon 6-caly hybrid." *Journal of Applied Polymer Science* **1993**, 49(7), 1259-1264.

Krishnamoorti, R.; Vaia, R.A.; Giannelis, E.P. "Structure and dynamics of polymer-layered silicate nanocomposites." *Chemistry of Materials* **1996**, 8, 1728-1734.

Kuhn, W.; Grün, F. "Beziehungen zwischen elastischen Konstanten und Dehnungsdoppelbrechung hochelastischer." *Kolloid-Zeitschrift* **1942**, 3, 248−271.

Larson R.G. *The structure and rheology of complex fluids* Oxford University Press, New York, **1999**.

Laurienzo, P. "Marine Polysaccharides in Pharmaceutical Applications: An Overview." *Marine Drugs* **2010**, 8, 2435−2465.

Lin, Y.M.; de Kreuk, M.; van Loosdrecht, M.C.M.; Adin, A. "Characterization of alginate-like exopolysaccharides isolated from aerobic granular sludge in pilot-plant." *Water Research* **2010**, 44(11), 3355-3364.

Lin, Y.M.; Sharma P.K.; van Loosdrecht, M.C.M. "The chemical and mechanical differences between alginate-like exopolysaccharides isolated from aerobic flocculent sludge and aerobic granular sludge." *Water Research* **2013**, 47(1), 57-65.

Lin Y.M.; Nierop K.G.J.; Girbal-Neuhauser E.; Adriaanse M.; van Loosdrecht M.C.M. "Sustainable polysaccharide-based biomaterial recovered from waste aerobic granular sludge as a surface coating material." *Sustainable Materials and Technologies* **2015**, 4, 24-29.

Linker, A.; Jones, R. S. "A New Polysaccharide Resembling Alginic Acid Isolated from Pseudomonads." *Journal of Biological Chemistry* **1966**, 241, 3845−3851.

Liu, T.; Tjiu, W.C.; Tong, Y.; He, C.; Goh, S.S.; Chung, T.S. "Morphology and fracture behavior of intercalated epoxy/clay nanocomposites." *Journal of Applied Polymer Science* **2004**, 94, 1236-1244.

Liu, Y.; Soer, W. J.; Scheerder, J.; Satgurunathan, G.; Keddie, J. L. "Water Vapor Sorption and Diffusion in Secondary Dispersion Barrier Coatings: A Critical Comparison with Emulsion Polymers." *ACS Applied Materials & Interfaces* **2015**, 7, 12147-12157.

Losego, M.D.; Grady, M.E.; Sottos, N.R.; Cahill, D.G.; Braun, P.V. " Effects of chemical bonding on heat transport across interfaces." *Nature Materials **2012**,* 11, 502-506.

Losego, M. D.; Blitz, I. P.; Vaia, R. A.; Cahill, D. G.; Braun, P. V. "Ultralow Thermal Conductivity in Organoclay Nanolaminates Synthesized via Simple Self-Assembly." *NANO Letters **2013**,* 13, 2215-2219.

Long, F. A.; Richman D. "Concentration Gradients for Diffusion of Vapors in Glassy Polymers and their Relation to Time Dependent Diffusion Phenomena." *Journal of American Chemical Society* **1960**, 82, 513-519.

Luckhurst, G. R.; Zannoni, C. "Why is the Maier–Saupe theory of nematic liquid crystals so successful?" *Nature* **1977**, 167, 412−414.

Maier, W.; Saupe, A. Z. "Eine einfache molekular-statistische Theorie der nematischen kristallinflüssigen Phase 1" *Naturforsch* **1959**, A14, 882.

Maier, W.; Saupe, A. Z. "Eine einfache molekular-statistische Theorie der nematischen kristallinflüssigen Phase 2." *Naturforsch* **1960**, A15, 287.

Matthew, I. R.; Browne, R. M.; Frame, J. W.; Millar, B. G. "Subperiosteal behaviour of alginate and cellulose wound dressing materials." *Biomaterials* **1995**, 16, 275−278.

Meeks, K. W.; Carino, N. J. "Curing of High-Performance Concrete: Report of the State-of-the-Art." National Institute of Standards and Technology Report, NISTIR 6295, **1999**.

Messersmith, P. B.; Giannelis, E. P. "Synthesis and barrier properties of poly (ε-caprolactone)-layered silicate nanocomposites." *Journal of Polymer Science Part A: Polymer Chemistry* **1995**, 33, 1047-1057.

Meyers, M. A.; Lin, A. Y.; Chen, P.; Muyco, J. "Mechanical strength of abolone nacre: Role of the soft organic layer." *Journal of the Mechanical Behavior of Biomedical Materials* **2008**, 1(1), 76-85.

Miano, F.; Rabaioli, M. R. "Rheological scaling of montmorillonite suspensions: the effect of electrolytes and polyelectrolytes." *Colloids and Surfaces A: Physicochemical and Engineering Aspects* **1994**, 84, 229-237.

Miller, S. A.; Horvath, A.; Monteiro, P. J. "Readily implementable techniques can cut annual CO_2 emissions from the production of concrete by over 20%." *Environmental Research Letters* **2016**, 11, 074029.

Munch, E.; Launey, M. E.; Alsem, D. H.; Saiz, E.; Tomsia, A. P.; Ritchie, R. O. "Tough, bio-inspired hybrid materials." *Science*, **2008**, 322, 1516-1520.

Naficy, S.; Jalili, R.; Aboutalebi, S. H.; Gorkin III, R. A.; Konstantinov, K.; Innis, P. C.; Spinks, G. M.; Poulin, P.; Wallace, G. G. "Graphene oxide dispersions: tuning rheology to enable fabrication." *Materials Horizon* **2014**, 1, 326-331.

Narayanan, R. P.; Melman, G.; Letourneau, N. J.; Mendelson, N. L.; Melman, A. "Photodegradable iron(III) cross-linked alginate gels." *Biomacromolecules* **2012**, 13, 2465-2471.

Neville, A. M. *Properties of concrete* Wiley, New York, **1995**.

Nielsen, L. E. "Models for the permeability of filled polymer systems." *Journal of Macromolecular Science, Chemistry* **1967**, 1, 929−942.

Okada, A.; Usuki, A. "The chemistry of polymer-clay hybrids." *Material Science and Engineering, C* **1995**, 3, 109−115.

Picken, S. J. "Orientational order in aramid solutions determined by diamagnetic susceptibility and birefringence measurements." *Macromolecules* **1990**, 23, 464-470.

Picken, S. J.; Aerts, J.; Visser, R.; Northolt, M. G. "Structure and rheology of aramid solutions: X-ray scattering measurements." *Macromolecules* **1990**, 23, 3849-3854.

Picken, S.J.; Aerts, J.; Doppert, H.L.; Reuvers, A.J.; Northolt, M.G. "Structure and rheology of aramid solutions: transient rheological and rheooptical measurements." *Macromolecules* **1991**, 24, 1366-1375.

Picken, S.J.; van der Zwaag, S.; Northolt, M.G. "Molecular and macroscopic orientational order in aramid solutions: a model to explain the influence of some spinning parameters on the modulus of aramid yarns." *Polymer* **1992**, 33, 2998-3006.

Powers, T.C.; Brownyard, T.L. *Journal of the American Concrete Institute* **1946-1947**, 18, 1-9.

Putz, K.W.; Compton, O.C.; Segar, C.; An, Z.; Nguyen, S.T.; Brinson L.C. "Evolution of order during vacuum-assisted self-assembly of graphene oxide paper and associated polymer nanocomposites." *ACS Nano* **2011**, 5 (8), 6601-6609.

Ramezanianpour, A.A.; Malhorta, V.M. "Effect of curing on the compressive strength, resistance to chloride-ion penetration and porosity of concretes incorporating slag, fly ash or silica fume." *Cement and Concrete Composites* **1995**, 17(2), 125-133.

Ray, S. S.; Okamoto, M. "Polymer/layered silicate nanocomposites: a review from preparation to processing." *Progress in Polymer Science* **2003**, 28(11), 1539-1641.

Richardson, I.G. "The nature of the hydration products in hardened cement pastes." *Cement and Concrete Composites* **2000**, 22, 97-113.

Roderick, G.L. "Water vapor sodium montmorillonite ineraction" Iowa State University of Science and Technology, Ames, 1965.

Ross, A. B.; Hall, C.; Anastasakis, K.; Westwood, A.; Jones, J. M.; Crewe, R. J. "Influence of cation on the pyrolysis and oxidation of

alginates." *Journal of Analytical and Applied Pyrolysis* **2011**, 91, 344-351.

Rowbotham, J. S.; Dyer, P. W.; Greenwell, H. C.; Selby, D.; Theodoru, M. K. "Copper(II)-mediated thermolysis of alginates: a model kinetic study on the influence of metal ions in the thermochemical processing of microalgae*"Interface Focus* **2013**, 3, 20120046.

Russo, R.; Malinconico, M.; Santagata, G. "Effect of cross-linking with calcium ions on the physical properties of alginate films." *Biomacromolecules* **2007**, 8, 3193-3197.

Schult, K. A.; Paul, D. R. "Techniques for measurement of water vapor sorption and permeation in polymer films." *Journal of Applied Polymer Science* **1996**, 61, 1865-1876.

Sehaqui, H.; Kochumalayil, J.; Liu, A.; Zimmermann, T.; Berglund, L. A. "Multifunctional nanoclay hybrids of high toughness, thermal, and barrier performances." ACS Applied Materials & Interfaces **2013**, 5, 7613-7620.

Shchipunov, Y.; Ivanova, N.; Silant'ev, V. "Bionanocomposites formed by in situ charged chitosan with clay." *Green Chemistry* **2009**, 11, 1758-1761.

Shchipunov, Y. "Bionanocomposites: Green sustainable materials for the near future." *Pure and Applied Chemistry* **2012**, 84(12), 2579-2607.

Shell, H. R.; Ivey K. H. "Fluorine micas" Bureau of Mines, Bulletin 647, US Department of the interior **1969**.

Siddique, R.; Kahn, M. I. *Supplementary Cementing Materials,* Springer, Berlin/Heidelberg, **2011**.

Sun, Y. M. "Sorption/desorption properties of water vapour in poly (2-hydroxy-ethyl methacrylate): 2. two-stage sorption models." *Polymer* **1996**, 37, 3921-3928.

Sutherland I. W. "Biofilm exopolysaccharides: a strong and sticky framework." *Microbiology* **2001**, 147, 3-9.

Tang, Z.; Kotov, N. A.; Magonov, S.; Ozturk, B. "Nanostructured artificial nacre." *Nature Materials* **2003**, 2, 413−418.

Tateyama, H.; Scales, P. J.; Ooi, M.; Nishimura, S.; Rees, K.; Healy, T. W. "X-ray diffraction and rheology study of highly ordered clay

platelet alignment in aqueous solutions of sodium tripolyphosphate." *Langmuir* **1997**, 13, 2440−2446.

Taylor, H. F. W. *Cement Chemistry* Thomas Telford publishing, London, **1997**, ISBN 978-0727725929

Te Nijenhuis, K. "On the nature of crosslinks in thermoreversible gels." *Polymer Bulletin* **2007**, 58, 27-42.

Ten Brinke, A. J. W.; Bailey, L.; Lekkerkerker, H. N. W.; Maitland, G. C. "Rheology modification in mixed shape colloidal dispersions. Part I: pure components." *Soft Matter* **2007**, 3, 1145-1162.

Theng, B. K. G. "The Clay Minerals." *Developments in Clay Science* **2012**, 4, 3-45.

Tjong, S. C. "Structural and mechanical properties of polymer nanocomposites." *Materials Science and Engineering R* **2006**, 73-197.

Van Es, M. A. "Polymer-Clay Nanocomposites: The importance of particle dimensions." Applied Sciences, Delft University of Technology, Delft, 2001.

Vanorio, T.; Prasad, M.; Nur, A. "Elasric properties of dry clay mineral aggregates, suspensions and sandstones." *Geophisical Journal International* **2003**, 155(1), 319-326.

Vlasveld, D. P. N. "Fibre reinforced polymer nanocomposite." Applied Sciences, Delft University of Technology, Delft, 2005.

Walther, A.; Bjurhager, I.; Malho, J. M.; Pere, J.; Ruokolainen, J.; Berglund, L. A.; Ikkala, O. "Large-area, lightweight and thick biomimetic composites with superior material properties via fast, economic, and green pathways." *Nano Letters* **2010**, 10, 2742−2748.

Walther, A.; Bjurhager, I; Malho, J. M.; Ruokolainen, J.; Berglund, L.; Ikkala, O.; "Supramolecular control of stifness and strength in lightweight high-performance nacre-mimetic paper with fire-shielding properties." *Angewandte Chemie International Edition*, **2010,** 49(36), 6448-6453.

Wang, J.; Dhir, R. K.; Levitt, M. "Membrane curing of concrete: moisture loss." *Cement and Concrete Research* **1994**, 24, 1463-1474.

Wang, R. Z.; Suo, Z.; Evans, A. G. "Deformation mechanisms in nacre." *Journal of Material Research* **2001**, 16(9), 2485-2493.

Watanabe, T.; Sato, T. "Expansion characteristics of montmorillonite and saponite under various relative humidity conditions." *Clay Science* **1988**, 7, 129−138.

Wegst, U. G. K.; Bai, H.; Saiz, E.; Tomsia, A.P.; Ritchie R. O.; "Bioinspired structural materials." *Nature Materials* **2014**, 14, 23-35.

Wu, L.; Ohtani, M.; Takata, M.; Saeki, A.; Seki, S.; Ishida, Y.; Aida, T. "Magnetically induced anisotropic orientation of graphene oxide locked by in situ hydrogelation." *ACS Nano* **2014**, 8, 4640−4649.

Yao, H. B.; Tan, Z. H.; Fang, H. Y.; Yu, S. H. "Artificial nacre-like bionanocomposite films from the self-assembly of chitosan–montmorillonite hybrid building blocks." *Angewandte Chemie International Edition* **2010**, 49, 10127−10131.

Zlopasa, J.; Koenders, E. A. B.; Picken, S. J. "A novel bio-based curing compound for cement-based materials." V. Mechtcherine, C. Schroefl (Eds.), *Proceedings of the international RILEM conference application of superabsorbent polymers and other new admixtures in concrete construction*, Dresden, Germany, Sept 14–17, RILEM Publications S.A.R.L. **2014**.

Zlopasa, J.; Koenders, E. A. B.; Picken, S. J. "Using bio-based polymers for curing cement-based materials." *AMS '14 Proceedings of the international conference on ageing of materials & structures*, Delft 26 - 28 May 2014, The Netherlands.

Zlopasa, J.; Norder, B.; Koenders, E. A. B.; Picken, S.J. "Origin of highly ordered sodium alginate/montmorillonite bionanocomposites." *Macromolecules* **2015**, 48, 1204-1209.

Zlopasa, J.; Norder, B.; Koenders, E. A. B.; Picken, S. J. "Rheological investigation of specific interactions in Na Alginate and Na MMT suspension." *Carbohydrate Polymers* **2016**, 151, 144-149.

Summary

Nature displays a multitude of fascinating materials, from beautiful colors of butterfly wings to the toughness of mullosc shells, which are formed in mild enviornmental conditions with commonly occuring materials, such as chitosan or calcium carbonate. These composite materials display an intricate interplay of biopolymers and minerals forming highly ordered structure. The function of these materials is primarily determined by the selective pressure of the enviornment that certain organisms are placed in. It varies from the "delicate" signaling colors to a robust impact resistence.

In **Chapter 2**, we have analysed the in-plane alingment of the Na-Alg/MMT bionanocomposite films by environmental scanning electron microscopy (ESEM) and wide-angle X-ray scattering (WAXS). Looking at the 2D X-ray scattering images we observed a clear angle dependency, which confirms preferential orientation of montmorillonite (MMT) platelets. The order parameter ($<P_2>$) was calculated from azimuthal intensity profiles derived from WAXS measured over the MMT 001 reflection, using the Maier−Saupe and the affine deformation model. These models are used to analyse the origin of the nanostructural ordering of the bionanocomposites, and it present two plausable extreme cases how the development of the highly ordered structure. The Maier-Saupe model is used in liquid crystals theory to describe the spontaneous ordering of nematic crystals, while the affine deformation model describes the change in orinetational order in an ideal rubber due to elongation. From our results we find that the affine deformation model describes our system more accuratelly and it further requires a gel formation achieved by alginate adsorption on the edges of MMT, which develops yield stress and deforms the MMT platelets during drying resulting in high range $<P_2>$ values. We observed that the $<P_2>$ values have a MMT concentration dependency, which is also explained by the MMT−alginate interaction. The perfered orientation of the MMT platelets in the NA-Alg/MMT system was further analysed under a polarizing optical microscope, where we imposed two directions of drying and showed a dependancy the direction of the MMT orientation.

Following the assumption that the interaction of the MMT platelets and the alginate are required for the development of the highly ordered structure, in **Chapter 3,** the Na-Alg/MMT suspensions were examined by small amplitude oscillatory shear experiments. The viscoelastic behaviour of the Na-Alg/MMT suspension is

greatly affected by increasing the volume fraction of the MMT platelets. This has led to a gel-like behaviour of the suspension, which is attributed to interactions of MMT and alginate via H-bonding and attraction between the positive edges of the platelets and the anionic backbone of the biopolymer. A critical concentration for the measured system was observed at 20 wt.% montmorillonite, where a crossover to a gel-like structure was detected. The observed gel has a rubber plateau, which develops further with higher montmorillonite concentration. The physical gel has a measured relaxation maximum, which is attributed to the breaking and reformation of the bonds between the platelets and alginate. For this transient behavior, we find that a Maxwell type viscoelasticity quite well describes the relaxation time and the observed G'-G" crossover. We believe that this gel-like behavior plays an important role in formation of highly ordered nanostructures that develop during the drying of these bio-nanocomposite suspensions.

The thermomechanical and thermal properties of Na-Alg/MMT bionanocomposite films with varying MMT content are presented in **Chapter 4**. The highly organised "brick-and-mortar" structure is reflected in the measured mechanical properties. The unidirectional orientation of the reinforcing MMT platelets was described well by Halpin-Tsai model where we took in consideration the level of alignment, MMT loading, and the effective aspect ratio. The reinforcement efficiency is lower with increasing volume fraction of the filler, due to the stacking behaviour of MMT that reduces the effective aspect ratio. Additionally, the highly ordered structure resulted in complete non-flammibilty of the bionanocomposite that maintains and has considerable heat shielding.

In **Chapter 5**, motivated by non-flammibility presented in Chapter 4, we examined the water sorption kinetics of the Na-Alg/MMT bionanocomposites. The water sorption isotherms were analysed using a surface variable concentration model, which fitted the experimental results adequatelly. The bionanocomposite films displayed a decrease in the amount of water absorbed with increasing MMT content. By introducing impermeabile platelet-shaped filler (MMT) a tuorutous path is imposed to the diffusing molecules, which is reflected in considerable reduction of the calculated diffusion coefficient. The diffusion coefficient of a polymer clay nanocomposite depends on the orientation, overlap, effective aspect ratio, and the concnetration of clay. We used the $<P_2>$ values obtained in Chapter 2 to back-calculate the effective aspect ratio of the MMT platlets, using a modified Nielsen model. From this we noticed that with increasing MMT concentration the effective aspect ratio is decreasing, which is a result of re-stacking of the MMT platelets.

In **Chapter 6**, we have focused on the application of Na-Alg as a bio-based curing compound for cement-based materials. Nowdays, most concrete structures are designed and expected to last for at least 50 years or more. During their liftime, cement-based structures can be exposed to various environments, which can have detrimental effects on concrete itself, e.g. freeze-thaw, sulfate attack, or on corrosion of the steel reinforcement. On going cement hydration guarantees a durable cement-based microstructure in terms of bond between the aggregates, fewer voids, and depercolation of capillary pores, which is of particular importance for the near surface area of cement-based materials. A properly cured cement-based material is the ultimate preparation for a long service life, since it prevents the surface from drying. The principle of using Na-Alg as a curing compound is based on rapid cross-linking reaction with Ca^{2+} ions on the surface of cement-based material. In this way the curing compound does not penetrate inside the cement-based material (which can delay the cement hydration), forms a membrane on the surface that is prefered. The use od Na-Alg as a curing compound also has an advantage since it is water based and is enviromentally friendly. The performance of the alginate curing compound was examined experimentally, by Rapid Chloride Migration tests and Environmental Scanning Microscope observations on different samples to investigate the functional properties, e.g. ion transport, and microstructural investigation. The mortar samples were cured at 50% RH and 20 °C both with and without surface addition of the bio-based compound. Two different types of cement, CEM I and CEM III/B, were tested to study differences in curing performance. Significant beneficial effects were observed at the mortar surface when applying the bio-based curing compound showing reduced diffusivity. The results showed a very good quality surface with a high quality and durable microstructure. Also, a higher curing sensitivity was observed for the CEM III/B samples compared to samples prepared with CEM I. As we observed in Chapter 5, the highly ordered structure of Na-Alg/MMT bionanocomposte membranes considerably reduces the water diffusion, which means that the effectivness of the curing compound can be tuned based on how severe is the enviornment in which the cement-based material is placed in to hydrate.

In **chapter 7** the main conculsions have been drawn on the design, characterisation, and application of highly ordered Na-Alg/MMT bionanocomposites and its future prospects are briefly discussed. Through finding in this work new applications for the highly ordered bionanocomposites with varying filler and/or polymer matrix can be envisaged, which are based on control over the orientation of the filler. One of the biopolymers we have looked at was alginate-like exopolymer extracted

from the aerobic granular sludge wastewater treatment process, which shows great potential for making bionanocomposites.

Samenvatting

De Natuur zit vol met fascinerende materialen. Denk aan de prachtige kleuren van de vleugels van vlinders en de sterke schelpen van schaaldieren. Ze worden gevormd onder milde condities vanuit veel voorkomende natuurlijke ingrediënten, zoals chitosan en calciumcarbonaat. Deze natuurlijke composieten vertonen een subtiele wisselwerking tussen biopolymeren en minerale componenten en vertonen vaak regelmatig geordende structuren. De functie van deze materialen is ingegeven door selectiedruk uit de omgeving waarin de levende organismen zich bevinden. Dat varieert van de subtiliteit van signaalkleuren tot hoge mechanische slagvastheid. In **Hoofdstuk 2**, analyseren we de oriëntatie in het vlak van de films van Na-Alg/MMT bionanocomposieten door middel van "environmental scanning electron microscopy" (ESEM) en "wide-angle X-ray scattering" (WAXS). In de 2D Röntgendiffractie resultaten kan een hoge mate van oriëntatie worden vastgesteld, dat de hoge mate van uitlijning van de montmorilloniet (MMT) kleiplaatjes bevestigt en kwantificeert. De orde parameter ($<P_2>$) wordt berekend uit de door middel van WAXS gemeten azimuthale intensiteitsprofielen van de MMT (001) reflectie, door het fitten van het Maier-Saupe en het affiene deformatie model. Deze modellen worden tevens gebruikt om impliciet vast te stellen hoe deze waargenomen oriëntatie tot stand komt. Ze vertegenwoordigen twee extreme standpunten van plausibele mechanismen die de oriëntatie zouden kunnen verklaren. Het Maier-Saupe model wordt vaak gebruikt in het vakgebied van de vloeibare-kristallen en beschrijft spontaan oriënterende nematische vloeibare kristallen, terwijl het affiene deformatie model de oriëntatie beschrijft onder invloed van een homogene rek of compressie, bijvoorbeeld van rubbers. Uit onze waarnemingen volgt dat het affiene model de waargenomen oriëntatie beter beschrijft en dit impliceert het vormen van een gel tijdens het droogproces van de films. Vanaf een bepaalde concentratie ontstaat een zwichtspanning die de kleiplaatjes doet oriënteren. Dit wordt primair veroorzaakt door de interactie van de alginaat polymeerketens met de rand van de MMT kleiplaatjes en geeft uiteindelijk de gevonden tamelijk hoge $<P_2>$ waarden. Het waargenomen effect van het MMT gehalte op de oriëntatiegraad wordt ook verklaard door deze MMT/alginaat interactie. Het oriënteren van deze systemen is ook onderzocht door middel van optische polarisatie microscopie, waarbij kan worden vastgesteld dat de droogrichting de oriëntatie van de MMT nanodeeltjes beïnvloedt. Voortbordurend op de veronderstelling dat een specifieke interactie tussen alginaat en MMT plaatjes vereist is voor het vormen van een

hoog georiënteerd materiaal worden in **Hoofdstuk 3** metingen aan alginaat/MMT oplossingen onder invloed van een kleine dynamische belasting uiteengezet (small amplitude oscillatory shear). Inderdaad blijkt het gevonden viscoelastische gedrag van Na-Alg/MMT suspensies in sterke mate van het MMT gehalte af te hangen. De gevormde gel structuur wordt toegeschreven aan specifieke interacties van het negatief geladen alginaat polymeer met de positief geladen MMT klei-randen, waarbij overigens ook H-bruggen een factor kunnen zijn. Bij een MMT mengverhouding van 20 wt.% MMT wordt een kritische concentratie gevonden waar het systeem een gel begint te vormen. Deze gel heft een rubber plateau dat zich verder ontwikkelt bij toenemend MMT gehalte. Deze fysische gelen vertonen een maximum in de relaxatiemodulus met een tijdsconstante die wij toeschrijven aan het vormen en verbreken van bindingen tussen het alginaat polymeer en de MMT kleiplaatjes. Het waargenomen viscoelastische gedrag, het relaxatiemaximum en het G'-G" kruispunt laten zich uitstekend beschrijven door een zogenaamd Maxwell model. Naar onze overtuiging is het deze gelvorming die de door uitdroging verkregen hoge oriëntatiegraad in alginaat/MMT bionanocomposieten verklaart. De thermomechanische en thermische eigenschappen van Na-Alg/MMT bionanocomposiet films met verschillend MMT gehalte worden in **Hoofdstuk 4** besproken. De verkregen gestapelde structuur ("brick-and-mortar" structure) is ook terug te vinden in de gemeten mechanische eigenschappen. De eigenschappen van een hoog uitgelijnd systeem van MMT nanodeeltjes in alginaat wordt tamelijk goed beschreven door middel van het Halpin-Tsai model, waar we tevens de oriëntatiegraad, MMT gehalte en effectieve asverhouding (aspect ratio) in rekening moeten brengen. Het versterkende effect van de MMT nanodeeltjes wordt in relatieve zin minder bij hogere kleigehaltes, hetgeen door stapeling van de MMT deeltjes verklaard kan worden aangezien dit de effectieve asverhouding van de vulstof doet afnemen. Verder wordt gevonden dat de hoog geordende structuur van alginaat/MMT aanleiding geeft tot materialen die totaal onbrandbaar zijn en permanent enorme temperatuursgradiënten kunnen weerstaan, het materiaal vertoont een hoge mate van warmteafscherming. In **Hoofdstuk 5** wordt, aangespoord door de in Hoofdstuk 4 waargenomen onbrandbaarheid, het wateropname gedrag van Na-Alg/MMT bionanocomposieten onderzocht. De water sorptie isothermen worden geanalyseerd met een variabel oppervlakteconcentratie diffusie model, dat de experimentele resultaten nauwkeurig kan fitten. De bionanocomposiet films vertonen een afnemend wateropname vermogen bij stijgend MMT gehalte. Door de introductie van de MMT nanodeeltjes wordt een labyrinth-achtige structuur gevormd die de permeatie van kleine moleculen zoals water ernstig be-

lemmert (tortuous path), dit uit zich in een forse afname van de berekende diffusie coëfficiënt. De diffusiecoefficient in een polymeer/klei nanocomposiet hangt af van de klei oriëntatiegraad, de mate van overlap, de effectieve asverhouding en het gehalte aan kleideeltjes. De in **Hoofdstuk 2** verkregen <P2> waarden worden ingezet om de vereiste asverhoudig uit de gemeten sorptiecurven te bepalen, door middel van een gemodificeerd Nielsen model. Hieruit volgt (ook) dat bij toenemend MMT gehalte de effective asverhouding afneemt, hetgeen stapeling van de MMT kleiplaatjes impliceert. In **Hoofdstuk 6** richten we ons op de toepassing van Na-Alg als een bio-based curing compound voor cementhoudende bouwmaterialen. Tegenwoordig worden de meeste betonconstructeis ontworpen op een verwachte levensduur van minstens 50 jaar. Gedurende deze tijd wordt het beton blootgesteld aan diverse omgevingsinvloeden, zoals vries/dooi-cycli, sulfaat blootstelling en corrosie van de staalbewapening. Een goed verlopende hydratatie tijdens het uitharden van het beton bevordert het vormen van een dichte betonstructuur met een goede hechting van het cement aan de toeslagmaterialen, minder holtes en microscheuren en het voorkomen van percolatie in de microporeuse structuur. Dit is met name aan het oppervlak van het beton van groot belang. Een op de juiste wijze uitgehard beton is het ultieme middel om een lange levensduur van de constructie te waarborgen. Dit kan bereikt worden door te voorkomen dat het uithardende beton oppervlak vroegtijdig uitdroogt. Het principe om een Na-alginaat oplossing hiervoor te gebruiken, als curing compound) is aangegeven door de optredende snelle crosslinkingsreactie met Ca^{2+} ionen die aan het oppervlak van het beton ruimschoots voorhanden zijn. Hierdoor dringt het alginaat niet in het betonoppervlak maar blijft het als afdekkende laag aan het oppervlak hetgeen gewenst is (indringing zou juist de beton uitharding kunnen belemmeren). Het gebruiken van Na-alginaat als curing compound heeft als additioneel voordeel dat het een waterige oplossing van een milieuvriendelijk biopolymeer van natuurlijke oorsprong betreft. De effectiviteit van deze behandeling van beton met Na-alginaat is experimenteel onderzocht door middel van “Rapid Chloride Migration tests” en “Environmental Scanning Electron Microscopy” aan diverse samples, hiermee kan het ionentransport en de microstructuur van het materiaal onderzocht worden. De cementmonsters werden bij 50% RH en 20 °C uitgehard met en zonder oppervlaktebehandeling met de biobased curing compound. Twee soorten cement zijn gebruikt CEM I en CEM III/B, aangezien deze een nogal verschillend uithardingsgedrag vertonen, vooral in hun gevoeligheid voor onvolledige uitharding. Een significante verbetering van de beton microstructuur wordt gevonden bij het behandelde cementoppervlak met een mooi ontwikkelde dichte en dus duurzame

microstructuur. Met name is dit bij de CEM III/B samples gevonden aangezien dit cement veel gevoeliger is voor onvolledige uitharding dan CEM I. Zoals al was vastgesteld in **Hoofdstuk 5** kan een hoog georiënteerde Na-Alg/MMT bionanocomposiet film een behoorlijke reductie van waterdiffusie opleveren, we kunnen dus de effectiviteit van de coating aanpassen aan de te verwachten omgevingsinvloeden tijdens het uitharden van het beton (wind, zon, vochtigheid, temperatuur en dergelijke). In **Hoofdstuk 7** worden de belangrijkste conclusies nog eens samengevat en met name wordt gekeken naar de implicaties van het dit werk op toekomstig onderzoek aan en toepassing van deze klasse van materialen. Op basis van de in dit proefschrift beschreven resultaten kan additioneel onderzoek aan hoog georiënteerde bionanocomposieten met andere nanodeeltjes en/of een ander soort matrix polymeer worden gedaan, waarbij het kunnen manipuleren van de oriëntatie en dispersie-graad van het vulmiddel van groot belang is. Een van de voorbeelden daarvan zijn biopolymeren die verkregen kunnen worden uit waterzuiveringsinstallaties, het zogenaamde alginate-like exopolymer dat uit een aerobe korreslibreactor verkregen kan worden, dit lijkt een veelbelovende toekomst te hebben als grondstof voor het maken van uitstekende bionanocomposiet materialen.

Acknowledgements

This is an ideal place for reflections, which are necessary to identify where you are and how you got there. Many friends and colleagues bare co-responsibility for any value these chapters have, while the errors and lapses are mine alone.

First and foremost, I would like to express my gratitude to prof. Klaas van Breugel and prof. Eddie Koenders for giving me the opportunity to come to TU Delft and their continuous support during the work.

To prof. Stephen Picken, Stephen thank you for accepting to join the project. I was in good fortune that I have met a person that is so willing to help and share his vast knowledge. I hope I have not plagued you too much over the years. Whether we talk about food or science your deep level of understanding of the subject never ceases to amaze me.

I wish to express my acknowledgement to the Dutch taxpayers and the STW for financing this project.

I would like to thank the people from the Microlab for being helpful during my stay there. Especially Erik, Henk, Virginie, Lupita, Arjan, and John for their positivity and genuine interest that were more uplifting then they might know.

Lessons that I was honored to receive from Oriol, Amin, and Phu, that I shared an office with, have become a part of me and last time I checked "Why Don't Penguins' Feet Freeze?" was still in the office.

The outlook on research and life of the Environmental Biotechnology department makes it a very stimulating place. Mark and Yuemei, thank you for inviting me to be a participant on your research line of biopolymer recovery. The colleagues/friends from EBT are a unique group of people that I feel privileged to have a chance to work with.

The people I can call friends, which sometimes means a dinner or help with moving to a new apartment. Neven, Damian, Albert, Luis, Dimitris, Stella, Bob, and Lisanne, you made The Netherlands feel like home.

A special thanks goes out to my family: mom, Laura, Julija, Zdenka, Ben, Rudi, Evelin, Pia, Melissa, Peter, Cvita, and Matilda that give me support to which I will always be in debt for. Ben, thanks for the cool graphics in the chapters and on the cover.

Patricía, the most beautiful and kindest person I have ever met. When I am with you I am over the moon. Thank you for sharing your life with me.

More than this ...

Cirriculum vitæ

Jure Zlopasa was born on 15th of April 1987 in the city of Zagreb, Croatia. In 2005 he started his bachelor study at Faculty of Chemical Engineering and Technology, Univeristy of Zagreb, Croatia. In 2010 he finished the MSc study at the same University. In March 2011 he started his PhD research titled Post-casting effects of concrete durability, which was a part of a STW perspectif program IS2C in the Materials and Environment section of the Faculty of Civil Engineering and Geosciences at Delft University of Technology. The unpredictability of research had not led him to where he intended to go, but he has ended up where he ought to be. Since his fascination and motivation on biopolymers and bionanocomposites had not disappeared he started, in July 2015, a research at Environmental Biotechnology section in the Faculty of Applied Sciences at Delft University of Technology on extraction and characterization of exopolymeric substances from aerobic granular sludge wastewater treatment process.

List of publications

1. Zlopasa, J.; Koenders, E. A. B.; van der Horst, A. Q. C. "Influence of compaction on chloride ingress." *Proceedings of the 9th fib International PhD symposium in civil engineering.* Haist, M.; Acosta, F.; Muller, H. S. (eds.). Karlsruhe **2012**, 505-510.

2. Ukrainczyk, N.; Zlopasa, J.; Koenders, E. A. B. "Hydration process of portand cement blended with silica fume." *Advanced Materials Research*, **2013**, 578-583.

3. Zlopasa, J.; Norder, B.; Koenders, E. A. B., Picken, S. J. "Highly ordered biopolymer clay nanocomposites." Dutch Polymer days, The Netherlands. Poster **2013**.

4. Zlopasa, J.; Koenders, E. A. B.; Picken, S. J.; "Using bio-based polymers for curing cement-based materials." *Proceedings of the 1st international conference on ageing of materials and structures, AMS'14.* Koenders, E. A. B. & van Breugel, K.; (eds.). Delft: DCMat Ageing Centre, **2014**, p. 220-226.

5. Ukrainczyk, N.; Zlopasa, J.; Koenders, E. A. B.; Rocha, C. A. A.; Filho, R.

D. T. *Proceedings of the International Conference on Offshore Mechanics and Arctic Engineering - OMAE.* s.n. (eds.) New York: ASME **2014**.

6. Zlopasa, J.; Koenders, E. A. B.; Picken, S. J. "A novel bio-based curing compound for cement-based materials." *International RILEM Conference of Superabsorbent Polymers and Other New Admixtures in Concrete Construction* Mechtcherine, V. & Schroefl, C. (eds.) Dresden **2014**, 47-54.

7. Zlopasa, J.; Koenders, E. A. B.; Picken, S. J. "Biobased membrane compound for concrete surfaces." WO2015/050449, **2015**.

8. Zlopasa, J.; Norder, B.; Koenders, E. A. B.; Picken, S. J. "Origin of highly ordered sodium alginate/montmorillonite bionanocomposites." *Macromolecules*, **2015**, 48(4), 1204-1209.

9. J. Zlopasa, B. Norder, E.A.B. Koenders and S.J. Picken, "Advanced biopolymer nanocomposites." Dutch Polymer days, The Netherlands. Talk **2015**.

10. Zlopasa, J.; Norder, B.; Koenders, E. A. B.; Picken S. J. "Rheological investigation of specific interactions in Na Alginate and Na MMT suspension." *Carbohydrate Polymers* **2016**, 151, 144-149.

11. Vilcinskas, K.; Zlopasa, J.; Jansen, K. M. B.; Mulder, F. M.; Picken, S.J., Koper, G. J. M. "Water sorption and diffusion in (reduced) graphene oxide-alginate biopolymer nanocomposites." *Macromolecular Materials and Engineering* **2016**, 301(9), 1049-1063.